1. General

Inconel Alloy 718 is the most widely used superalloy, accounting for approximately one-third of all superalloy production. This alloy, developed by the International Nickel Company in the late 1950's for gas turbine applications, has excellent strength, ductility, and toughness throughout the range -423 to 1300F. A major attribute of Inconel 718 is its processing versatility. It can be fabricated over a wide range of temperatures, forging reductions, and strain rates to produce microstructures and associated properties tailored for specific requirements. Inconel 718 is unique among nickel-base alloys because of its outstanding weldability and good resistance to strain-age cracking. The superior weldability characteristics are associated with the sluggish precipitation characteristics of the primary strengthening gamma-double-prime phase. The sluggish age-hardening response also necessitates relatively long aging treatments. Inconel 718 possesses excellent corrosion and oxidation resistance in addition to good formability. It also has good sea water corrosion resistance and it is attractive for marine applications. The alloy is produced in both wrought and cast forms. It is used in structural applications in the aerospace, nuclear, and petrochemical industries. Typical aerospace applications include compressor and turbine discs, buckets, spacers, and bolts for jet engines, liquid-rocket components involving cryogenic temperatures, and power supply batteries for satellites (Refs. 1, 19, 38, 71-74, 87-92).

1.1 Commercial Designation

Inconel Alloy 718.

1.2 Alternate Designations

Inconel 718, UNS N07718, Udimet 718, Allvac 718, Pyromet Alloy 718, Haynes Alloy No. 718, Lescalloy 718, Inconel Alloy 718SPF.

1.3 Specifications

1.3.1 *[Table]* AMS specifications.

1.4 Composition

1.4.1 *[Table]* AMS specified compositions.

1.5 Heat Treatment

1.5.1 Microstructural Effects. Heat treatment schedules for wrought Inconel 718 are based primarily on considerations of solution and reprecipitation reactions of the gamma-prime and gamma-double-prime phases for strengthening and of delta phase for grain size control. The heat treatments generally involve a high temperature anneal for solutioning of these second phases followed by one or two lower temperature aging treatments to reprecipitate the strengthening phases in the desired distributions. Some strengthening precipitate generally forms on cooling from the solution annealing temperature. The first aging treatment coarsens this precipitate as well as forming additional precipitate. The second lower temperature aging treatment promotes additional fine precipitate for improved tensile strength and creep rupture life (Ref. 93).

	Ni
19	Cr
18	Fe
5.1	Cb+Ta
3	Mo
0.9	Ti
0.5	Al

Gamma-double-prime and delta phases are structural variations of the same compound, Ni_3Cb. The body-centered-tetragonal gamma-double-prime phase precipitates coherently with the matrix and is strengthening. However, the orthorhombic delta phase forms a noncoherent precipitate which is not strengthening but is useful for grain size control. Gamma-double-prime forms in the approximate temperature range 1300 to 1650F and has a solvus temperature of about 1675F (see Figure 2.1.2.1.1). Gamma-prime phase, which has the formula $Ni_3(Al,Ti)$, forms in the same approximate temperature range as gamma-double-prime but at longer times. Gamma-double-prime and gamma-prime often precipitate together but gamma-double-prime, being more abundant, is the principal strengthening phase under such circumstances. Gamma-double-prime precipitates as small disc-shaped particles having a fully aged diameter of several hundred angstroms. The gamma-prime particles are typically more spherical in shape and have a somewhat smaller diameter (Ref. 93). Gamma-double-prime strengthens by virtue of high coherency strains in the lattice, while gamma-prime causes strengthening through the necessity to disorder the particles as they are sheared.

Delta phase forms at higher temperatures, in the range of 1600 to 1850F, and has a solvus temperature of about 1850F. For wrought Inconel 718 processed below the delta solvus, grain boundary migration is inhibited by the presence of this phase and the microstructure retains a fine grain size. Subsequent thermal exposure above this temperature dissolves the delta phase and allows more rapid grain growth (Ref. 92). The precipitation behavior of Ni_3Cb delta phase is shown in Figure 1.5.1.1.

1.5.1.1 *[Figure]* Effect of annealing time at 1700F on delta phase precipitation.

The microstructure of Inconel 718 consists of equiaxed grains with numerous annealing twins and coarse MC-type carbide inclusions throughout the matrix, regardless of heat treatment temperature (Ref. 94).

Increased solution annealing temperature promotes larger grain size and increased creep rupture strength but lower short-time tensile strength. These trends are

This section produced with the support of NASA-Lewis Research Center.

shown in Figure 1.5.1.2 and Table 1.5.1.3. The highest tensile strengths are achieved with the direct-aged material (no solution anneal), with some reduction of creep rupture life. Creep rates also decrease with increasing solution temperature, as shown in Figure 1.5.1.4 (Ref. 95).

1.5.1.2 *[Figure]* Effects of variations in cold work and annealing temperature on grain size of sheet.

1.5.1.3 *[Table]* Effects of solution annealing temperature on tensile and creep rupture properties.

1.5.1.4 *[Figure]* Effects of solution annealing temperature on creep rate behavior at 1300F.

Excessive grain coarsening begins in the temperature range 1900 to 1920F, as shown in Figure 1.5.1.5. This behavior is attributed to dissolution of primary CbC (Ref. 97).

1.5.1.5 *[Figure]* Grain growth behavior at 1900 to 2000F.

Variations in cooling rate after solution annealing affect the subsequent age-hardening reactions. Rapid quenching and air cooling both produce an initially soft material which hardens substantially during subsequent aging. In contrast, slow cooling allows hardening during the cooling period with little additional hardening during aging, shown in Figure 1.5.1.6. These hardness increases are associated with precipitation of the gamma-double-prime phase (Ref. 98).

1.5.1.6 *[Figure]* Effects of solution anneal cooling rate and aging time on hardness.

Aging temperature and time also significantly affect properties. Aging at 1202F, for example, after solution annealing results in low-strength material with high impact energy. The yield strength increases and impact energy decreases with increasing aging temperature up to 1382F, as shown in Figure 1.5.1.7. The aging reaction is sluggish, as shown by the extended times required to reach maximum hardnesses in Figures 1.5.1.8 and 1.5.1.9. The slow aging behavior is attributed to the low diffusivity of columbium in nickel (Ref. 98).

1.5.1.7 *[Figure]* Effects of aging temperature on room temperature yield strength and impact energy of solution annealed alloy.

1.5.1.8 *[Figure]* Effects of aging time at various temperatures on the hardness of sheet.

1.5.1.9 *[Figure]* Effect of aging time at 1200F on hardness after high temperature annealing.

The effects of single and double aging on strength and toughness properties are shown in Table 1.5.1.10. The double-aged materials exhibit higher tensile strengths but lower fracture toughnesses than single aged materials.

1.5.1.10 *[Table]* Effects of single and double aging treatments on mechanical properties of solution annealed alloy.

1.5.2 Standard Heat Treatments. Wrought Inconel 718 is normally used in the solution annealed and aged condition, but the exact treatment times and temperatures vary with the property requirements of the intended applications. Two heat treatment procedures are widely used by most producers. The first procedure, designated as the conventional heat treatment (CHT), is generally recommended for an optimum balance of creep rupture properties, room temperature tensile and yield strengths, and fatigue life. This procedure involves solution annealing below the delta solvus temperature followed by a two-step aging treatment, as follows:

Anneal at 1725 to 1825F for one-half to one hour, AC or faster; age at 1325F, eight hours, FC to 1150F, hold at 1150F for total age time of 18 hours, AC (alternatively, age at 1325F, eight hours, cool at 100F per hour to 1150F, age at 1150F, eight hours, AC).

CHT material is fine grained (average grain size ASTM 4 to 6) and contains coarse lenticular delta phase precipitates and blocky carbides along grain boundaries. The primary strengthening precipitate, body-centered-tetragonal gamma-double-prime Ni_3Cb, is disk-shaped, fine, and closely spaced throughout the matrix (Ref. 88).

The second widely-used procedure involves slightly higher solutioning and aging temperatures. It is used for optimum ductility and low temperature toughness in heavy sections, although it can also produce notch brittleness in creep rupture. This heat treatment involves solution annealing above the delta solvus temperature, as follows:

Anneal at 1950F, one-half to one hour, AC or faster; age at 1400F, 10 hours, FC to 1200F, hold at 1200F for total age time of 20 hours, AC.

Tensile properties for material heat treated according to these two procedures are given in Table 1.5.2.1 for hot-rolled rounds of various diameters and in Table 1.5.2.2 for pancake forgings. Tensile strengths of the solution annealed alloy are significantly increased by aging, with the 1325/1150F age giving higher strength than the 1400/1200F age. Tensile ductilities decrease with increasing strength.

1.5.2.1 *[Table]* Tensile properties in longitudinal orientations of hot-rolled rounds of several sizes and in various heat-treated conditions.

1.5.2.2 *[Table]* Tensile properties of pancake forgings of various sizes in different heat-treated conditions.

(See also Figures 3.2.1.1, 3.3.1.10, 3.3.1.11, 3.3.3.3, 3.3.7.1.5, and 3.5.2.2, and Tables 3.2.1.4, and 3.2.3.1.)

Particularly for the annealing treatment, a slightly reducing atmosphere with very low sulfur content is recommended to prevent the formation of heavy scale, which is difficult to remove (Ref. 1).

1.5.3 Thermomechanical Processing. Heat treatment of Inconel 718 is frequently considered as part of an overall thermomechanical approach to processing. Three general thermomechanical processing techniques, termed – standard processing, high strength processing, and direct age processing, have been developed in recent years. Typical tensile properties and fatigue properties for materials processed by these techniques are shown in Figures 1.5.3.1 and 1.5.3.2.

1.5.3.1 *[Figure]* Effects of temperature and processing technique on tensile strength.

1.5.3.2 *[Figure]* Effects of processing technique on low-cycle fatigue behavior at 1000F.

Standard processing is used primarily for noncritical or difficult to make shapes. Microstructures typically have a mixed grain structure with an average grain size of ASTM 4 to 6. Forging is conducted above the delta solvus temperature. Initial forging is conducted in the temperature range 1950 to 2000F, while finish forging is done at 1900 to 1950F. Cooling during the final stages of finish forging allows precipitation of a small amount of beneficial delta phase grain boundary platelets. After forging, parts are heat treated as follows:

Anneal at 1775F for two hours, WQ;
age at 1325F, eight hours, FC to 1150F,
hold at 1150F for eight hours.

This treatment is essentially equivalent to the CHT described above. Standard processed material contains a small amount of grain boundary delta phase and has good creep rupture ductility and freedom from notch embrittlement (Ref. 92).

High strength processing is useful for highly stressed components having a relatively simple configuration. The grain structure is usually smaller than that of standard processed material, with an average grain size of ASTM 8 or finer. The tensile and low-cycle fatigue properties are improved over those of standard processed material, primarily because of the finer grain size. The finer grain size is promoted by larger forging reductions near or below the delta phase solvus temperature. Initial forging is accomplished at 1900 to 1950F to minimize grain growth. Finish forging is initiated in the range 1850 to 1900F and completed below the delta phase solvus temperature of about 1850F. Processing conditions are more critical than for standard processing in order to achieve the necessary uniform forging reduction at the proper temperature. After forging, the parts are solution annealed and aged as described above for standard processing (Ref. 92).

The direct age processing technique is a further extension of the approach used in high strength processing to improve tensile strength and low-cycle fatigue properties. Grain sizes which are smaller and more uniform than that of high strength processed alloy are achieved through larger forging reductions at even lower temperatures. Following the forge processing, parts are heat treated using only the duplex age cycle described above for standard processing. The solution treatment used for standard and high strength processed alloy is omitted (see Figures 1.6.2 and 3.5.3.4 and Table 1.5.1.3.) (Ref. 92).

1.5.4 Weld Heat Treatments. Heat treatment of fusion weld joints requires special consideration because of the presence of cast structure in the weld area. The sluggish age-hardening response of Inconel 718 results in a relatively low-strength, high ductility joint in the as-welded condition. An additional solution annealing and aging treatment is required if high strength is required in the weld area. However, post-weld heat treatment can produce microfissuring and reduced ductility in the heat-affected zone. Microfissuring is thought to result from the presence of brittle Laves phase in the interdendritic regions of the weld metal or from grain boundary liquation of CbC and Laves phase. The following special post-weld heat treatment, sometimes referred to as the modified heat treatment (MHT), is useful to restore the toughness of embrittled heat-affected zones:

Anneal at 2000 to 2025F, one hour,
cool at 150F per hour to 1325F,
hold four hours, cool at 100F per hour to 1150F,
hold 16 hours, cool at 250F per hour to below 700F,
AC.

The high temperature solution anneal largely dissolves the Laves phase and restores adequate impact ductility in the fusion zone, while the slower cooling rates tend to reduce thermal stresses. Both the high solution anneal temperature and the slow cooling rate after solution annealing differentiate this treatment from the standard treatments and are important to produce the desired effects. (Refs. 88-89, 99, 127, 167). Although the MHT has beneficial effects on both the strength and toughness of welds compared with the standard treatments, it appears to have slightly detrimental effects on the toughness and both the creep crack and fatigue crack growth resistance of parent metal (see Figures 1.5.1.4, 3.3.7.2.1, 3.4.19, 3.5.3.10, 4.3.1.3, 4.3.1.14, and 4.3.1.19.) (Refs. 31-33, 58, 77, 81).

1.5.5 Casting Heat Treatments. Structural castings can have interdendritic segregation high in columbium, resulting in formation of Laves phase and coarse carbides not found in the wrought product. The Laves phase can be reduced by a homogenization anneal at 2050F or higher. However, dissolution of the grain boundary delta phase during homogenization annealing promotes notch creep rupture sensitivity; the delta phase can be reformed by solution treating at 1600F (below the delta solvus) (Ref. 95). A two-step homogenization procedure has been recommended for cast alloy. The first step involves heating at 2080 to 2150F to remove the Laves phase and increase the incipient

melting point. The second step is heating at 2200F to reduce columbium segregation (Ref. 100).

1.5.6 Special Heat Treatments. Additional heat treating procedures have been reported to provide tailored properties in wrought material for special purposes. A process similar to the standard process described above, termed delta processing, employs a heat treatment between the primary and finish forging steps. This in-process anneal is conducted in the range between the gamma-double-prime and delta solvus temperatures in order to precipitate delta phase at the grain boundaries. Presence of the delta phase promotes a finer, more uniform grain structure with accompanying more uniform mechanical properties in the final product (Ref. 101).

A heat treatment has been suggested which reduces fatigue and creep crack growth rates at 1200F by factors of two and five, respectively, compared with material processed by the CHT. This heat treatment consists of:

Solution anneal 1890F, one hour, FC to 1550F, hold four hours, plus partial solution anneal 1700F, FC to 1325F, hold eight hours, FC to 1150F, hold eight hours, AC (Ref. 97).

For improved resistance to creep-crack growth at temperatures of 800F and above, the following heat treatment procedure has been recommended (see Figure 3.4.19):

Anneal at 1700F, 10 hours, FC; age at 1300F, 48 hours, AC.

This treatment has slightly detrimental effects on tensile properties compared with those resulting from the standard treatments (Refs. 33, 78). The following treatment is recommended to remove the effects of precipitation hardening or cold work and to promote the softest most workable condition (Ref. 75):

Anneal at 1750 to 1800F, one-half hour, AC.

For applications requiring high toughness and resistance to hydrogen embrittlement and stress-corrosion cracking, such as in the oil and gas industry, the following procedure is recommended:

Anneal at 1850 to 1950F; age at 1200 to 1500F.

1.6 Hardness

(See also Figures 1.5.1.6, 1.5.1.8, and 1.5.1.9 and Table 1.5.1.10.)

1.6.1 *[Table]* Hardness ranges typical of a wide variety of product forms in various conditions.

1.6.2 *[Figure]* Effects of cold rolling and aging on the hardness of sheet at room temperature.

1.7 Forms and Conditions Available

Inconel 718 is available in a full range of products including rod, bar, forgings, shapes, tubes, plate, sheet, strip, wire, welding electrodes, and castings. The various products can normally be supplied either in the annealed or annealed-and-aged condition (Ref. 1).

1.8 Melting and Casting Practice

Standard commercial practice consists of vacuum induction melting and vacuum arc remelting (VIM/VAR). Alternate remelting processes and combinations of processes have been evaluated as means of reducing solidification segregation and effecting improved microstructural cleanliness (such as by removing white spots and agglomerated inclusions), which in turn leads to better low-cycle fatigue properties. These other processes include electroslag refining (ESR), electron-beam cold hearth refining (EBCHR), plasma-melt refining (PMR), and vacuum-arc double-electrode refining (VADER). ESR reduces sulfur content, removes large inclusion agglomerations and entrapped slag, and produces a fully dense structure with no shrinkage cavities. This ingot can then be used as the VAR electrode, with VAR processing being dedicated to controlling the solidification structure. VIM/ESR/VAR is significantly cleaner than the conventional VIM/VAR material and provides improvement in the reliability and quality of rotating-disk components (Refs. 95, 102).

Alloy cleanliness with respect to inclusions has a significant effect on low-cycle fatigue life. The fatigue behavior of alloy prepared by EBCHR is compared to that of VIM alloy in Figure 1.8.1. Inclusions in VIM alloy are effectively reduced by about an order of magnitude as a consequence of EBCHR. Concurrently, low-cycle fatigue life of ASTM 10 grain-size alloy is increased by about an order of magnitude. The improvement is somewhat less for ASTM grain size 8 alloy under similar conditions. These changes are related to the number of near-surface inclusions, which act as initiation sites for low-cycle fatigue cracks (Refs. 102-105).

1.8.1 *[Figure]* Effects of vacuum induction melting and electron-beam cold hearth refining on fatigue life at 1000F in air.

Inconel 718 has also been produced in cast form and by powder metallurgy methods (Ref. 106). Vacuum plasma spray techniques can be employed to produce near net shapes with properties similar to those of cast alloy (Ref. 107).

1.9 Special Considerations

1.9.1 Thermo-mechanical processing and heat treatments can be tailored to emphasize properties particularly desired for a given application. Higher tensile and fatigue strengths can be achieved by direct age processing than by standard processing (see Figures 1.5.3.1 and 1.5.3.2 and accompanying discussion). Improved fracture toughness results from heat treatment including a solution anneal at 2000F than from one including an anneal at 1750F (see Figure 3.3.7.2.1 and accompanying discussion).

1.9.2 Microstructural cleanliness is very important to improved low-cycle fatigue resistance. Special consolida-

tion processes such as electroslag refining and electron-beam cold hearth refining can be can be combined with vacuum induction melting to produce alloy with very low inclusion contents which exhibits up to 10-fold improvement in low-cycle fatigue life (see Section 1.8).

1.9.3 Small grain size is a major factor in achieving high fatigue strength in Inconel 718. The lower solution temperature in the CHT promotes fine grain size and superior fatigue properties (see Figures 3.5.1.6 and 3.5.2.2 and accompanying discussions).

1.9.4 The alloy is embrittled by internally induced hydrogen and by exposure to hydrogen atmospheres in the presence of plastic strain (see Section 2.3.3).

1.9.5 The tensile properties of cast alloy are lower than those of wrought alloy but can be improved by heat treatment or by hot isostatic pressing (see Table 3.2.1.14 and Figure 3.3.1.18 and accompanying discussions).

1.9.6 Under creep conditions, Inconel 718 has a tendency to be notch sensitive (see Figures 3.4.12 through 3.4.16 and accompanying discussions). It is believed that high finishing temperatures during hot work contribute to this behavior (see Figure 4.1.2).

1.9.7 The heat-affected zones of welds are susceptible to microfissuring caused by grain boundary liquation during weld solidification when fusion welded under conditions of high restraint. Ductility can be restored by post-weld annealing at 1950F or higher (see Section 4.3.3).

2. Physical Properties and Environmental Effects

2.1 Thermal Properties

2.1.1 Melting Range. The melting and solidification temperatures reported by various investigators are summarized in Table 2.1.1.1. Liquidus temperatures show the least variation and average 2443+/-26F. The observed solidus and eutectic temperatures exhibit a wider range of variability, due in part to differences in degree of segregation from one sample to another.

2.1.1.1 *[Table]* Melting and solidification temperatures for Inconel 718.

During quasi-isothermal solidification, the elements molybdenum, titanium, and columbium segregate to the residual melt, while nickel, iron, and chromium segregate to the primary solidifying crystals. Columbium exhibits particularly extreme segregation behavior (Ref. 108).

The primary dendrite arm spacing decreases with increasing cooling rate during solidification. With decreasing cooling rate, the elemental partition coefficients approach the ideal value of unity. However, a pronounced reduction in segregation is achievable only at the cost of significant extension of the dendrite arm spacing, which increases the diffusion distance during subsequent homogenization treatments (Ref. 108).

2.1.2 Phase Changes.

2.1.2.1 Time-temperature-transformation diagrams. In the solid state, chromium and molybdenum partition largely to the austenitic nickel-iron matrix. Chromium provides oxidation resistance while both chromium and molybdenum contribute to solid solution strengthening. Columbium, titanium, and aluminum govern the phase precipitation characteristics of the alloy while small additions of carbon and boron enhance grain boundary strength and ductility (Ref. 92).

The principal microstructural phases present in solution annealed and aged Inconel 718 consist of:

1. A face-centered-cubic (fcc) gamma matrix of nickel containing iron, chromium, and molybdenum in solid solution.

2. An ordered body-centered-tetragonal (DO_{22}) gamma-double-prime phase which is coherent with the matrix and has the ideal composition Ni_3Cb. This phase is favored in nickel-base superalloys with high iron contents and is the principal strengthening agent in Inconel 718.

3. An fcc (Ll_2) gamma-prime phase of $Ni_3(Al,Ti)$ which precipitates coherently with the matrix and is the prime strengthener in most nickel-base superalloys. However, in Inconel 718, this phase contributes little if any high temperature strength. Columbium and chromium also substitute in gamma-prime.

4. Delta phase, which has the same composition as gamma-double-prime but an orthorhombic crystal structure. It precipitates incoherently at temperatures above that to which gamma-double-prime is stable and is non-strengthening.

5. MC carbide phases, which precipitate during solidification both intergranularly and within the grains, frequently interdendritically. These carbides have the formula (Cb,Ti)C and tend to decompose slowly during service into $M_{23}C_6$ and M_6C.

6. Other minor phases, including topologically close-packed phases. Laves phase occurs in cast or welded microstructures but not in wrought material. Laves phase has the formula A_2B, where A is nickel, iron, manganese, chromium, and silicon and B is columbium, molybdenum, and titanium. The formation of Laves phase is promoted by silicon, titanium, columbium, and chromium. Nickel tends to discourage Laves formation (Ref. 100).

7. Body-centered-cubic alpha chromium, which forms as globular particles in regions where nickel is depleted due to extensive precipitation of intermetallic phases (Refs. 92-94, 98).

Like other high temperature alloys, Inconel 718 is metastable with respect to precipitation and overaging of the primary precipitates and transformation into other phases, as shown in the TTT diagram in Figure 2.1.2.1.1 (Ref. 109). Extended exposure of solution annealed and aged alloy (e.g., for 10,000 hours) at 1070F causes additional gamma-double-prime precipitation, resulting in further strengthening. At 1200F, little change occurs during exposures up to about 1000 hours, but longer time exposures cause particle coarsening and reductions in tensile and creep strengths. At higher temperatures, coarsening of the gamma-double-prime precipitate occurs at shorter times with a concomitant loss of strength (Ref. 110).

For exposure times in excess of 10 hours, gamma-double-prime begins to decompose into either gamma-prime (stable after long times at 1200 to 1560F) or delta (stable after long times at 1380 to 1830F). For example, after 3000 hours at 1470F, the precipitate morphology changes from a fine dispersion of gamma-double-prime to coarse gamma-prime combined with large delta plates (Ref. 110). Gamma-prime phase usually forms in regions where columbium is depleted due to heavy gamma-double-prime or delta precipitation (Ref. 98). Intergranular chromium globules also form after exposure times of 3000 hours or more in regions of nickel depletion. Both the gamma-double-prime and gamma-prime phases in Inconel 718 are metastable with respect to delta, which forms as intragranular laths along {111} or by a cellular reaction at grain boundaries (Ref. 92).

2.1.2.1.1 *[Figure]* Time-temperature-transformation (TTT) diagram.

The volume fractions of gamma-double-prime and gamma-prime can vary from 10 to 20 percent and from three to five percent, respectively, depending on the bulk alloy composition, heat treatment schedule, and degree of elemental segregation (Ref. 111)

Physical association between gamma-prime and gamma-double-prime particles occurs frequently during precipitation and growth at 1382F, leading to a variety of composite precipitate morphologies (such as two particles connected by a "neck," for example). For both phases, the particle size during coarsening shows a linear dependence on the cube root of aging time (Ref. 112).

The predominant carbide phase in Inconel 718 is a columbium-rich MC phase. This phase is present as coarse, irregular particles, both intergranularly and within the grains in solution annealed alloy. Additional carbide phase precipitates during aging, as shown in Figure 2.1.2.1.2. These carbide precipitates nucleate exclusively at grain boundaries and are accompanied by formation of zones which are free of gamma-prime and gamma-double-prime particles.

Transformation of MC to $M_{23}C_6$ occurs at long aging times (Ref. 113). The phase M_6C forms also during exposure at about 1200F but only under conditions of stress (Ref. 94).

2.1.2.1.2 *[Figure]* Time-temperature-precipitation diagram for grain boundary carbides.

The temperature dependence of hydrogen diffusivity is expressed by an Arrhenius-type equation as:

$$D = D_o \exp(-Q_D/RT)$$

where D_o is the frequency factor and Q_D is the activation energy of diffusion. Values of D_o and Q_D have been determined as 0.0107 cm^2/sec and 11,900 cal/g-atom, respectively for the diffusivity of hydrogen in Inconel 718 over the temperature range 302 to 932F. Similarly, the permeability P is expressed by:

$$P = P_o \exp(-Q_P/RT)$$

where P_o is the permeability factor and Q_P is the activation energy for permeation. Values of P_o and Q_P have been determined as 8.09×10^{-3} cm^3(NTP)/cm-sec-$atm^{1/2}$ and 13,330 cal/g-atom, respectively, over the same temperature range. The apparent solubility of hydrogen is calculated as the ratio P/D. The diffusivities are essentially unaffected by heat treatment. However, the permeabilities and apparent solubilities are higher for solution annealed and aged material than for mill annealed or solution annealed material (Ref. 114).

2.1.3 Thermal Conductivity.

2.1.3.1 *[Figure]* Thermal conductivity from -450 to 2000F.

2.1.4 Thermal Expansion.

2.1.4.1 *[Figure]* Thermal expansion from -320 to 2000F.

2.1.5 Specific Heat. 0.104 Btu/lb-F (0.104 cal/g-C) at 70F (Ref. 1).

2.1.6 Thermal Diffusivity.

2.2 Other Physical Properties

2.2.1 Density. 0.296 lb/in^3 (8.18 g/cm^3) in the annealed condition; 0.297 lb/in^3 (8.20 g/cm^3) in the annealed-and-aged condition (Ref. 1).

2.2.2 Electrical Properties.

2.2.2.1 *[Figure]* Electrical resistivity at low temperatures of annealed and annealed-and-aged alloy.

2.2.2.2 *[Figure]* Electrical resistivity at elevated temperatures of annealed and annealed-and-aged alloy.

2.2.3 Magnetic Properties. Permeability at 200H and 70F: annealed, 1.0013; annealed-and-aged, 1.0011 (Ref. 1).

Curie temperature: annealed, < -320F; annealed-and-aged, -170F (Ref. 1).

Inconel 718 is paramagnetic at normal temperatures but becomes strongly magnetic at temperatures near that of liquid hydrogen. Magnetic susceptibility reaches a maximum between 15 and 19K, near the boiling point of liquid hydrogen (20K), as shown in Figure 2.2.3.1. The peak susceptibility varies by a factor of eight with minor variations in nickel and iron content within specified compositional ranges for the alloy (Ref. 115).

2.2.3.1 *[Figure]* Effects of compositional variations on low temperature susceptibility.

2.2.4 Emittance.

2.2.5 Damping Capacity.

2.3 Chemical Environments

2.3.1 General Corrosion. Inconel 718 has good resistance to corrosion by many inorganic and organic compounds throughout wide ranges or acidity and alkalinity.

Both general and pitting corrosion resistance are reduced by higher aging temperatures. This behavior is attributed to localized carbide formation and chromium depletion (Ref. 96).

Marine corrosion resistance is excellent, with corrosion rates of less than 0.04 mil/year during 45-year exposures to marine atmosphere at Kure Beach, NC (Ref. 116).

2.3.2 Stress Corrosion. The alloy is highly resistant to chloride stress corrosion at temperatures up to 300F, but it becomes susceptible at higher temperatures, particularly when exposed to aqueous environments containing sodium and magnesium chlorides (Ref. 27).

Inconel 718 has good resistance to marine stress corrosion. Both unwelded and welded specimens showed no failures after 24-year exposures under stress to marine atmosphere at Kure Beach, NC (Ref. 116). However, the room temperature fatigue resistance is reduced in distilled water and in aqueous salt solutions as compared to air, as shown in Figure 2.3.2.1.

2.3.2.1 *[Figure]* Effects of environments of distilled water and solutions of sodium chloride on fatigue life of bar at room temperature.

The alloy has excellent resistance to stress corrosion and to pitting and crevice corrosion in environments containing hydrogen sulfide (Ref. 82). Inconel 718 is susceptible to stress corrosion when exposed to the hydrazine family of fuels (Ref. 18).

2.3.3 Hydrogen Effects. Hydrogen can have a deleterious effect on the mechanical properties of Inconel 718. Hydrogen can be absorbed by exposure to the gas at elevated temperatures or by cathodic charging. These two processes introduce measurable amounts of hydrogen internally which diffuse outwardly very slowly at room temperature. Exposure to hydrogen at room temperature does not result in absorption but can exert a damaging effect through adsorption on freshly exposed surfaces such as fatigue cracks. This latter effect is frequently called hydrogen environment embrittlement (HEE) and is of particular importance for hydrogen fueled rockets and for space power battery systems.

Temperature and Pressure Induced Absorption: The effect of absorbed hydrogen on tensile properties was investigated for annealed cold rolled (20 and 35 percent reductions) and cold rolled plus solution treated and aged sheet. Specimens were subjected to continuous or cyclic exposure to hydrogen at 15 psi for 100 or 1000 hours at temperatures between 800 and 1400F. The contents of absorbed hydrogen varied from four to six ppm with no clear trend depending on the exposure conditions. For unexposed specimens, the baseline values were two to three ppm. Hydrogen content had no apparent effect on the tensile strength. However, substantial embrittlement was revealed by loss of elongation (see Figures 2.3.3.1 and 2.3.3.3) for the annealed plus cold worked condition. These losses were only minor for the solution treated plus aged condition (see Figures 2.3.3.2 and 2.3.3.4). The embrittlement increased with increasing exposure temperature but was not clearly different for exposures of 100 or 1000 hours. The effects of cyclic exposures were not significantly different from continuous exposures. No microstructural features could be associated with the hydrogen embrittlement. Post hydrogen exposure for three hours at 1200F in air or vacuum resulted in outgassing which restored from 75 to 80 percent of the unexposed elongation values. One month exposure in air at room temperature did not restore the initial properties (Ref. 38).

2.3.3.1 *[Figure]* Effect of elevated temperature exposure to 15 psi hydrogen on room temperature tensile elongation of annealed sheet.

2.3.3.2 *[Figure]* Effect of elevated temperature exposure to 15 psi hydrogen on room temperature tensile elongation of solution treated and aged sheet.

2.3.3.3 *[Figure]* Effect of elevated temperature exposure to 15 psi hydrogen on room temperature tensile elongation of annealed and cold rolled sheet.

2.3.3.4 *[Figure]* Effect of elevated temperature exposure to 15 psi hydrogen on room temperature tensile elongation of cold rolled and solution treated and aged sheet.

More recent data showed the effects of elevated temperature exposure to hydrogen at five ksi on the tensile properties of sheet tensile tested subsequent to exposure in five ksi helium or five ksi hydrogen. The results (see Table 2.3.3.5) show no clear effect on the tensile and yield strengths but substantial reductions in the ductility values for absorbed hydrogen contents between 47 and 55 ppm. These reductions are essentially the same for tests in helium or in hydrogen.

2.3.3.5 *[Table]* Effect of elevated temperature exposure to high pressure hydrogen on the tensile properties of sheet in 5000 psi helium or 5000 psi hydrogen.

In another investigation, unwelded and GTA welded solution treated and aged center cracked tensile specimens were exposed to 1000 psi hydrogen at elevated temperature. The welded specimens had the crack tip located at the weld edge. The absorbed hydrogen contents were between two and 30 ppm. Crack growth resistance curves (see Figure 2.3.3.6) were unaffected by the absorbed hydrogen. However, the hydrogen contents between 18 and 30 ppm resulted in substantial reduction in the critical stress intensity for unstable fracture (see Table 2.3.3.7). It should be kept in mind that these values will depend on specimen size and configuration.

2.3.3.6 *[Figure]* Effect of hydrogen content on crack growth resistance curves for sheet.

2.3.3.7 *[Table]* Effect of hydrogen on critical stress intensity for unstable crack growth of sheet at room temperature.

Induced Absorption by Cathodic Charging: Solution treated and aged sheet tensile specimens having saw cut notches were cathodically charged with hydrogen resulting in absorbed hydrogen contents up to 50 ppm. In slow displacement tests (see Figure 2.3.3.8), the room temperature notch tensile strength decreased substantially with increasing hydrogen content, being about 57 percent of the uncharged value at 50 ppm. Hydrogen reduces the threshold stress intensity for subcritical crack growth (see Figure 2.3.3.9). The effect is substantial at 10 ppm hydrogen for all test temperatures and increases with increasing hydrogen contents to about 20 ppm and then appears to level off. At temperatures between 122 and 212F, the damping effect of absorbed hydrogen does not appear to be temperature sensitive.

2.3.3.8 *[Figure]* Effects of cathodically charged hydrogen on room temperature notched tensile strength.

2.3.3.9 *[Figure]* Effects of cathodically charged hydrogen on the threshold stress intensity for subcritical crack growth.

Hydrogen Environment Embrittlement (HEE): Exposure of Inconel 718 to extreme hydrogen pressures (up to 8000 psi) over a wide range of temperatures occurs in high performance hydrogen fueled rocket engines (e.g., the Space Shuttle main engine). The damaging effect of hydrogen, highly temperature and pressure dependent, is revealed by losses in smooth bar ductility. There is little or no effect on the tensile stress-strain curves (see Figure 2.3.3.10) at low strains. However, hydrogen promotes crack formation as the plastic strains increase. These cracks drastically reduce the tensile ductility (see Figure 2.3.3.11) with the largest effects being observed between zero and 400F; this can in turn reduce the ultimate strength (see Figure 2.3.3.12 and Table 2.3.3.15). The smooth bar fatigue strength (see Figure 2.3.3.13) is reduced substantially by high pressure hydrogen for test temperatures of 80 and 1200F and probably at temperatures between these extremes.

2.3.3.10 *[Figure]* Tensile stress-strain curves for plate at various temperatures in atmospheres of hydrogen at 5000 psi.

2.3.3.11 *[Figure]* Effect of temperature on the tensile ductility in hydrogen at 7500 psi pressure to that in air at atmospheric pressure for annealed plate.

2.3.3.12 *[Figure]* Effect of elevated temperature on tensile properties of annealed and aged plate in atmospheres of helium and hydrogen at 5000 psi.

2.3.3.13 *[Figure]* Fatigue life of smooth bar in two heat-treated conditions in environments of high pressure hydrogen and helium at two temperatures.

Static notched bar tensile specimens have been used frequently to assess HEE because their strength is very sensitive to the embrittling effects of high pressure hydrogen. These tests generally employed specimens with notches of about one mil radius giving a K_t of eight. The ratio of notch strength in hydrogen to that in helium has been used as a measure of HEE. According to the results from such tests (see Figure 2.3.3.14), the embrittlement increases linearly with the reciprocal square root of the hydrogen pressure. The HEE seems to vary widely with the heat and the heat treatment of the alloy. The reasons for these metallurgical effects have not been established.

2.3.3.14 *[Figure]* Hydrogen embrittlement as a function of hydrogen pressure for a mixture of heats and heat treatments.

2.3.3.15 *[Table]* Comparison of room-temperature tensile and notched-tensile properties of bar in atmospheres of helium and hydrogen at 10,000 psi.

Of special concern is the accelerating influence of hydrogen on the crack growth rates. In 10,000 psi hydrogen the crack growth rates increase with decreasing frequency with the largest effects being observed at very low frequencies (see Figure 2.3.3.16). Even at very low pressures (see Figure 2.3.3.17), the accelerating effects of low frequencies are present. The stress intensities for crack arrest decrease with increase in hydrogen pressure (see Figure 2.3.3.18) with a rough estimate of K_{iscc} being about 30 ksi$\sqrt{in}$. A K_{th} value of about 5 ksi$\sqrt{in}$. has been reported (Ref. 162) for tests in pure hydrogen at R of 0.4.

2.3.3.16 *[Figure]* Crack growth rates as a function of cyclic frequency for a forging.

2.3.3.17 *[Figure]* Crack growth rates at low cyclic frequencies for a forging in helium and low pressure hydrogen.

2.3.3.18 *[Figure]* Stress intensity at crack arrest for a forging as function of hydrogen pressure.

Protection Against HEE: Inhibition of electrolytic charging can be achieved by modification of the surface to produce a diffusion barrier (Ref. 165). In the case of HEE, small amounts of oxygen are effective in reducing the damaging effects of hydrogen. However, the concentrations required have not been well established. The inhibiting effects of oxygen are of special interest to the designer of Inconel 718 pressure vessels for the Ni-H_2 batteries used in electric power systems for satellites and for space stations. These thin-walled vessels (23 to 40 mils thick) contain un-heat-treated Inconel 718 highly constrained closure welds which are difficult to produce without microcracks. The batteries contain hydrogen at about 1000 psi plus KOH and water vapor. Pressure cycle frequencies can be as low as 16 per day and lives of many years are expected. Oxygen is produced during charging and discharging of the batteries but is not present on open circuit and is reduced by recombination with hydrogen to form water vapor. One investigator (Ref. 163) concluded from measurements on a cell used in the Hubble spacecraft that an oxygen content from 80 to 100 ppm characterizes the cell environment during normal operation. Recent studies have attempted to determine the influence of the cell environment on the crack growth rates of Inconel 718 in the solution annealed and aged condition. Water vapor plus KOH (see Figure 2.3.3.19) reduces the crack growth rates in an otherwise pure hydrogen atmosphere. Another investigation (Ref. 164) attempted to assess the influence of adding small amounts of oxygen to the KOH. Unfortunately these results are clouded by uncertainties concerning the calibrations of the trace oxygen analyzer. However, the beneficial effects of KOH alone on the crack growth rates in pure hydrogen were reported. While these preliminary results appear encouraging, considerable additional work is necessary to establish their significance in actual battery service.

2.3.3.19 *[Figure]* Fatigue crack growth rates of solution treated and aged sheet in air, pure hydrogen and in a simulated Ni-H_2 battery environment without oxygen.

In some critical applications (not practical for the present design of the Ni-H_2 batteries), it is possible to protect Inconel 718 from hydrogen by the use of coatings. Copper and gold have been shown to be effective in preventing the loss of tensile ductility in static tests in 1200 psi hydrogen. However, in low cycle fatigue, the protective effect of copper is eventually lost because the copper cracks before Inconel 718 in the solution treated and aged condition (Ref. 162).

2.3.4 Oxidation. Inconel 718 has good resistance to oxidation at temperatures throughout its normal operating range, but oxidizes and scales appreciably at higher temperatures (Ref. 36).

During oxidation in air at 1472 to 1832F, the initial oxide film consists of Cr_2O_3 with two nickel spinels, $NiCr_2O_4$ and $NiFe_{2-x}Cr_xO_4$ ($0<x<1$). Iron is present as Fe_2O_3 and mixed oxides. Exposure at 1832F produces a thick Cr_2O_3 film (Ref. 124).

Exposure of thin (0.010-inch thick) sheet to low pressure air (eight torr), such as encountered on reentry, results in very low thickness loss for times up to 5000 hours at 1400F but much greater thickness loss at 1800F, as shown in Figure 2.3.4.1. Tensile ductility, however, is degraded by short term exposures at 1400F, as shown in Figure 2.3.4.2.

2.3.4.1 *[Figure]* Loss of thickness due to oxidation of sheet continuously exposed to still air at a pressure of eight torr (0.01 atmosphere) at both 1800 and 1400F.

2.3.4.2 *[Figure]* Room temperature tensile properties of annealed sheet after exposures to elevated temperatures at eight torr (0.01 atmosphere) air pressure both with and without stress.

As a result of diffusion of oxygen into the grain boundaries, creep crack growth and fatigue crack growth rates for Inconel 718 at elevated temperatures, as well as for other superalloys, are faster in air than in inert environments (see Figures 3.4.20, 3.4.21, and 3.5.3.3). Under fatigue conditions, this detrimental effect of air environments becomes more pronounced with decreasing cycle frequency (see Figures 3.5.3.3 and 3.5.3.9).

Inconel 718 has good resistance to hot corrosion (sulfidation) within its normal service-temperature range. At 1100F, the hot corrosion resistance of Inconel 718 is slightly inferior to that of Inconel 601 but better than that of Inconel 617, as shown in Figure 2.3.4.3. The superiority of the Inconel 601 is attributed to its higher chromium content, and the inferiority of Inconel 617 is believed to be a result of its greater molybdenum content (Ref. 79).

2.3.4.3 *[Figure]* Maximum penetration by hot corrosion of Inconel 718 and two other nickel-base superalloys exposed for various times at 1100F to air and to a fused salt mixture of potassium sulfate and sodium sulfate.

The resistance to frictional ignition in oxygen is an important consideration in some aerospace applications. The data in Table 2.3.4.4 indicate that Inconel 718 has intermediate resistance to frictional ignition in comparison with a number of other aerospace alloys. This listing also indicates that resistance to frictional

ignition among the various alloys generally increases with increasing nickel content (Ref. 125).

2.3.4.4 *[Table]* Frictional ignition of Inconel 718 and other aerospace alloys.

The flammability (promoted combustibility) of Inconel 718 in high pressure oxygen is comparable to those of Waspaloy and stainless steels, as shown in Table 2.3.4.5 (Ref. 126).

2.3.4.5 *[Table]* Relative rankings of selected aerospace alloys for promoted combustion in high-pressure gaseous oxygen.

2.4 Nuclear Environments

2.4.1 *[Figure]* Effects of long-time elevated temperature exposures to inert environments and to various neutron-fluence levels on tensile properties determined at exposure temperatures.

3. Mechanical Properties

3.1 Specified Mechanical Properties

3.1.1 *[Table]* AMS specified room-temperature properties.

3.1.2 *[Table]* AMS specified elevated-temperature properties.

3.2 Mechanical Properties at Room Temperature

3.2.1 Tension Stress-strain Diagrams and Tensile Properties.

Stress-strain curves, shown in Figure 3.2.1.1, indicate that the room temperature flow stresses are higher for alloy solution annealed at 1750 or 1850F and aged than for alloy solution annealed at 1950 or 2050F and aged.

3.2.1.1 *[Figure]* Stress-strain curves for sheet in four heat-treated conditions.

The effects of heat treatment and test orientation on the tensile properties of several product forms are given in Tables 3.2.1.2 through 3.2.1.6. Lowest strengths and highest ductilities are exhibited in the solution annealed condition, seen in Tables 3.2.1.2 and 3.2.1.3. Double aging at 1325/1150F or 1400/1200F increases the ultimate strength by about 50 percent and significantly reduces the ductility as compared to the solution annealed only condition, shown in Tables 3.2.1.3 through 3.2.1.5. Highest strengths are observed for alloy directly aged after hot rolling (no solution anneal), shown in Table 3.2.1.6. Rounds and plate are slightly weaker and less ductile in the transverse direction than in the longitudinal direction for both solution annealed and solution annealed and aged conditions, seen in Tables 3.2.1.2 through 3.2.1.4.

3.2.1.2 *[Table]* Tensile properties in longitudinal and transverse orientations of hot-rolled, annealed rounds of two sizes.

3.2.1.3 *[Table]* Effects of heat treatment on tensile properties of plate at room temperature.

3.2.1.4 *[Table]* Tensile properties in longitudinal and transverse orientations of hot-rolled rounds in annealed-and-aged conditions.

3.2.1.5 *[Table]* Tensile properties of annealed-and-aged sheet at room temperature.

3.2.1.6 *[Table]* Tensile properties of round and flat bars in the hot-rolled-plus-aged condition.

Prestraining of annealed alloy up to 50 percent produces up to 67 percent increase in ultimate strength and substantial decrease in ductility, shown in Figure 3.2.1.7. Aging at 1325F after prestraining further increases the strength and also improves ductility at higher prestrain levels, as seen in Figure 3.2.1.8. Variation in prestrain temperatures between 70 and -423F has an inconsistent effect on subsequent tensile properties. Similar effects are observed for cold rolling with and without a subsequent 1325/1150F aging treatment, shown in Figure 3.2.1.9. Similar effects are also observed for cold drawing to reductions of 20 to 50 percent, shown in Figures 3.2.1.10 through 3.2.1.12. Higher strengths are obtained by subsequently double aging at 1275/1150F than at 1325/1150F or 1450/1150F.

3.2.1.7 *[Figure]* Effects of prestraining at room and low temperatures on the room-temperature tensile properties of annealed sheet.

3.2.1.8 *[Figure]* Effects of prestraining at room and low temperatures followed by aging at 1325F on the room-temperature tensile properties of annealed-and-aged sheet.

3.2.1.9 *[Figure]* Effects of cold rolling and aging on tensile properties of sheet at room temperature.

3.2.1.10 *[Figure]* Effects of cold drawing and various subsequent aging treatments on tensile strength of bar at room temperature.

3.2.1.11 *[Figure]* Effects of cold drawing and various subsequent aging treatments on yield strength of bar at room temperature.

3.2.1.12 *[Figure]* Effects of cold drawing and various subsequent aging treatments on elongation of bar at room temperature.

Long time exposure of fully heat treated alloy at 1000 or 1100F moderately improves subsequent room temperature tensile properties. However, similar exposures at 1200 or 1300F result in decreased strength and ductility, possibly due to overaging, as shown in Figure 3.2.1.13.

3.2.1.13 *[Figure]* Room-temperature tensile properties after long-time exposures to temperatures from 1000 to 1300F.

Heat treatment at 2175F improves the tensile properties of VIM/VAR cast alloy compared to the as-cast condition, as shown in Table 3.2.1.14. Further improvement is effected by the conventional double

aging treatment, but strengths and ductilities of the cast alloy remain lower than those of heat treated wrought alloy, shown in Tables 3.2.1.3 through 3.2.1.5. No orientation effect is apparent on the tensile properties of the cast alloy (Ref. 100).

3.2.1.14 *[Table]* Effects of heat treatment and orientation on tensile properties of cast alloy at room temperature.

3.2.2 Compression Stress-strain Diagrams and Compression Properties.

3.2.3 Impact.

3.2.3.1 *[Table]* Charpy V-Notch impact properties at room temperature of forged and hot-rolled rounds of various sizes in two heat-treated conditions.

3.2.4 Bending.

3.2.5 Torsion and Shear.

3.2.6 Bearing.

3.2.7 Stress Concentration.

3.2.7.1 Notch properties.

3.2.7.1.1 *[Figure]* Nominal tensile properties at room temperature of sheet with sharp scratches.

3.2.7.2 Fracture toughness.

(See Figure 3.3.7.2.1, Tables 4.3.1.14 and 4.3.1.15, and Section 3.3.7.2.)

3.2.8 Combined Loading.

3.3 Mechanical Properties at Various Temperatures

3.3.1 Tension Stress-strain Diagrams and Tensile Properties. Stress-strain curves for annealed and aged alloy at -423 to 1400F are shown in Figures 3.3.1.1 to 3.3.1.4.

3.3.1.1 *[Figure]* Tensile stress-strain curves at room and elevated temperatures for solution-treated-and-aged bar.

3.3.1.2 *[Figure]* Tensile stress-strain curves at room and elevated temperatures for specimens cut from roll-formed E and L shapes.

3.3.1.3 *[Figure]* Tensile stress-strain curves for sheet at room and low temperatures.

3.3.1.4 *[Figure]* Tensile stress-strain curves for bar at room and low temperatures.

The effects of test temperature on the tensile properties of annealed sheet are shown in Figure 3.3.1.5 and of annealed and double-aged sheet and bar in Figures 3.3.1.6 through 3.3.1.9. The fully heat treated alloy maintains a substantial strength advantage over the annealed-only alloy at temperatures up to at least 1500F. A ductility minimum exists at 1400F for both the annealed and annealed-plus-aged conditions.

3.3.1.5 *[Figure]* Effect of temperature up to 1600F on tensile properties of annealed sheet.

3.3.1.6 *[Figure]* Effects of low temperatures on the tensile properties of sheet in the annealed and annealed-and-aged conditions.

3.3.1.7 *[Figure]* Effects of temperatures from -320 to 1350F on tensile properties of sheet in two heat-treated conditions.

3.3.1.8 *[Figure]* Tensile properties of annealed-and-aged bar at temperatures from -320 to 1300F.

3.3.1.9 *[Figure]* Effect of elevated temperatures on tensile properties of annealed-and-aged bar.

Test orientation has little effect on the ultimate and yield strengths of forgings at room and cryogenic temperatures. Ductilities, however, are highest for longitudinal and substantially lower for the short transverse orientation, as shown in Figure 3.3.1.10. Solution annealing at 1800F and double-aging at 1325/1150F results in higher yield strengths than solution annealing at 1950F and double aging at 1400/1200F, as shown in Figures 3.3.1.10 and 3.3.1.11.

3.3.1.10 *[Figure]* Effects of low temperatures on tensile properties of forging in three principal orientations after two different heat treatments.

3.3.1.11 *[Figure]* Effects of low temperatures on short-transverse tensile properties of forging in two annealed-and-aged conditions.

Cold rolling of solution annealed alloy increases the strength and reduces ductility at -320F, as shown in Figure 3.3.1.12. Subsequent aging results in further substantial strength increases at room and cryogenic temperatures, as shown in Figures 3.3.1.12 and 3.3.1.13. These trends are similar to those at room temperature shown in Figures 3.2.1.7 through 3.2.1.12. Solution annealing and aging after a cold rolling reduction of 20 percent erases the effects of cold rolling. This material is not as strong as that which is direct aged after cold rolling, shown in Figure 3.3.1.14.

3.3.1.12 *[Figure]* Effects of cold rolling and aging on tensile properties of sheet at -320F.

3.3.1.13 *[Figure]* Tensile properties at 75 and -423F of sheet cold rolled various amounts prior to aging.

3.3.1.14 *[Figure]* Tensile properties at low and high temperatures of sheet cold-rolled and subsequently heat treated in two different manners.

Long time aging at 1000 to 1200F has no significant effect on subsequent tensile properties at 1200F. However, aging at 1300F reduces subsequent 1200F strength properties, as shown in Figure 3.3.1.15.

3.3.1.15 *[Figure]* Tensile properties of forging at 1200F after long-time exposure to temperatures from 1000 to 1300F.

The strength properties of heat treated castings at temperatures up to 1400F are less than those of wrought product, as seen by comparison of data in Figures 3.3.1.16 and 3.3.1.17 with those shown in Figures 3.3.1.6 through 3.3.1.10. Hot-isostatic-pressing of castings before heat treating improves tensile ductility but has little effect on strength at 75 and 1100F, shown in Figure 3.3.1.18.

3.3.1.16 *[Figure]* Effect of low temperatures on the tensile properties of annealed-and-aged castings.

3.3.1.17 *[Figure]* Effect of elevated temperatures on tensile properties of annealed-and-aged castings.

3.3.1.18 *[Table]* Effect of hot-isostatic-pressing (HIP) on tensile properties of precision castings at 75 and 1100F.

3.3.2 Compression Stress-strain Diagrams and Compression Properties (see Figure 4.1.1).

3.3.2.1 *[Figure]* Tensile and compressive strength properties of forged bars at high temperatures in the hot-working range.

3.3.3 Impact. Impact toughness is substantially greater in the solution annealed condition than after solution annealing and aging. Toughness is also greater in the longitudinal orientation than in the long transverse orientation and is higher after solution annealing at 1800F and double aging at 1325/1150F than after solution annealing at 1950F and double aging at 1400/1200F, as shown in Table 3.3.3.2 and Figure 3.3.3.3.

3.3.3.1 *[Table]* Impact properties of annealed-and-aged plate at room temperature and -320F.

3.3.3.2 *[Table]* Effects of heat treatment and low temperatures on the Charpy V-Notch impact properties of plate.

3.3.3.3 *[Figure]* Effects of low temperatures on longitudinal and transverse impact properties of forgings in two heat treated conditions.

3.3.4 Bending.

3.3.5 Torsion and Shear.

3.3.6 Bearing.

3.3.7 Stress Concentration.

3.3.7.1 Notch properties. For several notch tests Inconel 718 sheet is notch-sensitive at temperatures from cryogenic to 1000F, as shown in Figures 3.3.7.1.1 and 3.3.7.1.2. The alloy is less notch-sensitive in the solution annealed condition than in the solution annealed and aged condition, shown in Figure 3.3.7.1.3. The tensile strengths and ductility are reduced with increasing scratch depth, as shown in Figure 3.3.7.1.4. Forged alloy is not notch-sensitive (for the notch test used) in the short transverse direction, as indicated in Figure 3.3.7.1.5.

3.3.7.1.1 *[Figure]* Comparison of tensile strength and notch tensile strength of sheet at various temperatures after cold rolling and subsequent heat treatment in two different manners.

3.3.7.1.2 *[Figure]* Comparison of tensile strength and notch tensile strength of annealed-and-aged sheet at low temperatures.

3.3.7.1.3 *[Figure]* Effect of low temperatures on notch strength ratio (K_t = 10) of sheet in two heat-treated conditions.

3.3.7.1.4 *[Figure]* Nominal tensile properties at -320F of sheet with sharp scratches.

3.3.7.1.5 *[Figure]* Comparison of tensile strength and notch tensile strength of annealed-and-aged forging at low temperatures.

3.3.7.2 Fracture toughness. The high fracture toughness of Inconel 718 at elevated temperatures usually precludes the use of conventional linear-elastic K_{Ic} fracture mechanics techniques. However, a fracture toughness K_{Jc} can be calculated by a linear elastic conversion of J_{Ic} determined from the elastic-plastic approach. Data for K_{Jc} presented in Figure 3.3.7.2.1 indicate that the J_{Ic} fracture toughness at 75 to 1000F can be increased considerably by use of the modified heat treatment (MHT), which includes solution annealing at 2000F, rather than at the conventional heat treatment (CHT), which includes solution annealing at 1750F. The rather wide range of toughness values in Figure 3.3.7.2.1 reflects microstructural differences resulting from variations in thermal-mechanical history among the different shapes tested. This MHT is thus of interest for structural components where fracture resistance is a primary concern. During the early stages of plastic straining, primary microvoids nucleate at broken MC-type carbides. Secondary microvoids nucleated at coarse delta-phase particles promote crack extension in the CHT materials. The higher solution temperature in the MHT dissolves the delta precipitate particles and enhances fracture resistance by supressing secondary microvoid nucleation (Ref. 88).

3.3.7.2.1 *[Figure]* Effects of heat treatment on equivalent fracture toughness at temperatures to 1000F.

3.3.8 Combined Loading.

3.4 Creep and Creep Rupture Properties

Representative data for times-to-given-strains and for rupture lives of heat treated Inconel 718 sheet and bar at 1000 to 1400F are presented in Figures 3.4.1 through 3.4.10. Strengths are comparable for sheet in both longitudinal and transverse orientations, as seen by comparison of sheet data in Figures 3.4.6 through 3.4.8, and 3.4.10 with data for bar in Figures 3.4.1 and 3.4.3 through 3.4.5.

3.4.1 *[Figure]* Creep rupture curves for bar in the temperature range 1000 to 1300F.

3.4.2 *[Figure]* Creep rupture curves for sheet at 1000 and 1200F.

3.4.3 *[Figure]* Rupture life and steady creep rate of bar as functions of stress in the temperature range 1100 to 1300F.

3.4.4 *[Figure]* Isochronous stress-strain curves at 1100, 1200, and 1300F for time range 1 to 1000 hours.

3.4.5 *[Figure]* Stresses required to cause various amounts of creep and rupture in 100, 1000, and 10,000 hours at temperatures from 1100 to 1300F.

3.4.6 *[Figure]* Time to various amounts of creep strain as a function of stress for sheet in longitudinal orientation at 1000F.

3.4.7 *[Figure]* Time to various amounts of creep strain as a function of stress for sheet in longitudinal orientation at 1400F.

3.4.8 *[Figure]* Time to various amounts of creep strain as a function of stress for sheet in transverse orientation at 1000F.

3.4.9 *[Figure]* Time to various amounts of creep strain as a function of stress for sheet in transverse orientation at 1200F.

3.4.10 *[Figure]* Time to various amounts of creep strain as a function of stress for sheet in transverse orientation at 1400F

Imposed stresses relax only about 10 percent after 10,000 hours at 1100F, but relax more rapidly at 1200 and 1300F, as shown in Figure 3.4.11.

3.4.11 *[Figure]* Stress relaxation of bar loaded in tension to 60 ksi at various temperatures and held at constant strain for times up to 10,000 hours.

Rupture strength is notch-sensitive at 1000 to 1350F. The creep rupture strength decreases with increasing notch acuity for sheet, as shown in Figures 3.4.12 through 3.4.14. Notch sensitivity is similar for both longitudinal and transverse orientations, as shown in Figures 3.4.15 through 3.4.17. Although the variables that influence this condition are not thoroughly understood, it is believed that high finishing temperatures during hot work are a contributing factor (see Figure 4.1.2). For minimum notch sensitivity of this type, maximum finishing temperatures of 1650 to 1750F and maximum annealing temperatures of 1750F have been suggested (Refs. 2, 33, 78).

3.4.12 *[Figure]* Effects of notch acuity on the creep rupture properties of sheet at 1000 and 1200F.

3.4.13 *[Figure]* Creep rupture curves for smooth and notched sheet specimens at 1300F.

3.4.14 *[Figure]* Creep rupture curves at 1000 and 1200F for smooth and sharp-notched sheet specimens in the annealed-and-aged condition.

3.4.15 *[Figure]* Effects of notch acuity on the notch creep rupture properties of sheet at 1000F.

3.4.16 *[Figure]* Creep rupture curves at 1000 and 1200F for smooth and sharp-notched specimens in the cold-worked-and-aged condition.

3.4.17 *[Figure]* Creep rupture curves for sharp-notched sheet at 800 to 1200F.

Creep crack growth rates in air tend to increase with increasing temperature, as shown in Figure 3.4.18. Creep crack growth rates vary with heat treatment as shown in Figure 3.4.19, being lowest for the special heat treatment involving solution annealing at 1700F and aging at 1350F. Oxidation causes a significant acceleration in creep crack growth rates during testing in air. Crack growth rates in air are up to 100-fold greater than those in helium or vacuum at the same temperatures, as shown in Figures 3.4.20 and 3.4.21.

3.4.18 *[Figure]* Creep crack growth rates of plate at 1000, 1200, and 1400F in air.

3.4.19 *[Figure]* Effects of various heat treatments on creep crack growth rate at 1200F in air.

3.4.20 *[Figure]* Creep crack growth rates of plate at 1200F in environments of air and helium.

3.4.21 *[Figure]* Creep crack growth rates of plate at 1000F and 1200F in air and vacuum.

Steady creep rates for Inconel 718, shown in Figure 3.4.22, exhibit log-log dependencies on the applied stress ranging from nine to 15. These high apparent stress dependencies suggest that a back stress associated with the second phase precipitates and the defect structure within the alloy is operative and that the effective creep stress is less than the applied stress (Ref. 128). High temperature creep deformation is thus controlled by an effective stress which is equal to the applied stress minus the back stress. This relationship is expressed by:

$$\dot{e}_s = A(S_a - S_o)^{n_e} \exp(-Q_c/RT)$$

where $\dot{e}_s$ = steady creep rate
A = creep rate proportionality constant

S_a = applied stress
S_o = back stress
n_e = effective stress dependency of creep
Q_c = effective activation energy for creep
R = gas constant
T = absolute temperature

Power law creep is observed (n_e = 3 to 6) at 1112 and 1157F at stresses above 108 ksi and the back stress is proportional to the applied stress. The ratio of back stress to applied stress is about 0.25. In the low stress region, below 104 ksi, the diffusional creep process controls deformation (n_e = 1) and a threshold stress exists which is independent of applied stress. The threshold stress varies with temperature as shown in Figure 3.4.23. The threshold stress also varies with gamma-double-prime precipitate size and exhibits a maximum value at a particle size of slightly greater than 200 angstroms at 1112F. The resultant steady creep rates concurrently exhibit a minimum at this particle size, as shown in Figure 3.4.24 (Refs. 129, 130).

3.4.22 *[Figure]* Steady creep rate behavior at 1076 to 1238F in argon.

3.4.23 *[Figure]* Effect of temperature on threshold stress for diffusional creep in argon.

3.4.24 *[Figure]* Effects of gamma-double-prime particle size on steady creep rates at 1112F in argon.

3.5 Fatigue Properties

3.5.1 Conventional High-cycle Fatigue.

Representative high-cycle fatigue data for heat treated sheet and bar at -423 to 1200F are shown in Figures 3.5.1.1 through 3.5.1.3.

3.5.1.1 *[Figure]* Bending fatigue strength at room and low temperatures of sheet with 11 RMS surface finish.

3.5.1.2 *[Figure]* Bending fatigue strength at room and low temperatures of sheet with 64 RMS surface finish.

3.5.1.3 *[Figure]* Axial fatigue strength at room and low temperatures of sheet with 32 RMS surface finish.

The fatigue strength is affected by microstructure and is higher for hot-rolled-and-aged and for fully heat treated alloy than for material which has been solution annealed only, as shown in Figure 3.5.1.4 and Table 3.5.1.5. Grain size, in particular, has a strong effect on fatigue strength. Small grain size promotes higher fatigue strength, as shown in Figure 3.5.1.6.

3.5.1.4 *[Figure]* Fatigue strength at 10^6, 10^7, and 10^8 cycles for hot-rolled plate in several heat-treated conditions.

3.5.1.5 *[Table]* Comparison of the effects of aging after annealing on tensile properties and fatigue strength of forgings at room temperature.

3.5.1.6 *[Figure]* Effect of grain size on fatigue strength of plate at 10^8 cycles.

The high-cycle fatigue strength is notch-sensitive at temperatures from -423 to 1400F, as shown by the low temperature data in Figures 3.5.1.7 and 3.5.1.8 and the room and elevated temperature stress-range diagrams in Figures 3.5.1.9 through 3.5.1.12. Both solution annealed and fully heat treated alloy are notch-sensitive.

3.5.1.7 *[Figure]* Axial fatigue strength at room and low temperatures of both smooth and notched specimens of annealed-and-aged sheet.

3.5.1.8 *[Figure]* Axial fatigue strength at room and low temperatures of both smooth and notched specimens of annealed sheet.

3.5.1.9 *[Figure]* Stress-range diagram for notched and smooth sheet at 75F.

3.5.1.10 *[Figure]* Stress-range diagram for notched and smooth sheet at 1000F.

3.5.1.11 *[Figure]* Stress-range diagram for notched and smooth sheet at 1200F.

3.5.1.12 *[Figure]* Stress-range diagram for notched and smooth sheet at 1400F.

3.5.2 Low-cycle Fatigue.

Low-cycle fatigue data in air at room temperature are shown in Figure 3.5.2.1. The fatigue strength is higher at 1200F for alloy solution annealed at 1750F and double aged at 1325/1150F than for alloy solution annealed at 1900F and double aged at 1400/1200F, as shown in Figure 3.5.2.2. Tensile and/or compression holds reduce the fatigue life at 1200F, shown in Figure 3.5.2.3.

3.5.2.1 *[Figure]* Fatigue life of plate as a function of total cyclic strain range at room temperature.

3.5.2.2 *[Figure]* Fatigue life of plate in two heat-treated conditions as a function of total cyclic strain range at 1200F.

3.5.2.3 *[Figure]* Effects of holding at peak cyclic compressive and tensile strains on fatigue life as a function of total cyclic strain range at 1200F.

3.5.3 Fatigue Crack Propagation.

Fatigue crack growth rates (FCGRs) are essentially unchanged from liquid nitrogen temperature to room temperature for rates between about 10^{-5} and 10^{-4} inch/cycle, as shown in Figure 3.5.3.1. At higher temperatures in air, the rates increase with increasing temperature. This behavior, shown in Figure 3.5.3.2, is attributed primarily to oxidation effects. The FCGRs at room temperature in vacuum and at 1200F in helium are less than those in air, reflecting the deleterious effects of air oxidation at both temperatures, shown in Figures 3.5.3.3 and 3.5.3.4. This effect of air is increased by decreasing cyclic frequency. Similar behavior is also shown in creep crack propagation,

shown earlier in Figures 3.4.20 and 3.4.21 (Refs. 131-134).

3.5.3.1 *[Figure]* Fatigue crack growth rate for plate tested in air and in liquid nitrogen.

3.5.3.2 *[Figure]* Effects of elevated temperatures on fatigue crack growth rate of plate in air.

3.5.3.3 *[Figure]* Fatigue crack growth rates of plate at 1200F in environments of air and helium at two rates of cycling.

3.5.3.4 *[Figure]* Effects of grain size and test environment on fatigue crack growth behavior at 68F.

The effects of temperature on FCGRs in vacuum are dependent on grain size. Large-grained material exhibits an increase in FCGRs with increase in temperature from 68 to 1202F, as shown in Figure 3.5.3.5. In contrast, the FCGRs for fine-grained alloy are essentially unchanged over the same temperature range, seen in Figure 3.5.3.6 (Ref. 134). These differences in behavior may reflect the increasing importance of time-dependent deformation and of intergranular fracture modes in larger-grained material with increasing temperature.

3.5.3.5 *[Figure]* Effect of temperature on fatigue crack growth behavior of large-grained alloy in vacuum.

3.5.3.6 *[Figure]* Effect of temperature on fatigue crack growth behavior of fine-grained alloy in vacuum.

FCGRs exhibit three general ranges of frequency dependence, namely time, mixed, and cyclic dependence. Two of these ranges are illustrated in Figure 3.5.3.7. At frequencies below about $4x10^{-4}$ cpm at 1200F, FCGRs are fully time dependent and fracture is transgranular. At higher frequencies, from $4x10^{-4}$ to at least one cpm, FCGRs exhibit mixed time and cycle dependencies, along with mixed transgranular and intergranular fractures (Ref. 135). Behavior at higher frequencies at 1000F is shown in Figure 3.5.3.8. At frequencies from four to 400 cpm, crack growth is cycle-dependent and the frequency effect is small. Reduction of the frequency to 0.0833 cpm effects an increase in FCGRs, indicative of the change to mixed mode behavior. Similar but weaker frequency effects in helium at 1200F, shown in Figure 3.5.3.9, suggest that a non-environmental component such as creep is also present (Refs. 131, 133).

3.5.3.7 *[Figure]* Effect of cyclic frequency on fatigue crack growth behavior in air at 1200F.

3.5.3.8 *[Figure]* Fatigue crack growth rates in air at 1000F and cyclic frequencies from 0.0833 to 400 cpm.

3.5.3.9 *[Figure]* Effect of cycle frequency on fatigue crack growth rate at $\Delta K = 36.4$ ksi$\sqrt{in}$ and 1200F in air and helium.

The effects of heat treatment on the FCGRs are shown in Figure 3.5.3.10. Higher FCGRs are observed for material given the conventional heat treatment (CHT) than for material with a modified heat treatment (MHT). The higher solution annealing temperature of 2000F for the MHT is sufficient to resolution the Laves and delta phases, both of which are known to increase FCGRs. In contrast, these two phases are present after the CHT solution anneal at 1750F (Ref. 131). Similarly, alloy heat solution annealed at 1800F and double aged at 1325/1150F has higher FCGRs at 75 and -320F than alloy solution annealed at 1950F and double aged at 1325/1150F, as shown in Figure 3.5.3.11.

3.5.3.10 *[Figure]* Effects of heat treatment on fatigue crack growth rates of plate at 800 and 1000F in air.

3.5.3.11 *[Figure]* Fatigue crack growth rate of forging billets at room temperature and -320F in two conditions of heat treatment.

Heat treatment also affects FCGRs through grain size. As shown in Figure 3.5.3.12, the FCGRs of similarly heat treated lots from different producers at elevated temperatures under hold-time conditions are less for large-grained material than for fine-grained material. The lowest FCGRs are obtained with a "necklace" microstructure, consisting of large grains surrounded by necklaces of very small grains. Similar grain size effects on FCGRs have been noted under continuous cycling conditions (not shown); the lower rates exhibited in Figure 3.5.3.10 by MHT material may be due in part to the larger grain size of this material as compared to the CHT material (Ref. 131). The gamma-double-prime precipitate size also affects FCGRs, with the FCGRs being lower for coarse precipitate than for fine precipitate, regardless of grain size (Ref. 136).

3.5.3.12 *[Figure]* Effects of grain size on fatigue crack growth rates in air at 1000F.

The stress ratio (R) also significantly affects FCGRs. Although most laboratory tests are conducted with R values close to zero, service values of R are frequently much higher. The effects of varying stress ratios can be compensated for by expressing the stress intensity as an effective stress intensity which is calculated as:

$$K_{eff} = K_{max} (1-R)^m$$

where K_{eff} = effective stress intensity range
K_{max} = maximum applied stress intensity
K_{min} = minimum applied stress intensity
R = stress ratio = K_{min}/K_{max}
m = empirical exponent

The exponent "m" approximates 0.6 to 0.7 and decreases slightly with increasing temperature, as shown in Figure 3.5.3.13 (Ref. 131).

3.5.3.13 *[Figure]* Effect of temperature on stress ratio correlation exponent.

At elevated temperatures in air, the addition of a hold time at the maximum tensile portion of the loading cycle results in FCGRs that are faster than those for continuous cycling. This behavior is shown in Figures 3.5.3.14 and 3.5.3.15 (Ref. 131).

3.5.3.14 *[Figure]* Effects of various hold times at maximum cyclic tensile load on fatigue crack growth rate of plate at 1000F.

3.5.3.15 *[Figure]* Effects of various hold times at maximum cyclic tensile load on fatigue crack growth rate of plate at 1200F.

The fatigue crack growth behavior for loading spectra consisting of combinations of fatigue cycles and constant load hold-times can be estimated using the linear cumulative damage model when the hold-times are at maximum load. This model involves the simple summation of the individual contributions from cyclic crack growth and from constant load crack growth (Refs. 137, 156). However, actual service loading cycles are frequently more complex. Life prediction based on a linear summation of crack growth on a cycle-by-cycle basis is inadequate for those frequent situations where retardation or acceleration results from certain sequences of loading (Ref. 138).

The linear cumulative damage model can be useful in estimating the crack growth behavior under thermo-mechanical fatigue cycling. The model sums the separate contributions of cycle-dependent and time-dependent behavior, neglecting any interaction effects. The dominant mechanisms at the two extremes of the thermo-mechanical fatigue cycle are mechanical fatigue and environmentally-enhanced intergranular crack growth (Ref. 139)

Mechanistically, the FCGRs are governed by the nature of the crack tip fracture mode. This mode ranges from a cycle-dependent, transgranular process resulting in low crack growth rate to a time-dependent, intergranular process leading to accelerated crack growth. The cycle-dependent regime is independent of loading frequency and generally corresponds to low temperatures and low load ratios. In this regime, FCGRs are determined by the cyclic stress intensity only and are insensitive to alloy chemistry and microstructure (Ref. 140). The temperature at which the transition to time-dependent damage occurs is a function of the test frequency and has a high value for higher frequencies. In the intergranular damage regime, the FCGRs change with the reciprocal of frequency and are sensitive to hold-time durations imposed at maximum or minimum load levels. For hold-time conditions, the crack tip damage mode is found to depend on the frequency of the loading part of the test cycle. Furthermore, waveshape damage effects are sensitive to the combined frequency of the loading and unloading cycle segments in relation to the material transitional frequency (Ref. 133).

3.6 Elastic Properties

3.6.1 Poisson's Ratio.

3.6.1.1 *[Figure]* Poisson's ratio at temperatures from -450 to 2000F.

3.6.2 Modulus of Elasticity.

3.6.2.1 *[Figure]* Dynamic modulus of elasticity at temperatures from -450 to 1200F.

3.6.2.2 *[Figure]* Effects of elevated temperatures on static modulus of elasticity of plate in atmospheres of helium and hydrogen at 5000 psi.

3.6.3 Modulus of Rigidity.

3.6.3.1 *[Figure]* Dynamic modulus of rigidity at temperatures from -450 to 2000F.

3.6.4 Tangent Modulus.

3.6.5 Secant Modulus.

4. Fabrication

4.1 Forming

(See also Section 1.5.3.)

Because of its good strength at elevated temperatures, Inconel 718 has relatively high resistance to hot forming. The recommended hot-forming range is 2050F maximum to 1650F minimum (Ref. 106). Data from hot compression tests, summarized in Figure 4.1.1, are useful in selecting optimum forming temperature ranges. (Ref. 141). Heating above 2050F is undesireable because of the danger of severe grain coarsening (Refs. 1, 77).

4.1.1 *[Figure]* Effects of strain rate and temperature on compressive flow stress at a true strain of 0.3.

The hot forming temperature affects notch sensitivity under creep conditions, as shown in Figure 4.1.2. In order to minimize creep notch sensitivity, the metal should be worked uniformly with gradually decreasing temperature and with relatively light finishing reductions (20 to 25 percent for open-die work and 10 percent for closed-die work) in the 1750 to 1650F range. The work piece should be reheated if any part cools below 1650F before the desired amount of reduction has been achieved (Refs. 1, 77).

4.1.2 *[Figure]* Effects of hot forming temperature on smooth and notch creep rupture life and on creep ductility at 1200F and 100 ksi.

Annealed Inconel 718 can be cold formed by standard procedures used for steels and stainless steels. Since it work hardens rapidly (see Figures 1.6.2, 3.2.1.7 to 3.2.1.10, 3.3.1.12, and 3.3.1.13), frequent process anneals are necessary when large cold reductions are desired (Ref. 1).

The alloy should be clean and free of oil and paint when charged into the heating furnace to avoid sur-

face degradation. The furnace atmosphere should be slightly reducing and very low in sulfur content (Refs. 1, 77). For critical applications (e.g., Ni-H_2 batteries), annealing before cold work should be in vacuum or an inert atmosphere to avoid weld microcracking (Ref. 166).

Fine-grained Inconel 718 is capable of being formed superplastically. Alloy with a grain size of ASTM 10 or finer can be produced by appropriate hot and cold working of VIM/ESR-melted ingot. The true flow stresses under typical superplastic forming conditions are low, from about four to 10 ksi, as shown in Figure 4.1.3. This material is capable of elongations up to 760 percent during slow tensile straining at rates less than $4x10^{-3}$ min^{-1} at 1750F, as shown in Figure 4.1.4. Material formed under these conditions can be solution annealed and aged to restore tensile and creep properties to those of conventionally processed and heat treated alloy (Refs. 142, 143).

4.1.3 *[Figure]* Slow tensile deformation behavior of fine-grained alloy at 1750F.

4.1.4 *[Figure]* Slow tensile ductility of fine-grained alloy at 1750F.

4.2 Machining and Grinding

Like other nickel-base superalloys, the machinability of Inconel 718 is inferior to that of most steels including stainless steels. Nevertheless, with proper selection of tool materials, speeds, feeds, and coolants, it can be machined in either the annealed or age-hardened condition. The use of annealed material provides easier machining and longer tool life, but machining of the age-hardened alloy results in better chip action on chipbreaker tools and slightly better surface finish (Ref. 1).

4.3 Joining

4.3.1 Fusion Welding.

Inconel 718 has good weldability, particularly in conjunction with gas-tungsten-arc (GTA), plasma-arc, and electron-beam welding. Other processes such as shielded-metal-arc, gas-metal-arc, and submerged-arc welding may also be applicable in special cases (Ref. 86). Welding is generally carried out on annealed material, and appropriate post-weld heat treatment is employed to develop the desired properties. The age-hardened alloy is also weldable, but weld joints are relatively soft and weak until heat treated. A full post-weld anneal and aging treatment is often applied to obtain optimum properties in weldments, but in many instances comparable properties can be obtained with only post-weld aging if the base metal was originally in the annealed condition. Preheat is not required, but if the base metal is cold (below 35F), the area to be welded should be warmed to 60 to 70F to prevent moisture condensation, which can cause porosity in the weld metal (Refs. 1, 86).

The enhanced weldability characteristics of Inconel 718 are associated with sluggish precipitation kinetics of the primary strengthening phase, gamma-double-prime. This sluggish age hardening behavior results in a relatively high ductility heat-affected zone (HAZ) and fusion zone as welded, which permits relaxation of residual welding stresses and thereby improves the strain-age cracking resistance during post-weld heat treatment (Ref. 127).

However, when Inconel 718 is autogenously closure-welded under conditions of high restraint, HAZ microfissuring may be encountered (Ref. 144). This is a type of hot cracking which results from the formation of a liquid film at grain boundaries during the weld heating cycle, and the inability of this film to accomodate thermally induced stresses experienced during weld cooling. In the wrought alloy, grain boundary melting results from the constitutional liquation of Cb-rich MC carbides during rapid HAZ heating.

Significantly greater HAZ microfissuring susceptibility occurs in cast Inconel 718; this results from constitutional liquation of Laves phase that is residual from the original cast structure. The Laves phase liquation reaction initiates at temperatures below those required for liquation of Cb-rich carbides or Ti-rich carbonitrides, resulting in increased sensitivity to microfissuring in the cast alloy. Laves phase occurs only in the segregated cast structure and is not a concern in wrought alloy (Refs. 145-148).

The tendency to HAZ microfissuring can be minimized by using fine-grained base alloy (Ref. 149) and by avoiding excessively low weld heat input. Ductility and toughness can be restored to embrittled HAZ by post-weld annealing above 1950F, which results in complete dissolution of the Laves phase. Age hardening following the high temperature anneal results in a good combination of strength and toughness (see Section 1.5.4) (Refs. 31-33, 58, 77).

Microfissuring in the HAZ of fusion weldments is postulated to occur by sliding along grain boundaries containing a liquid phase. Both the detrimental liquid distribution on the grain boundary faces and the stress concentrations due to grain boundary sliding are accentuated by large grain size. The adverse effect of large grain size on microfissuring is illustrated in Figure 4.3.1.1 (Ref. 150).

4.3.1.1 *[Figure]* Effect of heat-affected-zone grain size and augmented strain on GTA weld hot cracking.

The microfissuring problem in cast Inconel 718 is due primarily to boron, followed by iron and columbium. Since these are required alloying elements, the problem appears unavoidable without a major change in alloy chemistry (Ref. 151). Increased levels of carbon and sulfur also promote microfissuring in cast alloy, as shown in Figure 4.3.1.2 (Ref. 146).

4.3.1.2 *[Figure]* Effects of sulfur and carbon contents and heat treatment on heat-affected-zone crack length in welded cast alloy.

In the as-welded condition, Inconel 718 exhibits substantially lower tensile strength but higher ductility than unwelded heat treated alloy from cryogenic temperature to 1200F, as shown in Figures 4.3.1.3 through 4.3.1.6. Heat treatments increase the strengths and decrease the ductility of weld metal to approximately the levels of the original heat treated base alloy, seen in Figures 4.3.1.3 through 4.3.1.7. Post-weld heat treatments which include solution annealing at 1950 or 2000F effect higher strength and ductility than those which include a solution anneal at 1750F, as indicated in Figures 4.3.1.4 through 4.3.1.6 and Table 4.3.1.8. Good tensile strength and ductility are also exhibited by weld metal in the aged-only condition, as seen in Tables 4.3.1.8 and 4.3.1.9 (with exception of poor ductility for 0.094-inch diameter wire in Table 4.3.1.8). The effects of varying aging temperature on weld joint tensile properties are shown in Figure 4.3.1.10.

4.3.1.3 *[Figure]* Effects of elevated temperatures on base plate and on Inconel 718 GTA deposit that formed butt joint between two segments of base plate.

4.3.1.4 *[Figure]* Effects of heat treatment on ultimate tensile strength of GTA weld metal at room temperature to 1200F.

4.3.1.5 *[Figure]* Effects of heat treatment on tensile yield strength of GTA weld metal at room temperature to 1200F.

4.3.1.6 *[Figure]* Effects of heat treatment on elongation of GTA weld metal at room temperature to 1200F.

4.3.1.7 *[Figure]* Effects of low and high temperatures on tensile properties of GTA butt-welded joints in 0.25-inch plate.

4.3.1.8 *[Table]* Tensile properties at room temperature of all-weld-metal deposited by the GTA technique and subjected to various post-weld treatments.

4.3.1.9 *[Table]* Tensile properties at room temperature of all-weld-metal and of butt-welded joint in 0.5-inch plate after two post-weld treatments.

4.3.1.10 *[Figure]* Effect of post-weld aging for 20 hours at various temperatures on room-temperature tensile properties of GTA butt joint in sheet.

Tensile properties of weld joints solution annealed at 1950F and double aged at 1400/1200F indicate absence of notch sensitivity at -423 to 1200F, as shown in Table 4.3.1.11.

4.3.1.11 *[Table]* Comparison at various temperatures of tensile and notch-tensile properties of parent metal and of butt-welded joints in forgings.

Shear strength is slightly higher than the tensile yield strength in the as-welded condition, as indicated in Table 4.3.1.12..

4.3.1.12 *[Table]* Tensile and shear properties of GTA weld deposit in the as-welded condition.

Post-weld solution annealing at 2000F or above alleviates the problems of low ductility and low toughness of weldments resulting from formation of brittle Laves phase in interdendritic regions during cooling after welding. As shown in Figure 4.3.1.13, the impact strength of weldments is almost quadrupled by annealing at 2000 or 2100F as compared with annealing at 1700 to 1900F (Ref. 87). However, aging after welding reduces the impact energy compared to the as-welded condition, as shown in Figure 4.3.1.14.

4.3.1.13 *[Figure]* Effect of post-weld annealing temperature on the impact strength of the heat-affected zones of GTA welds.

4.3.1.14 *[Table]* Effects of aging before and after welding on tensile and impact properties of GTA butt-welded joints in 1.0-inch plate.

In the as-welded condition, Inconel 718 has adequate toughness for most low strength applications. Modified heat treatment after welding results in higher fracture toughness than the CHT, shown in Table 4.3.1.15 (Refs. 89, 127).

4.3.1.15 *[Table]* Effects of heat treatment and test temperature on fracture toughness of welded bar.

Long-term thermal aging causes a lesser reduction in fracture toughness of GTA weld metal post-weld heat treated by the MHT procedure than in similar material heat treated by the CHT procedure. Aging of MHT weld metal for 5,000, 10,000, or 20,000 hours at 1051F results in a 25 percent reduction in J_{Ic} at 1000F compared to the unaged alloy (not shown). Similar exposures produce lower fracture toughness values and larger data scatter in CHT weld metal. Critical flaw sizes under comparable conditions are estimated to be approximately 15-fold greater for MHT material than for CHT material after aging. The lower fracture resistance in the CHT material results from aging-induced delta phase precipitation, which enhances microvoid initiation (Ref. 152). The fracture toughness of various types of fusion weldments in Inconel 718 is shown in Table 4.3.1.16.

4.3.1.16 *[Table]* Tensile strength and fracture toughness of base metal and weld metal at 75 and -320F for butt joints produced by various welding methods in plate.

Creep rupture life and ductility of welded and heat treated alloy are lower than those of parent metal, shown in Table 4.3.1.17.

4.3.1.17 *[Table]* Comparison of creep rupture properties of parent metal and weld joints in GTA butt-welded sheet.

The fatigue strength of unheat-treated GTA welds at room and cryogenic temperatures, shown in Figure 4.3.1.18, is substantially lower than those of fully heat treated alloy (see Figures 3.5.1.1 through 3.5.1.3) or annealed alloy (see Figure 3.5.1.9).

4.3.1.18 *[Figure]* Fatigue strength of GTA as-welded butt joints in annealed sheet at room and low temperatures.

Fatigue crack growth rates (FCGRs) in weldments are greater than those of the unwelded base alloy, as seen by comparison of data in Figure 4.3.1.19 with those shown earlier for unwelded alloy in Figure 3.5.3.1. FCGRs in weldments heat treated with the MHT (2000F solution anneal) are less than those given the CHT (1750F solution anneal), shown in Figure 4.3.1.20. The lower FCGRs for the MHT alloy is attributed to dissolution of Laves phase during the high temperature solution anneal. The presence of welding defects such as porosity or inclusions does not appear to affect the FCGRs of weldments at room temperature or 1000F (Ref. 131).

4.3.1.19 *[Figure]* Fatigue crack growth rates of Inconel 718 weld deposit in butt-welded joint produced by GTA method.

4.3.1.20 *[Figure]* Fatigue crack growth rate at 800 and 1000F of GTA weld deposit after conventional heat treatment and modified post-weld heat treatment.

Welding hot cracks do not adversely affect the fatigue behavior of cast Inconel 718 any more than the presence of a typical fatigue crack. In fact, hot cracks appear to be less detrimental to the fatigue behavior than similar fatigue cracks possibly due to an incubation period for the hot crack to begin crack growth. The crack growth rates for as cast and weld hot cracked alloy at room temperature are shown in Figure 4.3.1.21 (Ref. 148).

4.3.1.21 *[Figure]* Fatigue crack growth behavior at room temperature in the cast condition and after weld hot cracking.

4.3.2 Resistance Welding.

4.3.2.1 *[Figure]* Effects of temperatures up to 1400F on tensile properties of annealed-and-aged resistance-flash-welded joints in 5/8-inch bar.

4.3.3 Brazing. Brazed joints in Inconel 718 can be produced by means of silver-base, copper-base, and nickel-base brazing alloys. Since maximum service temperatures are limited to about 400 and 950F for the silver-base and copper-base joints, respectively, the nickel-base brazing alloys are the most widely used with Inconel 718. These alloys, which contain various amounts of chromium, boron, silicon, and iron in addition to nickel, when properly used, produce joints with strength and oxidation resistance approaching that of the base metal at temperatures up to 2000F, but with relatively low ductility. The Inconel 718 base metal is sometimes nickel plated prior to brazing to facilitate uniform wetting and fusion between the braze metal and base metal. Brazing is carried out preferably in vacuum, at temperatures between 1750 and 2075F depending upon the particular brazing alloy. Age hardening is carried out after the brazing operation, which also serves as the annealing phase of the heat treat cycle. An alloy containing 18 percent nickel and 82 percent gold can also be used to braze Inconel 718. Although it is not as strong as the nickel-chromium-boron-silicon brazing alloys, it provides better resistance to oxidation and stress corrosion, better ductility, and improved ability to fill relatively large clearances (Ref. 86).

4.3.3.1 *[Figure]* Effects of various annealing temperatures, representing brazing exposures, on tensile properties of annealed-and-aged alloy at various temperatures.

4.3.4 Explosive Welding.

4.3.4.1 *[Figure]* Effect of elevated temperatures on tensile properties of annealed-and-aged inertia welds and base metal.

4.4 Surface Treating

4.4.1 Cleaning. Removal of hot-work and heat-treat sealer is best done by immersion in one of the commercially available caustic-base salt baths followed by pickling in hot sulfuric and hot nitric-hydrofluoric acid.

Table 1.3.1 AMS specifications (Refs. 4-12, 168)

Alloy	Inconel 718
AMS Specification	**Product Form**
5596G	Sheet, strip, plate
5597D	Sheet, strip, plate
5662J	Bars, forgings, rings
5663F	Bars, forgings, rings
5664D	Bars, forgings, rings
5589C	Seamless tubing
5590C	Seamless tubing
5832D	Welding wire
5383D	Investment castings

Table 1.4.1 AMS specified compositions (Refs. 4-12)

Alloy	Inconel 718					
AMS Specification	**5596G, 5597D, 5664D, 5589C, 5590C, 5832D**		**5662J, 5663F**		**5383D**	
	Elements (percent)					
	min	**max**	**min**	**max**	**min**	**max**
Nickel	50.00	55.00	50.00	55.00	50.00	55.00
Chromium	17.00	21.00	17.00	21.00	17.00	21.00
Columbium + Tantalum[a]	4.75	5.50	4.75	5.50	4.75	5.50
Molybdenum	2.80	3.30	2.80	3.30	2.80	3.30
Titanium	0.65	1.15	0.65	1.15	0.65	1.15[b]
Aluminum	0.20	0.80	0.20	0.80	0.40	0.80[b]
Cobalt	–	1.00	–	1.00	–	1.00
Carbon	–	0.08	–	0.08	–	0.08
Manganese	–	0.35	–	0.35	–	0.35
Silicon	–	0.35	–	0.35	–	0.35
Phosphorus	–	0.015	–	0.015	–	0.015
Sulfur	–	0.015	–	0.015	–	0.015
Boron	–	0.006	–	0.006	–	0.006
Copper	–	0.30	–	0.30	–	0.30
Lead	–	–	–	0.0005	–	–
Bismuth	–	–	–	0.00003	–	–
Selenium	–	–	–	0.0003	–	–
Iron	remainder		remainder		remainder	

a Tantalum content is 0.05 percent, maximum for AMS 5589C, 5597D, 5662J, and 5664D and 0.10 percent maximum for 5383D.

b Titanium plus aluminum content 1.75 percent maximum.

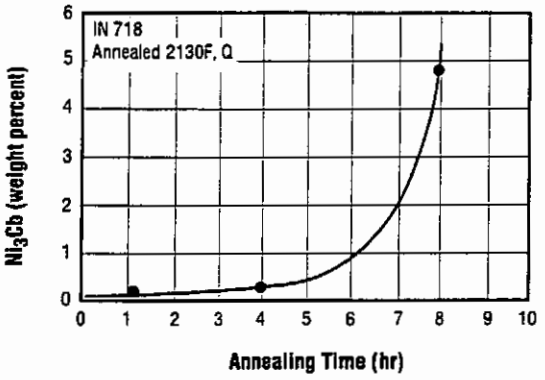

Fig. 1.5.1.1 Effect of annealing time at 1700F on delta phase precipitation (Ref. 90)

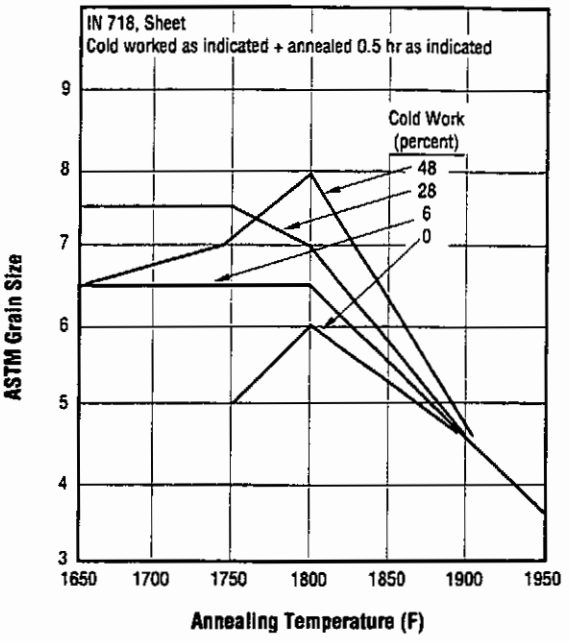

Fig. 1.5.1.2 Effects of variations in cold work and annealing temperature on grain size of sheet (Ref. 1)
Note: Increasing ASTM grain-size number is indicative of decreasing grain size.

Table 1.5.1.3 Effects of solution annealing temperature on tensile and creep rupture properties (Ref. 96)

Alloy	Inconel 718						
Solution Treatment[a]	**Tensile Properties at Room Temperature**				**Creep Rupture Properties at 1200F/100 ksi**		
	F_{ty} (ksi)	F_{tu} (ksi)	e (percent)	RA (percent)	Rupture Life (hr)	e (percent)	RA (percent)
None (direct aged)	193	221	19	34	95	24	31
1725F, 1 hr, AC	180	212	18	34	194	11	16
1750F, 1 hr, AC	171	206	20	38	122	14	19
1775F, 1 hr, AC	166	204	23	41	218	13	15
1800F, 1 hr, AC	170	204	24	43	200	6	10
1850F, 1 hr, AC	172	202	22	46	270	6	12
1900F, 1 hr, AC	169	198	25	48	225	2	8

[a] All materials aged 1325F, eight hours, cool at 100F/hour to 1150F, eight hours, AC.

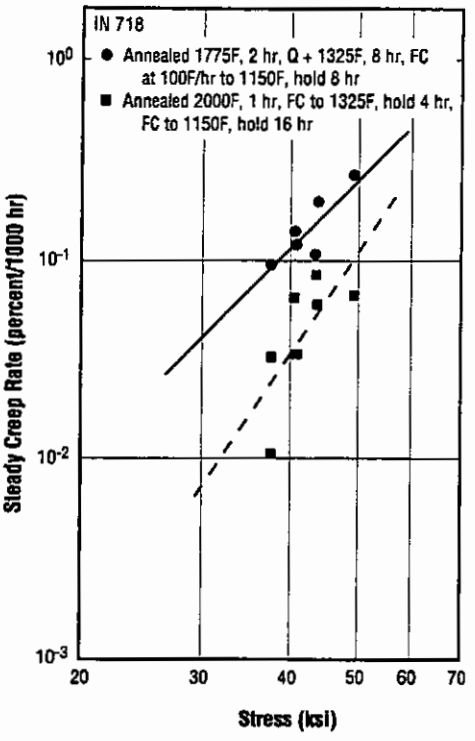

Fig. 1.5.1.4 Effects of solution annealing temperature on creep rate behavior at 1300F (Ref. 95)

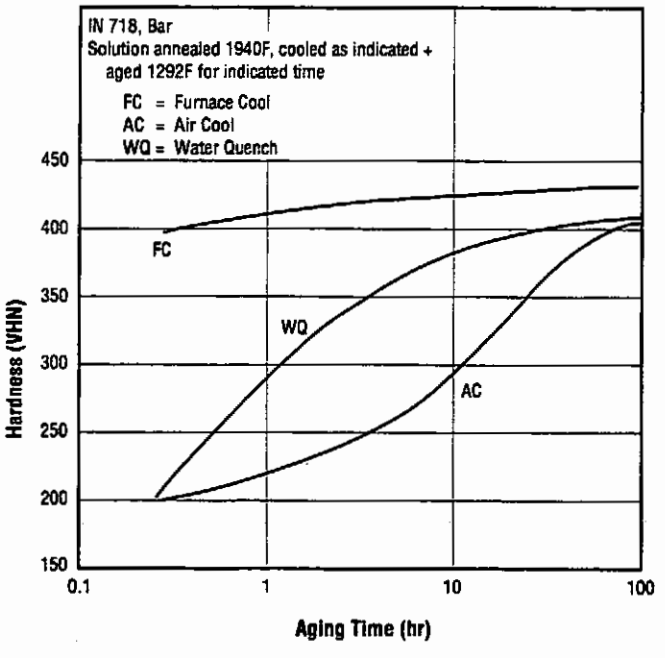

Fig. 1.5.1.6 Effects of solution anneal cooling rate and aging time on hardness (Ref. 98)

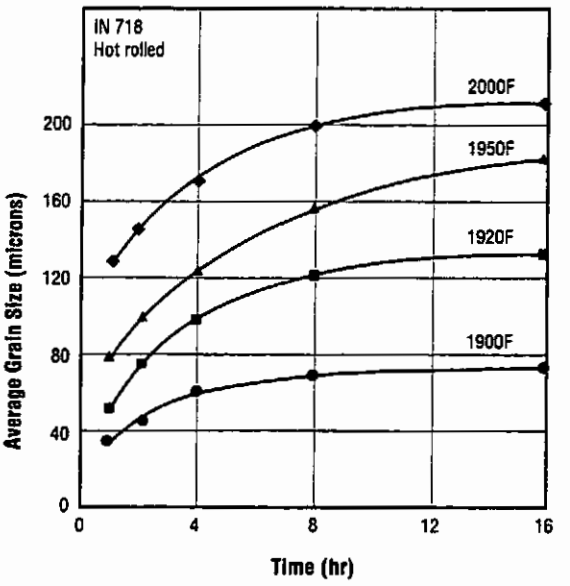

Fig. 1.5.1.5 Grain growth behavior at 1900 to 2000F (Ref. 97)

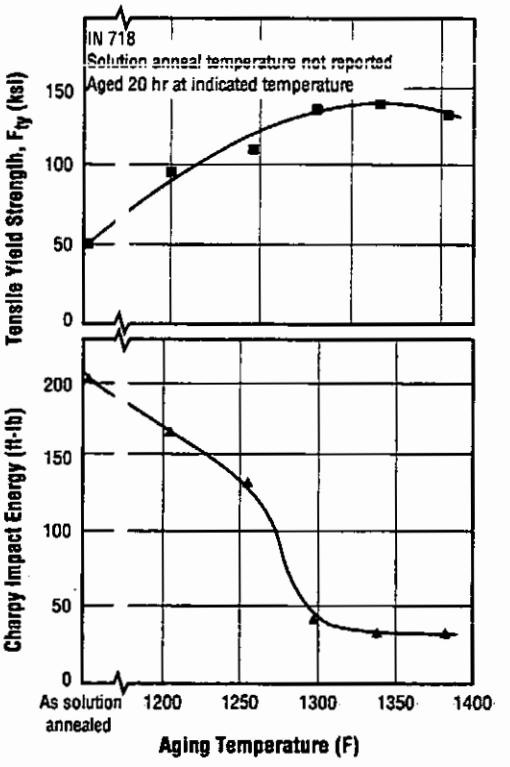

Fig. 1.5.1.7 Effects of aging temperature on room temperature yield strength and impact energy of solution annealed alloy (Ref. 96)

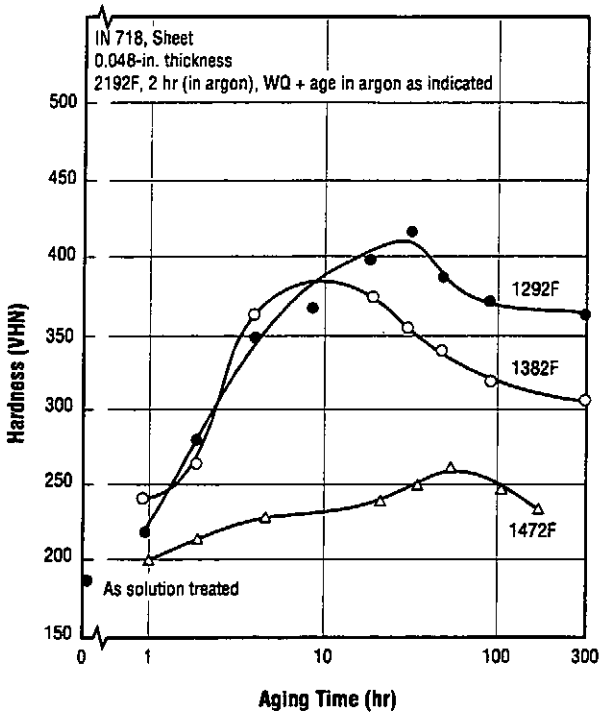

Fig. 1.5.1.8 Effects of aging time at various temperatures on the hardness of sheet (Ref. 84)

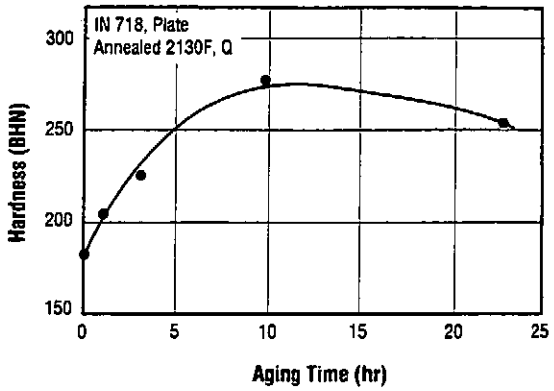

Fig. 1.5.1.9 Effect of aging time at 1200F on hardness after high temperature annealing (Ref. 90)

Table 1.5.1.10 Effects of single and double aging treatments on mechanical properties of solution annealed alloy (Ref. 96)

Alloy	Inconel 718					
Heat Treatment[a]	Tensile Properties				Hardness (HRC)	Fracture Toughness J_{Ic} (psi in.)
	F_{ty} (ksi)	F_{tu} (ksi)	e (percent)	RA (percent)		
A	161	190	19	–	40	546
B	124	174	28	51	35	1908
C	124	175	27	42	38	1631
D	164	193	23	48	42	572
E	182	205	17	41	44	480

[a] A = 1950F, one hour, AC.
B = 1875F, one hour, WQ + 1450F, six to eight hours, AC.
C = 1925F, one hour, WQ + 1400F, six hours, AC.
D = 1750F, two hours, WQ or AC + 1325F, eight hours, cool 100F/hour to 1150F, hold eight hours, AC.
E = 1925F, one hour, AC + 1400F, six hours, FC 100F/hour to 1200F, hold eight hours, AC.

Table 1.5.2.1 Tensile properties in longitudinal orientation of hot-rolled rounds of several sizes and in various heat-treated conditions (Ref. 1)

Alloy	Inconel 718				
Form	Hot-Rolled Rounds				
Diameter (in.)	**Condition**	**F_{ty} (ksi)**	**F_{tu} (ksi)**	**e, 2-in. (percent)**	**RA (percent)**
5/8	As-rolled	82.1	139.5	46	60
	1750F, 1 hr, AC	79.2	139.0	50	49
	1950F, 1 hr, AC	48.2	116.5	61	66
	1750F, 1 hr, AC + age[a]	179.8	208.2	21	39
	1950F, 1 hr, AC + age[b]	157.5	194.2	22	30
1	As-rolled	65.0	130.0	54	67
	1750F, 1 hr, AC	64.5	129.0	55	61
	1950F, 1 hr, AC	52.0	112.5	64	68
	1750F, 1 hr, AC + age[a]	175.0	201.5	20	36
	1950F, 1 hr, AC + age[b]	152.0	188.0	21	34
1-1/2	As-rolled	105.5	147.0	40	52
	1750F, 1 hr, AC	72.5	141.5	46	45
	1950F, 1 hr, AC	55.0	120.0	58	60
	1750F, 1 hr, AC + age[a]	167.5	205.0	20	28
	1950F, 1 hr, AC + age[b]	153.0	191.0	24	36
4	1750F, 1 hr, AC	55.0	117.5	53	52
	1950F, 1 hr, AC	48.0	112.5	60	63
	1750F, 1 hr, AC + age[a]	165.0	192.0	17	24
	1950F, 1 hr, AC + age[b]	165.0	195.5	21	34

[a] Age 1325F, eight hours, FC to 1150F, hold for total age of 18 hours, AC.

[b] Age 1400F, 10 hours, FC to 1200F, hold for total age of 20 hours, AC.

Table 1.5.2.2 Tensile properties of pancake forgings of various sizes in different heat-treated conditions (Ref. 1)

Alloy	Inconel 718					
Form	Pancake Forgings					
Forging Size (in.)	**Condition**	**Orientation**	**F_{ty} (ksi)**	**F_{tu} (ksi)**	**e, 2-in. (percent)**	**RA (percent)**
8 dia x 2-1/2	1700F, 1 hr, AC + age[a]	Radial				
		top edge	159.0	182.0	10	10.5
		center	160.0	196.0	24	33.0
		bottom edge	159.5	186.5	16	19.0
		Tangential				
		top edge	181.0	209.0	19	27.5
		bottom edge	179.0	210.0	18	29.5
7 dia x 1	1950F, 1/2 hr, AC + age[b]	Radial	153.0	189.5	19	29.8
		Tangential	153.2	185.2	19	27.2
5-1/2 dia x 1	1800F, 1 hr, WQ + age[a]	Radial	172.5	202.8	19	25.6
	1950F, 1 hr, WQ + age[b]	Radial	152.0	190.0	18	24.3

[a] Age 1325F, eight hours, FC to 1150F, hold for total age of 18 hours.

[b] Age 1400F, 10 hours, FC to 1200F, hold for total age of 20 hours.

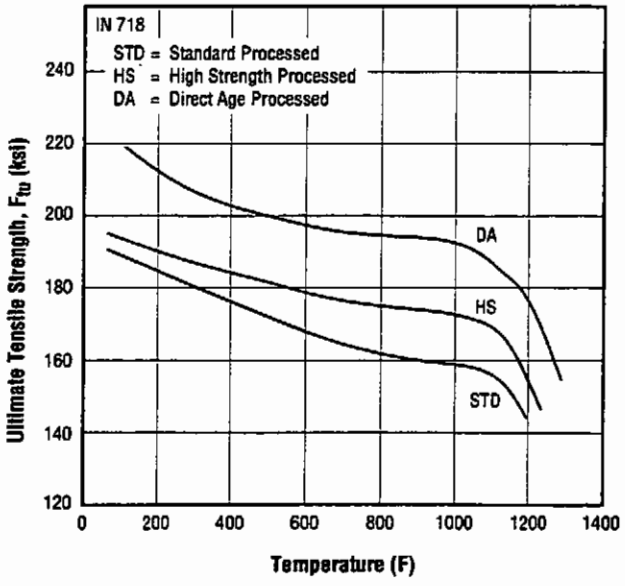

Fig. 1.5.3.1 Effects of temperature and processing technique on tensile strength (Ref. 92)

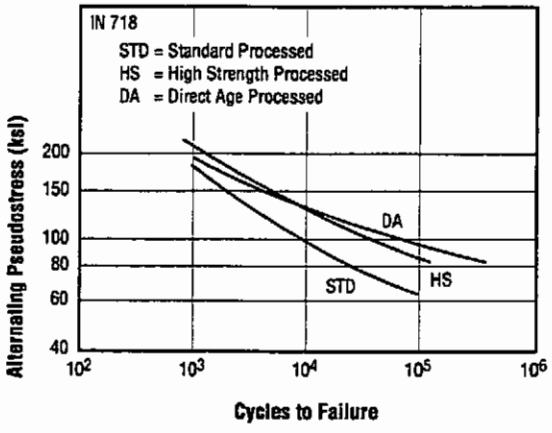

Fig. 1.5.3.2 Effects of processing technique on low-cycle fatigue behavior at 1000F (Ref. 92)

Table 1.6.1 Hardness ranges typical of a wide variety of production forms in various conditions (Ref. 1)

Alloy	Inconel 718
Condition	**Rockwell Hardness**
Annealed, 1700 to 1950F	B 85 - 98
Annealed + aged[a]	C 40 - 47
As-hot-rolled	C 17 - 30
Hot-rolled + aged[a]	C 40 - 46

[a] Aged in accordance with either one of the conventional schedules given in Sections 1.5.1 and 1.5.2.

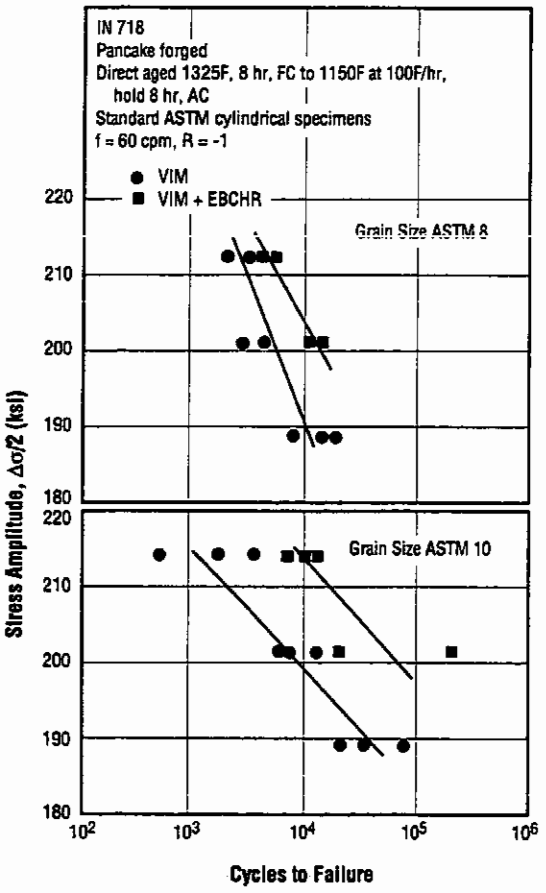

Fig. 1.8.1 Effects of vacuum induction melting and electron-beam cold hearth refining on fatigue life at 1000F in air (Ref. 103)

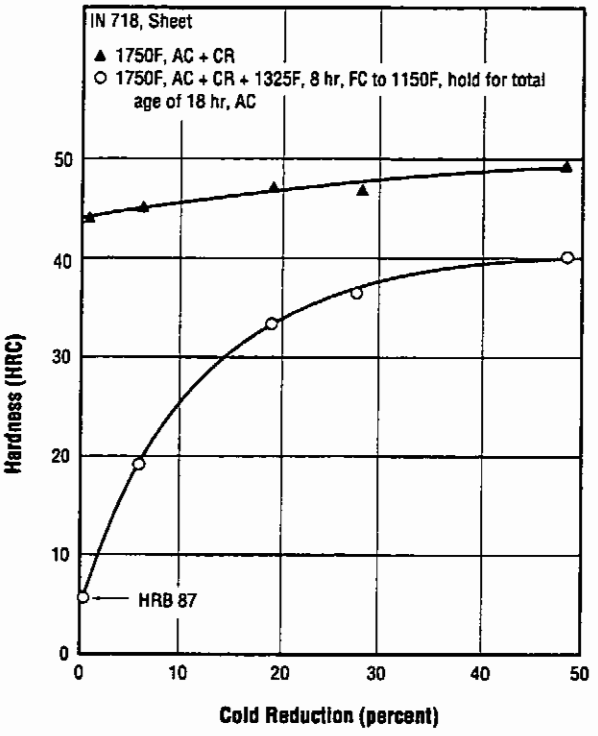

Fig. 1.6.2 Effects of cold rolling and aging on the hardness of sheet at room temperature (Ref. 1)

Table 2.1.1.1 Melting and solidification temperatures for Inconel 718

Alloy	Inconel 718						
Sample Condition	Process	Temperature (F)				Reference
		Liquidus	Solidus	γ/ CbC Eutectic	γ/Laves Eutectic	
As-Cast	Heating	2464	2269	2298	2156	153
	Cooling	2406	2214	2280	2120	153
Wrought	Heating	2469	2266	2340	–	153
	Cooling	2413	2178	2304	2106	153
a	a	2437	2300	–	–	1
a	a	2450	2200	–	–	106
Wrought	Heating	2453	2338	–	–	111
	Cooling	2401	–	–	–	111
a	a	2453	2273	–	–	108
a	Cooling	2478	–	2352	2120	108
	Heating	–	2327	–	–	154
Wrought	a	–	–	2150	–	150
As-Cast	Heating	2446	2269	2320 – 2410	2100 – 2151	100

a Not reported.

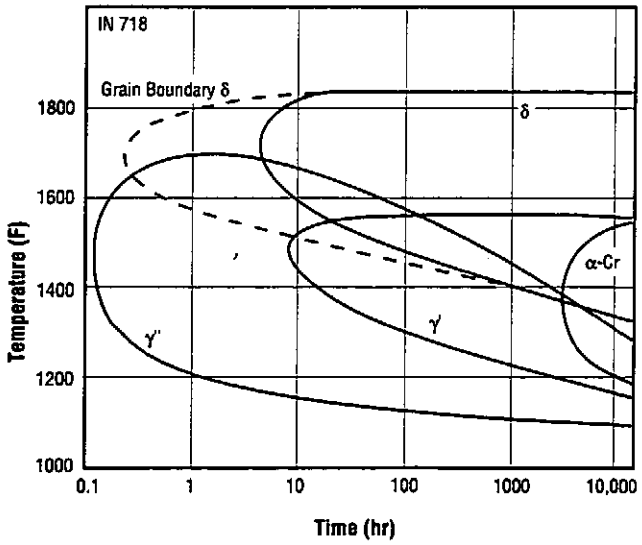

Fig. 2.1.2.1.1 Time-temperature-transformation (TTT) diagram (Ref. 98)

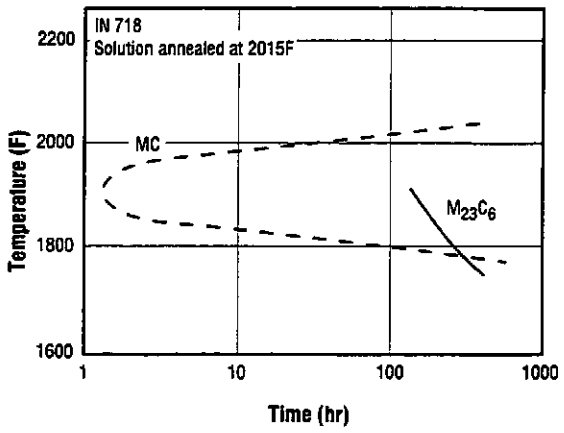

Fig. 2.1.2.1.2 Time-temperature-precipitation diagram for grain boundary carbides (Ref. 113)

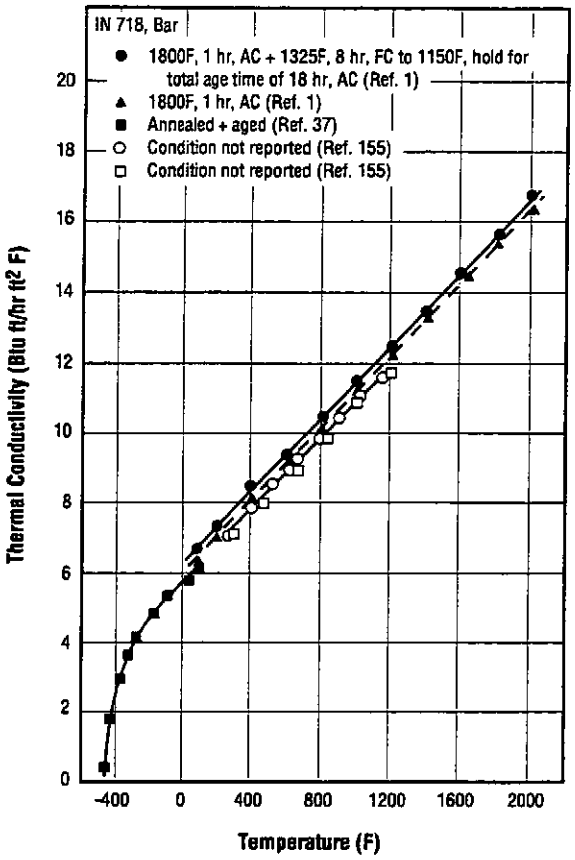

Fig. 2.1.3.1 Thermal conductivity from -450 to 2000F (Refs. 1, 37, 155)

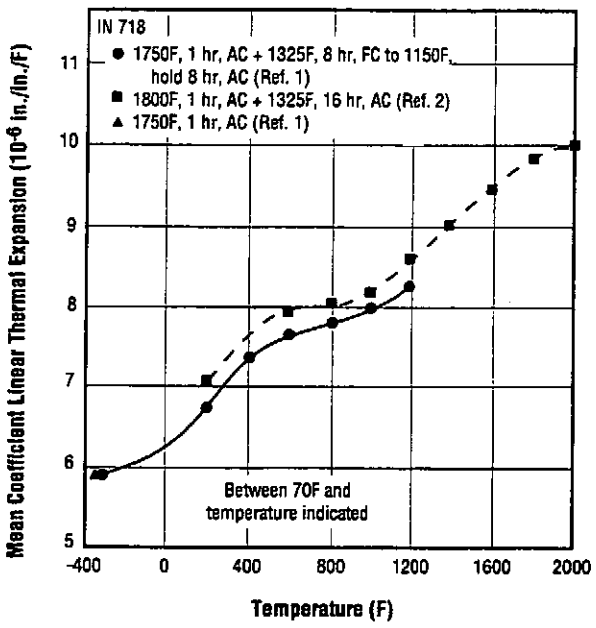

Fig. 2.1.4.1 Thermal expansion from -320 to 2000F (Refs. 1, 2)

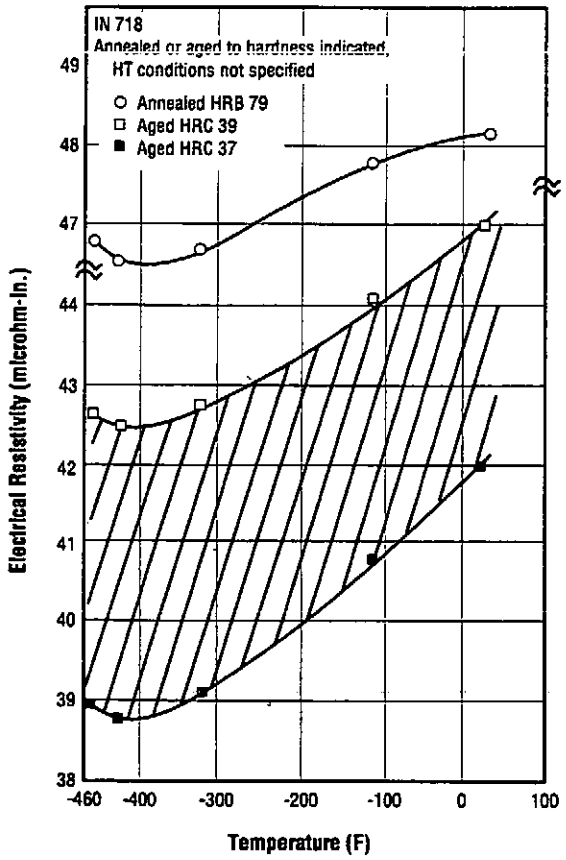

Fig. 2.2.2.1 Electrical resistivity at low temperatures of annealed and annealed-and-aged alloy (Ref. 3)

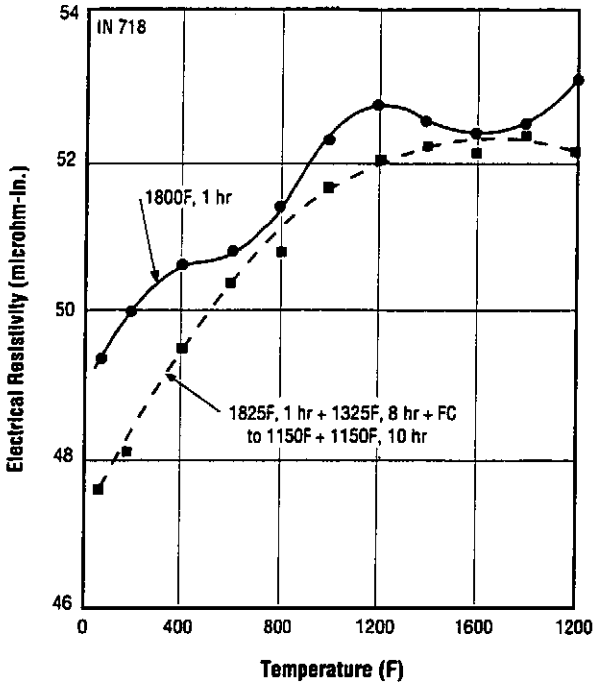

Fig. 2.2.2.2 Electrical resistivity at elevated temperatures of annealed and annealed-and-aged alloy (Ref. 2)

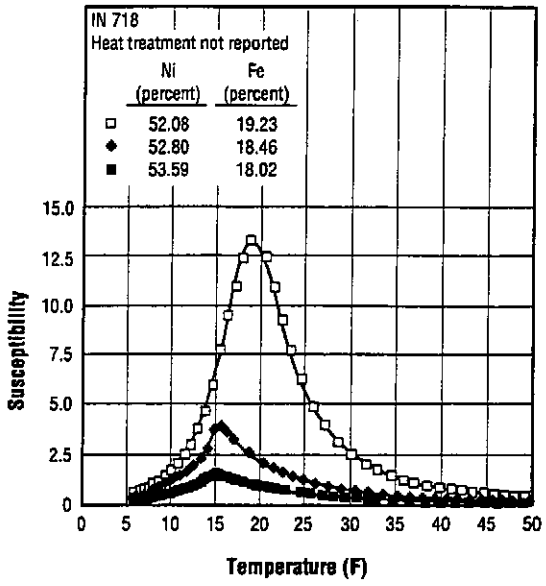

Fig. 2.2.3.1 Effects of compositional variations on low temperature susceptibility (Ref. 115)

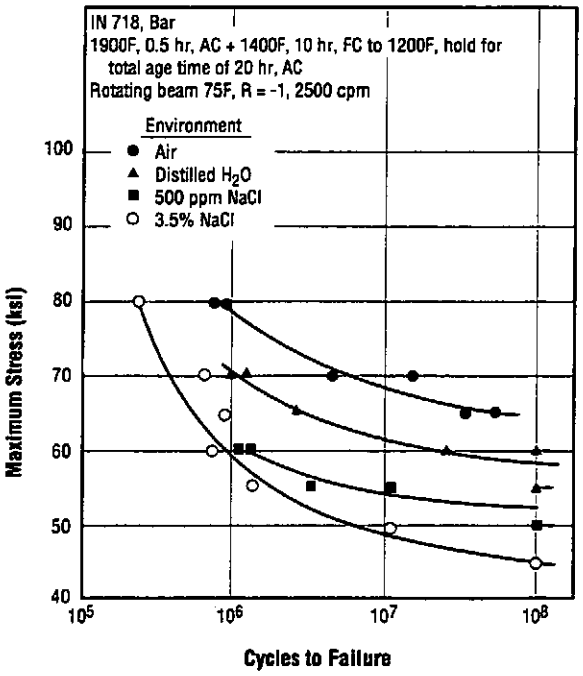

Fig. 2.3.2.1 Effects of environments of distilled water and solutions of sodium chloride on fatigue life of bar at room temperature (Ref. 28)

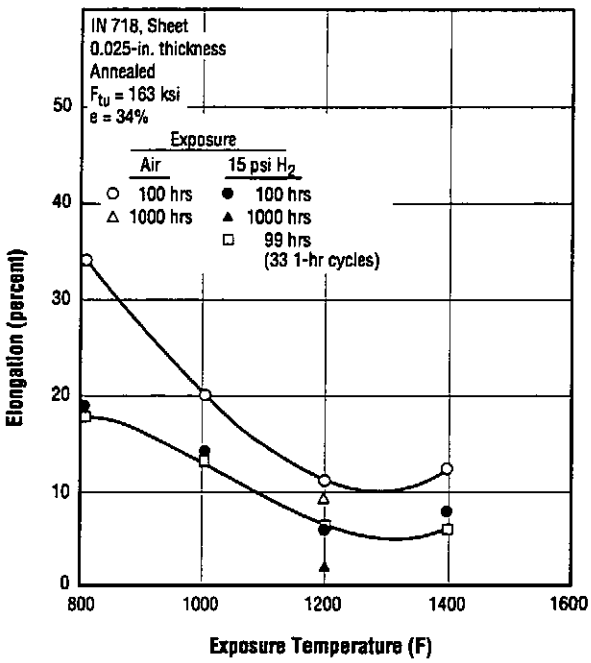

Fig. 2.3.3.1 Effect of elevated temperature exposure to 15 psi hydrogen on room temperature tensile elongation of annealed sheet (Ref. 38)

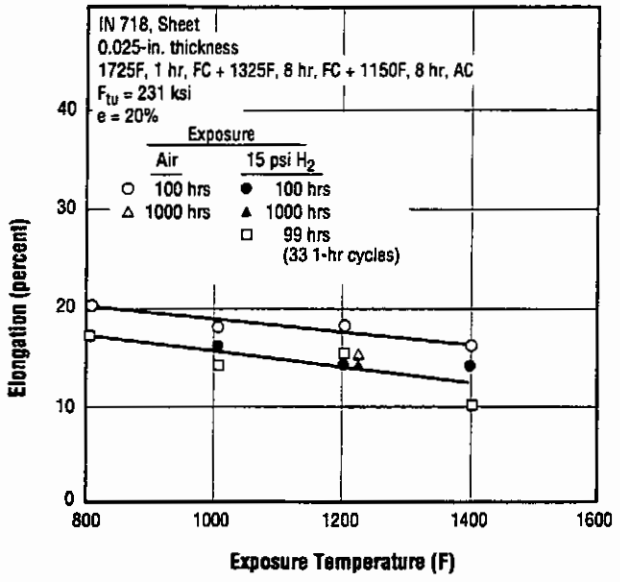

Fig. 2.3.3.2 Effect of elevated temperature exposure to 15 psi hydrogen on room temperature tensile elongation of solution treated and aged sheet (Ref. 38)

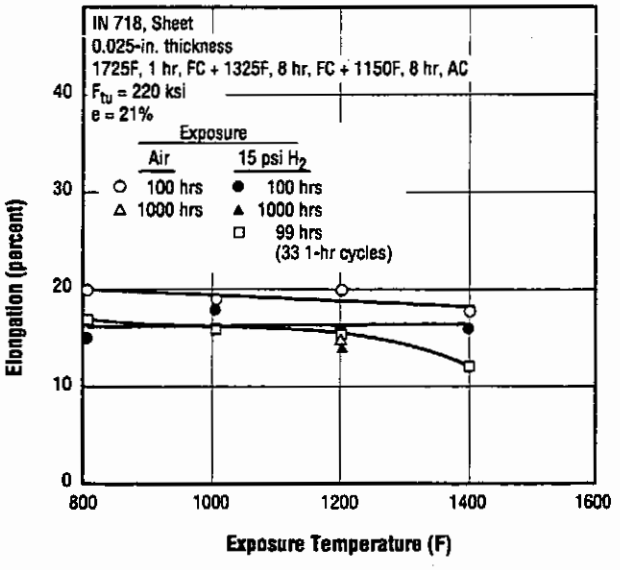

Fig. 2.3.3.4 Effect of elevated temperature exposure to 15 psi hydrogen on room temperature tensile elongation of cold rolled and solution treated and aged sheet (Ref. 38)

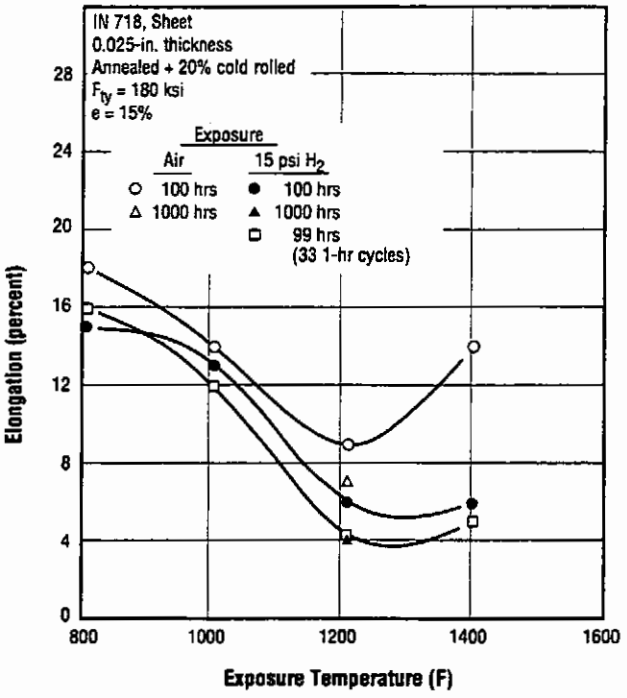

Fig. 2.3.3.3 Effect of elevated temperature exposure to 15 psi hydrogen on room temperature tensile elongation of annealed and cold rolled sheet (Ref. 38)

Table 2.3.3.5 Effect of elevated temperature exposure to high pressure hydrogen on the tensile properties of sheet in 5,000 psi helium or 5,000 psi hydrogen (Ref. 119)

Alloy			Inconel 718[a]							
Hydrogen Charging[b]			Tested in 5,000 psi Helium				Tested in 5,000 psi Hydrogen			
Temperature (F)	Time (min.)	Hydrogen Content (ppm)	F_{ty} (ksi)	F_{tu} (ksi)	e (percent)	RA (percent)	F_{ty} (ksi)	F_{tu} (ksi)	e (percent)	RA (percent)
c	–	0.65	175	207	18.3	34.4	176	204	11.9	15.1
800	15	50	166	208	8.4	7.3	169	201	8.8	5.9
1200	9	47	174	203	7.0	4.8	166	195	7.0	4.3
1200	15	55	175	198	4.3	8.6	177	203	4.4	7.8

a Annealed 1925F, 20 minutes + 1400F, 10 hours, FC to 1200F, hold for total aging time of 20 hours.

b Tensile specimens charged by exposing to 5,000 psi hydrogen for indicated times and temperatures.

c Not hydrogen charged.

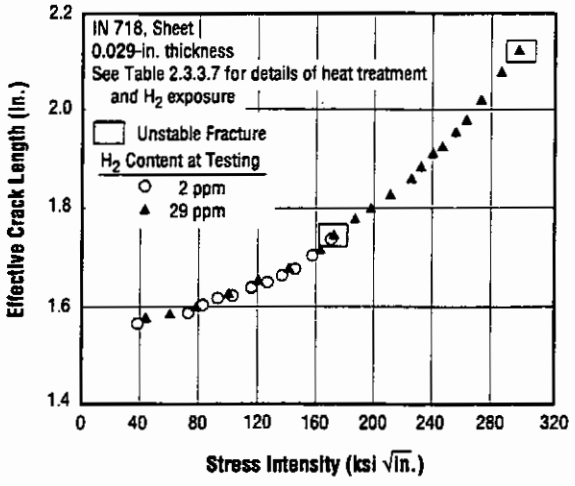

Fig. 2.3.3.6 Effect of hydrogen content on crack growth resistance curves for sheet (Ref. 122)

Table 2.3.3.7 Effect of hydrogen on critical stress intensity for unstable crack growth of sheet at room temperature (Ref. 122)

Alloy	Inconel 718			
Form	0.029-in. Sheet[a]			
Specimen Type[b]	Hydrogen Charging Conditions[c]		Hydrogen Content (ppm)	Critical Stress Intensity[d] (ksi $\sqrt{in.}$)
	Time (hr)	Temperature (F)		
Base Metal	Uncharged		NA	275
			NA	310
			NA	325
	24	200	2	305
			2	325
	37.5	500	28	170
			30	170
Weld Metal	24	200	3	195
			4	190
	37.5	500	18	150
			29	130
			30	110

[a] Heat treated 1900F, 0.25 hour, argon cool + 1325F, eight hours, cool to 1150F at 100F/hour, hold at 1150F, eight hours cool to below 600F in 0.17 hours.

[b] Center cracked sheet specimens, ASTM E 561.

[c] Charged in 1000 psig high purity hydrogen.

[d] Stress intensity factor for transition from stable to unstable crack growth under incrementally increasing loads.

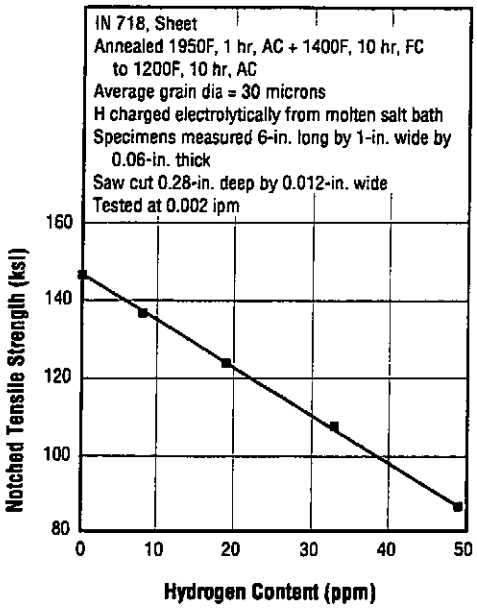

Fig. 2.3.3.8 Effects of cathodically charged hydrogen on room temperature notched tensile strength (Ref. 120)

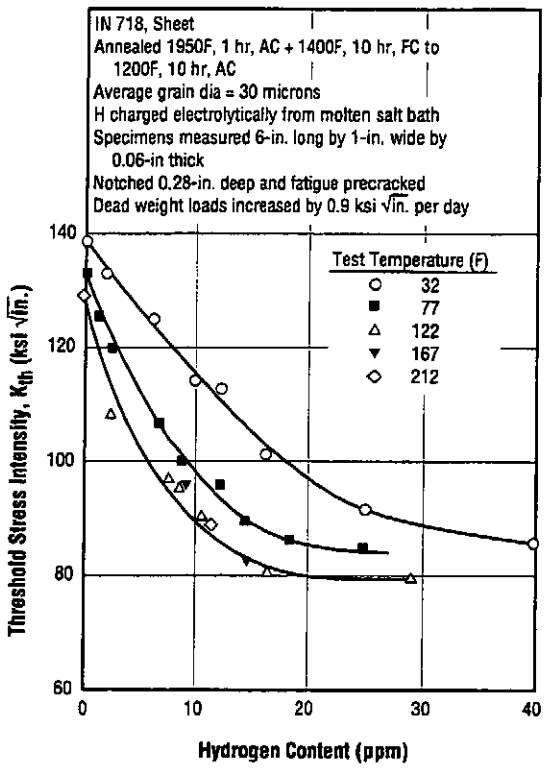

Fig. 2.3.3.9 Effects of cathodically charged hydrogen on the threshold stress intensity for subcritical crack growth (Ref. 121)

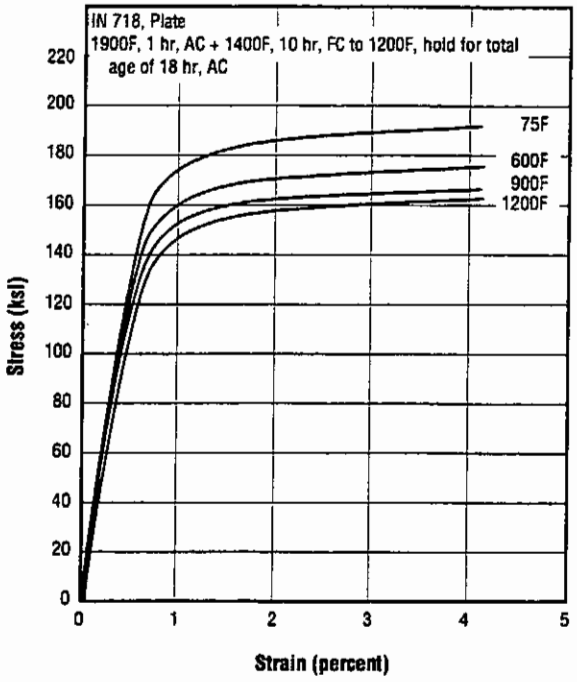

Fig. 2.3.3.10 Tensile stress-stain curves for plate at various temperatures in atmosphere of hydrogen at 5000 psi (Ref. 14)

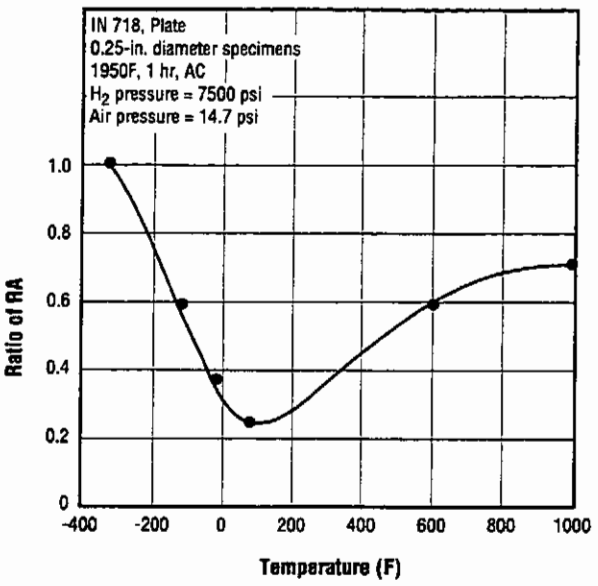

Fig. 2.3.3.11 Effect of temperature on the ratio of tensile ductility in hydrogen at 7500 psi pressure to that in air at atmospheric pressure for annealed plate (Ref. 65)

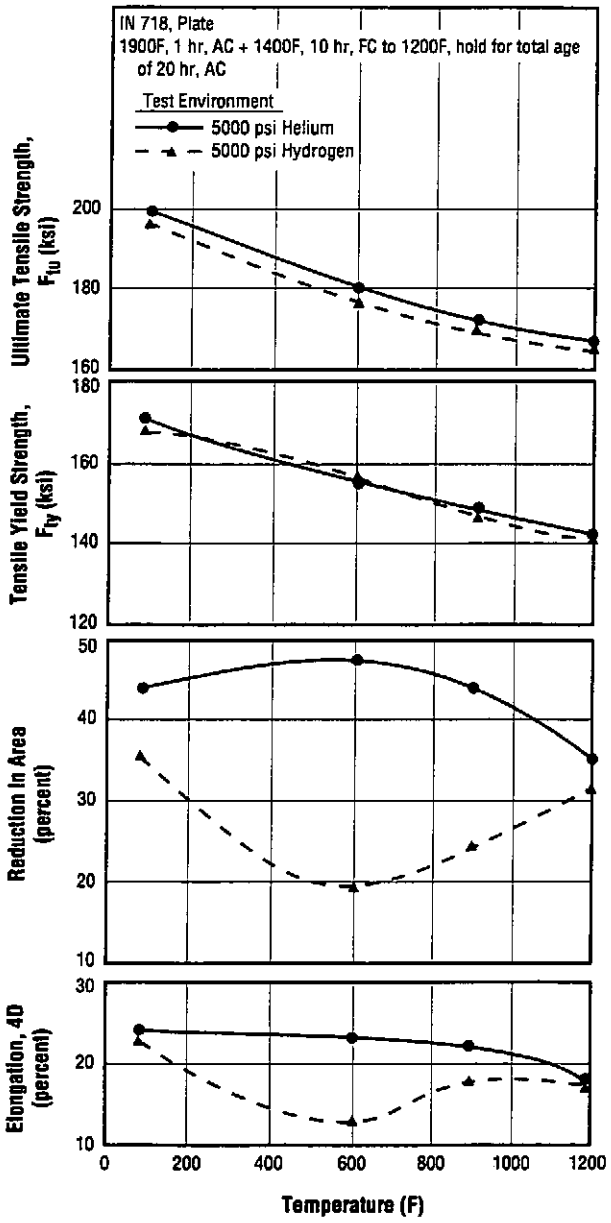

Fig. 2.3.3.12 Effect of elevated temperatures on tensile properties of annealed-and-aged plate in atmospheres of helium and hydrogen at 5000 psi (Ref. 14)

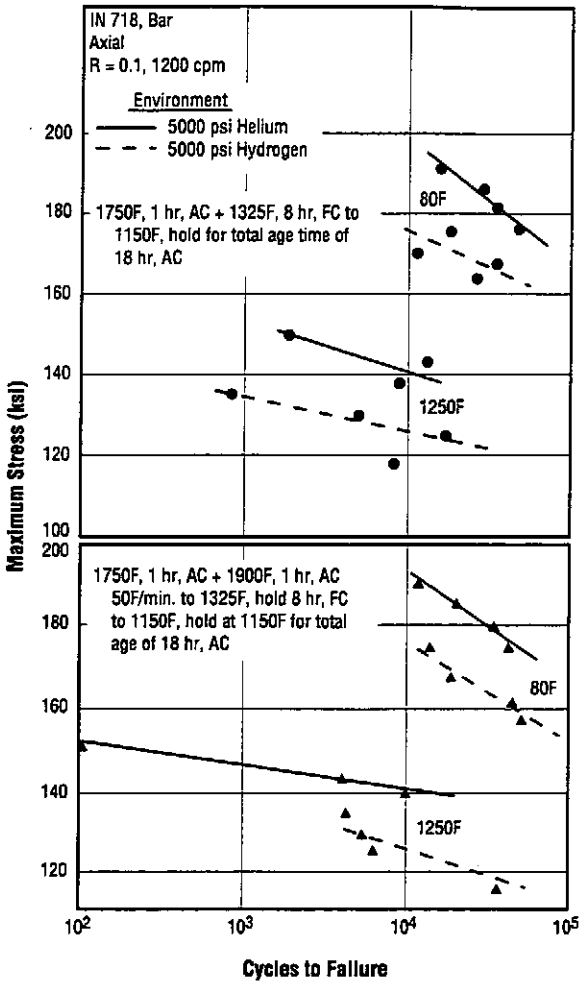

Fig. 2.3.3.13 Fatigue life of smooth bar in two heat-treated conditions in environments of high-pressure hydrogen and helium at two temperatures (Ref. 35)

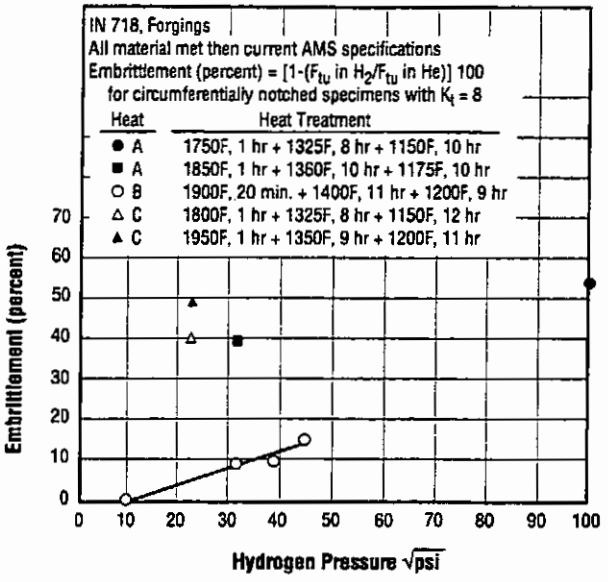

Fig. 2.3.3.14 Hydrogen embrittlement as a function of hydrogen pressure for a mixture of heats and heat treatments (Ref. 157)

Table 2.3.3.15 Comparison of room-temperature tensile and notched-tensile properties of bar in atmospheres of helium and hydrogen at 10,000 psi (Ref. 57)

Alloy	Inconel 718	
Form	Bar	
Condition	1750F, 1 hr, AC + 1325F, 8 hr, FC to 1150F, Hold 10 hr, AC	
Environment	**He (10 ksi)**	**H_2 (10 ksi)**
F_{ty} (ksi)	182	–
F_{tu} (ksi)	207	193
e, 4D (percent)	17	1.5
RA (percent)	26	0.8
NTS (ksi)	274	126
Notched RA (percent)	1.7	0.2

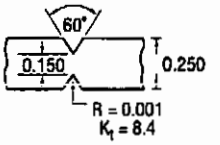

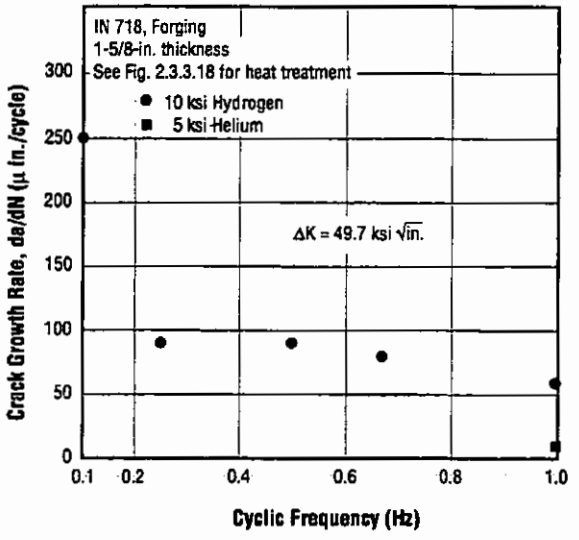

Fig. 2.3.3.16 Crack growth rates as a function of cyclic frequency for a forging (Ref. 158)

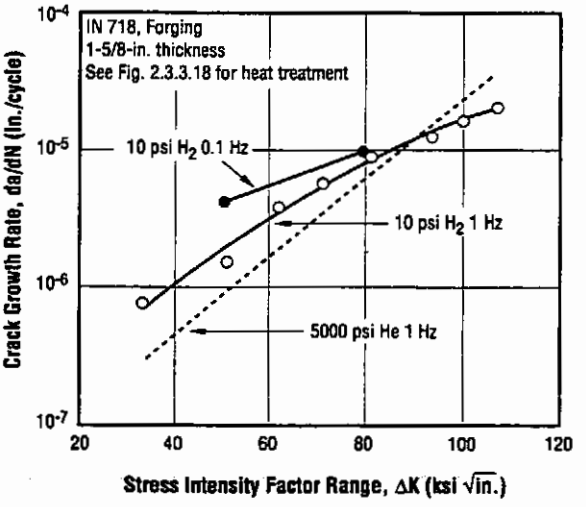

Fig. 2.3.3.17 Crack growth rates at low cyclic frequencies for a forging in helium and low pressure hydrogen (Ref. 158)

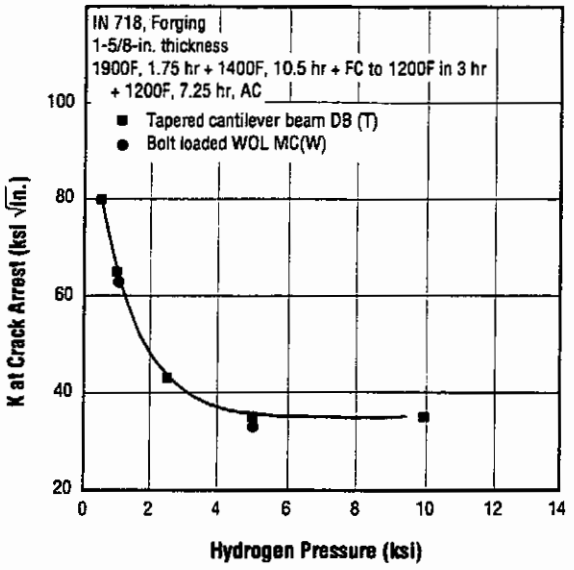

Fig. 2.3.3.18 Stress intensity at crack arrest for a forging as function of hydrogen pressure (Ref. 160)

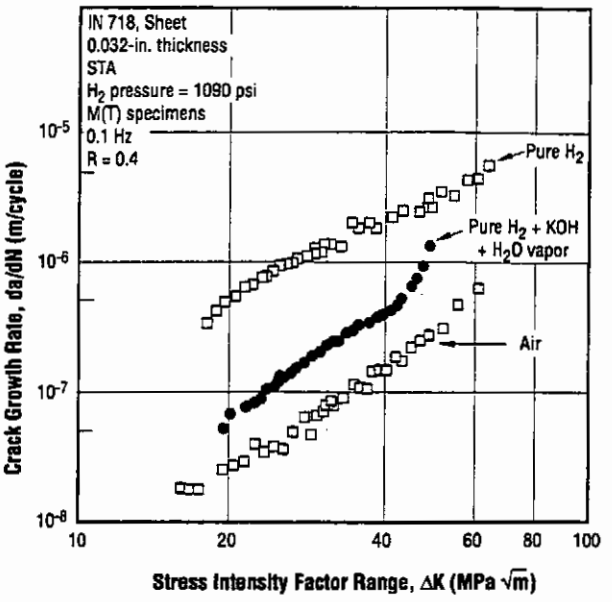

Fig. 2.3.3.19 Fatigue crack growth rates of solution treated and aged sheet in air, pure hydrogen and in a simulated Ni-H_2 battery environment without oxygen (Ref. 161)

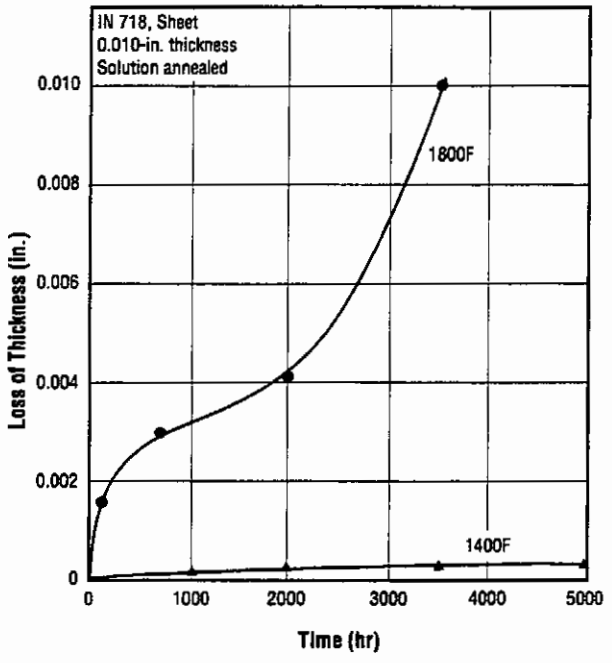

Fig. 2.3.4.1 Loss of thickness due to oxidation of sheet continuously exposed to still air at a pressure of 8 torr (0.01 atmosphere) at both 1800 and 1400F (Ref. 36)

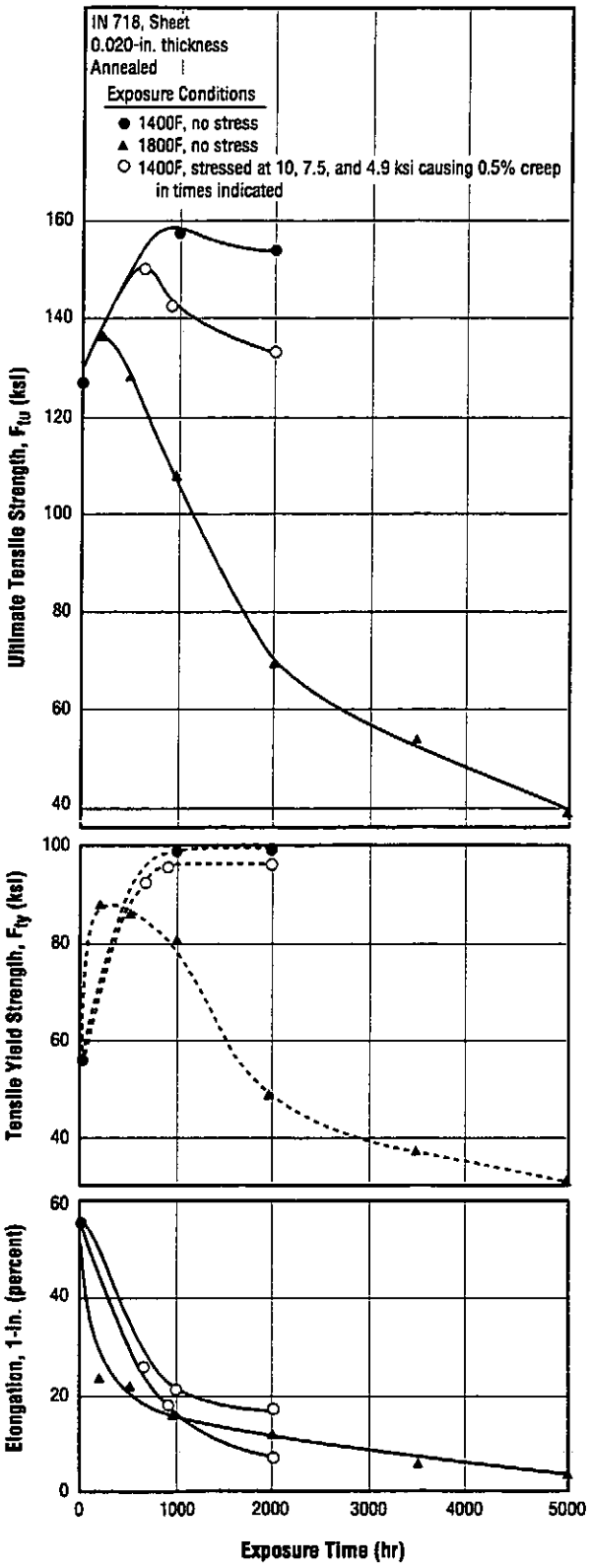

Fig. 2.3.4.2 Room-temperature tensile properties of annealed sheet after exposures to elevated temperatures at 8 torr (0.01 atmosphere) air pressure both with and without stress (Ref. 3)

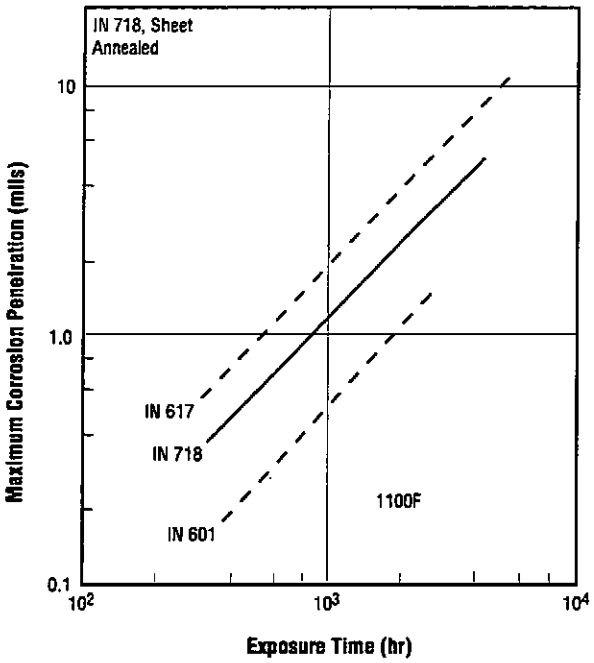

Fig. 2.3.4.3 Maximum penetration by hot corrosion of IN 718 and two other nickel-base superalloys exposed for various times at 1100F to air and to a fused salt mixture of potassium sulfate and sodium sulfate (Ref. 79)

Table 2.3.4.4 Frictional ignition of Inconel 718 and other aerospace alloys (Ref. 125)

Alloy[a]	Average Mechanical Energy Required for Ignition[b] ($W/in.^2 \times 10^{-12}$)
MA 754	> 26.5[c]
Inconel 600	16.1
MA 6000	14.7
Waspaloy	13.1
Monel K-500	9.7
Hastelloy X	7.7
Inconel 718	7.2
Incoloy 909	6.9
Type 304 Stainless Steel	6.7
Inconel 706	6.5
MA 956	4.4
Type 440C Stainless Steel	4.0

[a] Pairs of hollow cylinders pressed together with one cylinder fixed and other rotating at 17,000 rpm in 1000 psig oxygen.

[b] Mechanical energy equals Pv product, where:
P = contact pressure (psi)
v = linear surface velocity (ips).

[c] No ignition.

Table 2.3.4.5 Relative rankings of selected aerospace alloys for promoted combustion in high-pressure gaseous oxygen (Ref. 126)

Flammability Ranking[a]	Alloy
1	Monel 400
2	Inconel 600
3	Type 316 Stainless Steel
	Waspaloy
	Inconel 718
	17-4 PH
	Type 440C Stainless Steel
	Type 321 Stainless Steel
4	Aluminum 2219

[a] Composite ranking based on extinguishing pressure (highest pressure which will not sustain combustion), consumption velocity (specimen burn rate), ignition resistance, and specimen configuration. Resistance to combustion decreases with increasing ranking number.

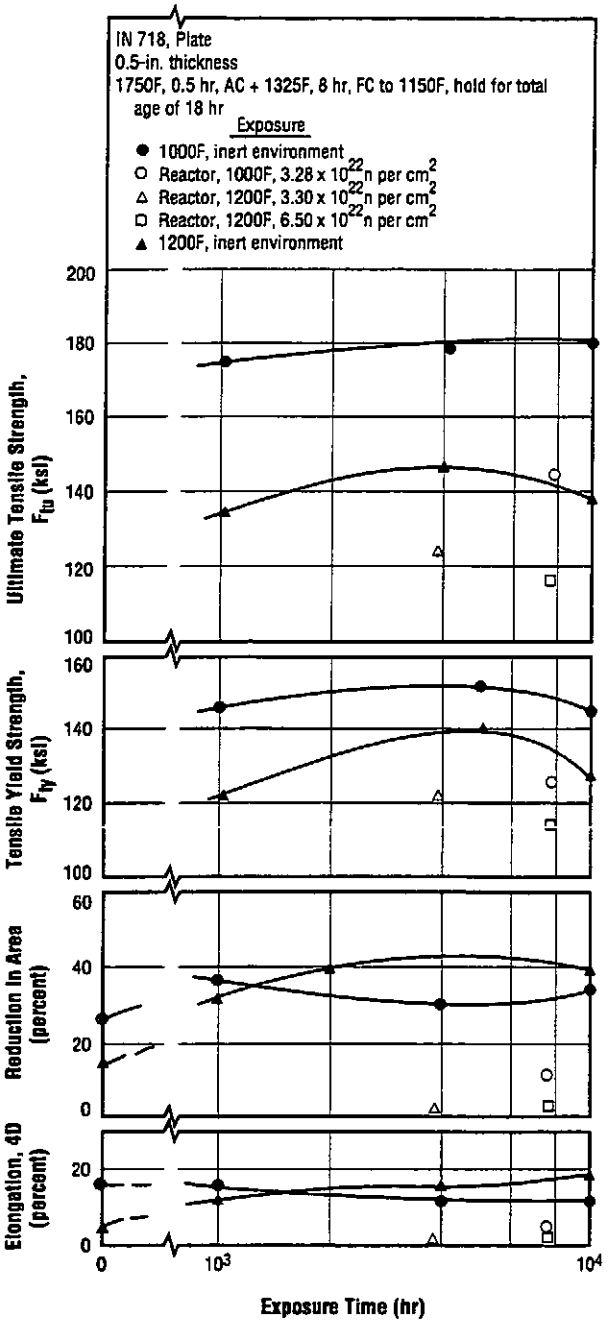

Fig. 2.4.1 Effects of long-time elevated temperature exposures to inert environments and to various neutron-fluence levels on tensile properties determined at exposure temperatures (Ref. 21)

Table 3.1.1 AMS specified room-temperature properties (Refs. 4-11)

Alloy	Inconel 718									
AMS Specification	Form	Condition	Tensile Properties						Hardness	
			F_{ty} (ksi)		F_{tu} (ksi)		e^e, min (percent)	RA, min (percent)		
			min	max	min	max			min	max
5596G	Sheet, strip, plate 0.010 – 0.187-in.	Anneal[a]	–	80	–	140	30	–	–	102 HRB
	0.188 – 1.0-in.		–	105	–	150	30	–	–	25 HRC
	0.010 – 1.0-in.	Anneal[a] + age[b]	150	–	180	–	12	–	36 HRC	–
5597D	Sheet, strip, plate	Anneal[c]	–	75		140	30	–	–	25 HRC
		Anneal[c] + age[d]	150	–	180	–	15	–	38 HRC	–
5662J and 5663F	Bars, forgings, rings L	Anneal[a] + age[b]	150	–	185	–	12	15	331HB	–
	L-T (forgings)		150	–	180	–	10	12	331HB	–
	T (bars)		150	–	180	–	6	8	331HB	–
5664D	Bars up to 3.0-in.	Anneal[c]	–	–	–	–	–	–	–	248 HB
	3.0 – 5.0-in.		–	–	–	–	–	–	–	285 HB
	5.0 – 10.0-in.		–	–	–	–	–	–	–	321 HB
	Forgings, rings		–	–	–	–	–	–	–	248 HB
	Bars up to 10.0-in.	Anneal[c] + age[d]	150	–	180	–	10	12	341 HB	–
	Forgings, rings		150	–	180	–	12	15	341 HB	–
5589C	Tubing, seamless	Anneal[a]	–	95	–	155	30	–	–	–
		Anneal[a] + age[b]	150	–	185	–	12	–	36 HRC	–
5590C	Tubing, seamless		–	–	–	–	–	–	–	–
5383D	Investment castings	Anneal[f]	–	–	–	–	–	–	–	25 HRC
		Anneal[f] + age[b]	110	–	125	–	5	10	34 HRC	44 HRC

Note: The original AMS documents should be consulted for complete specification details.

[a] 1725 to 1825F, AC.

[b] 1325F, eight hours, FC to 1150F, hold for total age of 18 hours.

[c] 1950F, AC.

[d] 1400F, 10 hours, FC to 1200F, hold for total age of 20 hours.

[e] 2-in. or 4D.

[f] 2000F, AC.

Table 3.1.2 AMS specified elevated-temperature properties (Refs. 4-11)

Alloy	Inconel 718[a]								
AMS Specification	Form	Test Temperature (F)	Tensile Properties				Stress-Rupture Properties		
			F_{ty}, min (ksi)	F_{tu}, min (ksi)	e, min (percent)	RA, min (percent)	Stress (ksi)	Rupture Time, min (hr)	e, min (percent)
5596G	Sheet, strip, plate	1200							
	0 – 0.015-in.		115	140	5	—	95	23	—
	0.016 – 0.025-in.		115	140	5	—	95	23	4
	0.026 – 1.0-in.		120	145	5	—	100	23	4
5662J and 5663F	Bars, forgings, rings		—	—	—	—	100	23	4
	L		125	145	12	15	—	—	—
	L-T (forgings)		125	140	10	12	—	—	—
	T (bars)		125	140	6	8	—	—	—
5589C	Tubing, seamless	1300	—	—	—	—	72.5	23	5
5383D	Investment castings		—	—	—	—	65	23	3

Note: The original AMS documents should be consulted for complete specification details

[a] 1725 to 1825F, AC, + 1325F, eight hours, FC to 1150F, hold for total age of 18 hours, AC.

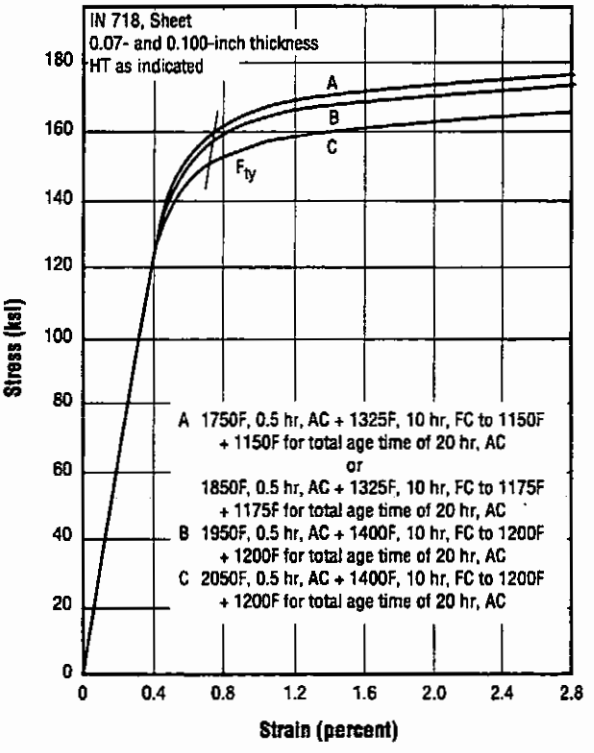

Fig. 3.2.1.1 Stress-strain curves for sheet in four heat-treated conditions (Ref. 53)

Table 3.2.1.2 Tensile properties in longitudinal and transverse orientations of hot-rolled, annealed rounds of two sizes (Ref. 1)

Alloy	Inconel 718					
Form	Hot-Rolled Rounds					
Condition	Annealed 1 hr, AC					
Diameter (in.)	**Annealing Temperature (F)**	**Orientation**	**F_{ty} (ksi)**	**F_{tu} (ksi)**	**e, 2-in. (percent)**	**RA (percent)**
2-1/2	1750	L	77.5	135.5	45	49
		T	73.5	129.5	32	29
	1950	L	50.4	114.0	62	65
		T	49.8	112.0	53	49
4	1750	L	63.5	122.0	49	51
		T	58.8	116.0	40	37
	1950	L	49.0	113.0	60	63
		T	48.7	116.5	45	40

Table 3.2.1.3 Effects of heat treatment on tensile properties of plate at room temperature (Ref. 34)

Alloy	Inconel 718				
Form	1-in. Plate				
Condition	**Orientation**	**F_{ty} (ksi)**	**F_{tu} (ksi)**	**e, 2-in. (percent)**	**RA (percent)**
1750F, 1 hr, AC	L	59	125	40	32
1750F, 1 hr, AC + age[a]	L	155	194	15	17
	T	152	186	11	14

[a] Age 1325F, eight hours, to 1150F, hold for total age of 18 hours, AC.

Table 3.2.1.4 Tensile properties in longitudinal and transverse orientations of hot-rolled rounds in annealed-and-aged conditions (Ref. 1)

Alloy	Inconel 718				
Form	Hot-Rolled Rounds, 4-in. diameter				
Condition	**Orientation**	**F_{ty} (ksi)**	**F_{tu} (ksi)**	**e, 2-in. (percent)**	**RA (percent)**
1750F, 1 hr, AC + age[a]	L	178.0	199.5	15	24
	T	178.5	198.5	12	16
1950F, 1 hr, AC + age[b]	L	164.0	197.0	17	23
	T	165.0	192.0	19	24

[a] Age 1325F, eight hours, FC to 1150F, hold for total age of 18 hours, AC.

[b] Age 1400F, 10 hours, FC to 1200F, hold for total age of 20 hours, AC.

Table 3.2.1.5 Tensile properties of annealed-and-aged sheet at room temperature (Ref. 1)

Alloy	Inconel 718		
Form	Sheet		
Condition	1950F, AC + 1400F, 10 hr, FC to 1200F, Hold for Total Age Time of 20 hr, AC		
Sheet Thickness (in.)	**F_{ty} (ksi)**	**F_{tu} (ksi)**	**e, 2-in. (percent)**
0.010	172.5	192.5	17
0.050	177.0	211.0	16
0.100	176.0	208.0	18
0.250	170.5	205.0	19

Table 3.2.1.6 Tensile properties of round and flat bars in the hot-rolled-plus-aged condition (Ref. 1)

Alloy	Inconel 718			
Form	Round and Flat Bar			
Condition	Hot-rolled + 1325F, 8 hr, FC to 1150F, Hold for Total Age of 18 hr, AC			
Sample (in.)	**F_{ty} (ksi)**	**F_{tu} (ksi)**	**e, 2-in. (percent)**	**RA (percent)**
21/32 diameter	189.5	206.5	19	34.5
5/8 diameter	181.8	208.2	22	45.0
13/16 diameter	181.0	209.0	22	43.0
5/8 x 1 flat	184.0	215.5	24	45.5
1-1/4 x 1-1/2 flat	210.0	227.5	17	40.8
1-1/2 x 1-3/4 flat	172.0	215.0	19	35.0

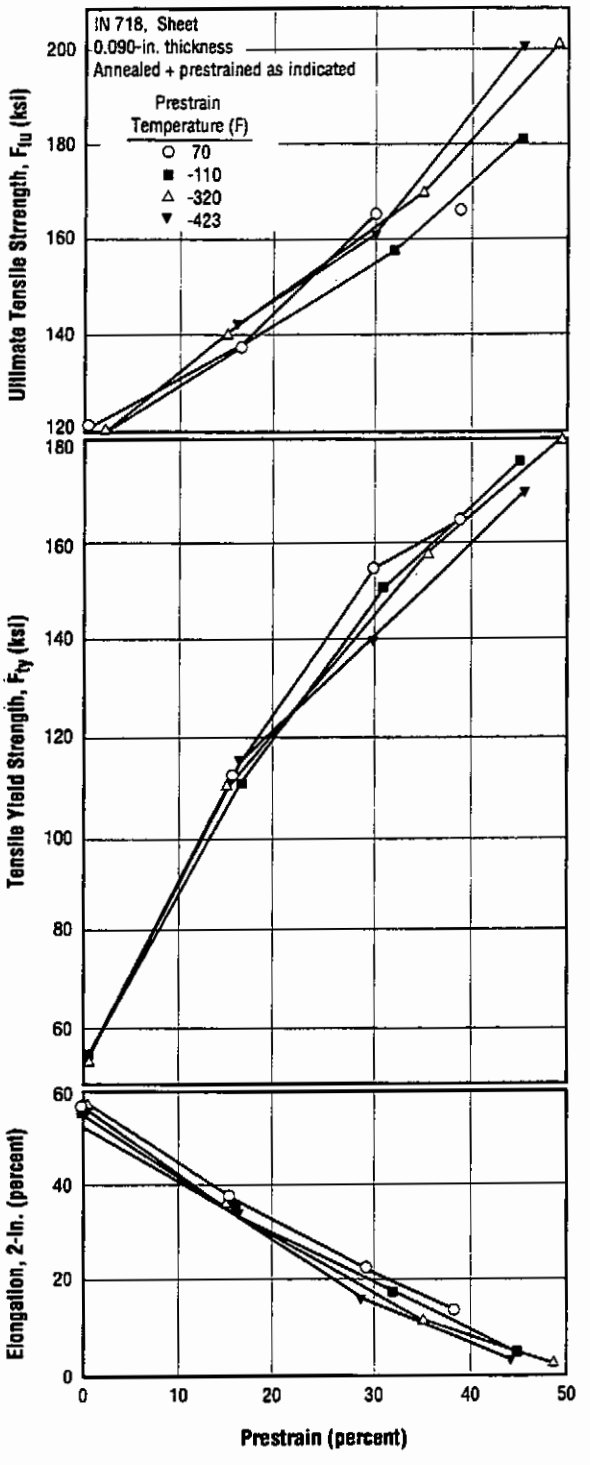

Fig. 3.2.1.7 Effects of prestraining at room and low temperature on the room-temperature tensile properties of annealed sheet (Ref. 54)

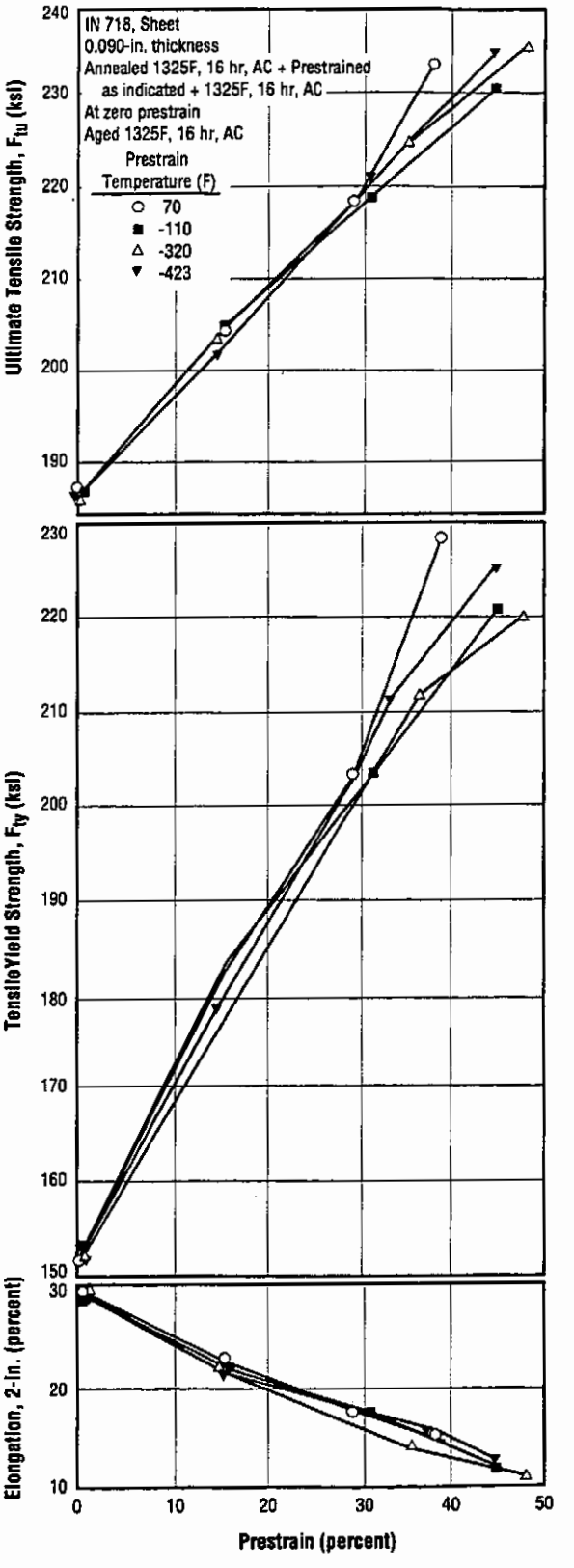

Fig. 3.2.1.8 Effects of prestraining at room and low temperatures followed by aging at 1325F on the room-temperature tensile properties of annealed-and-aged sheet (Ref. 54)

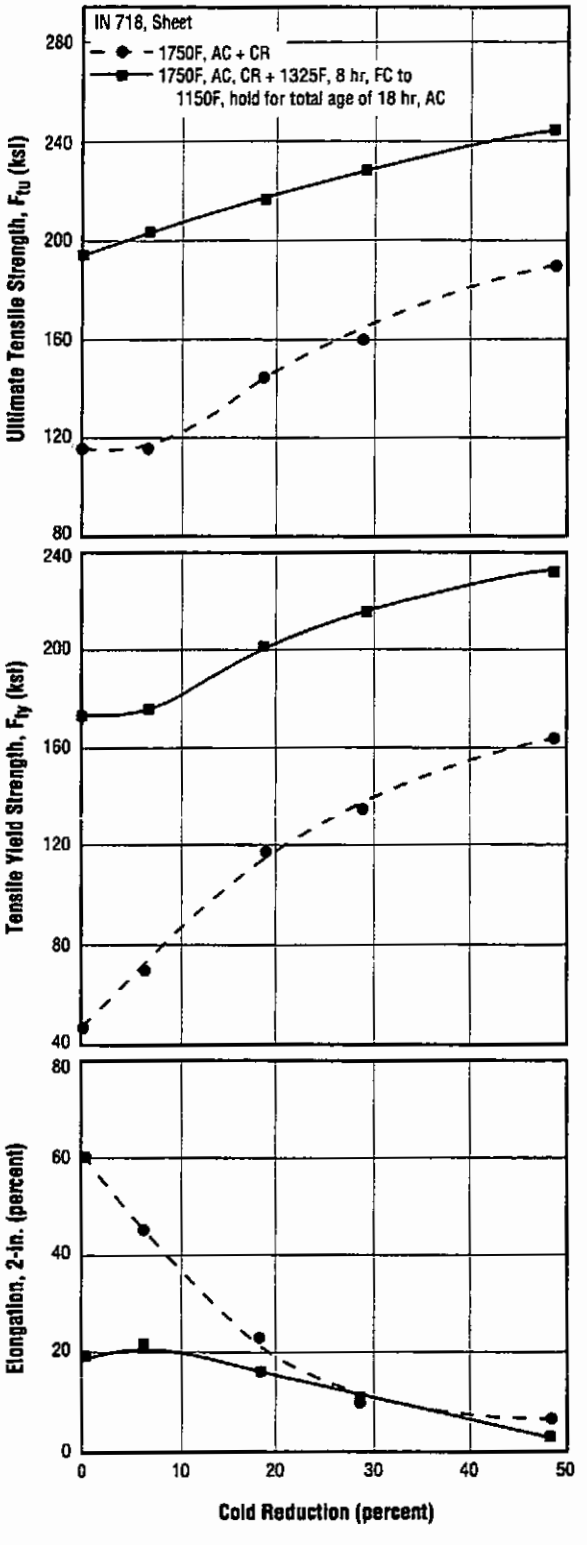

Fig. 3.2.1.9 Effects of cold rolling and aging on the tensile properties of sheet at room temperature (Ref. 1)

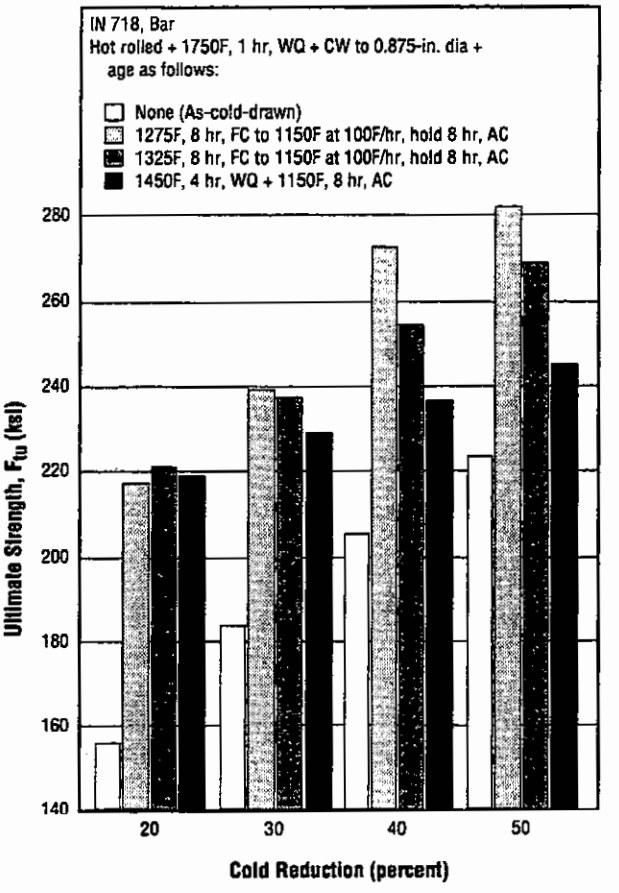

Fig. 3.2.1.10 Effects of cold drawing and various subsequent aging treatments on tensile strength of bar at room temperature (Ref. 55)

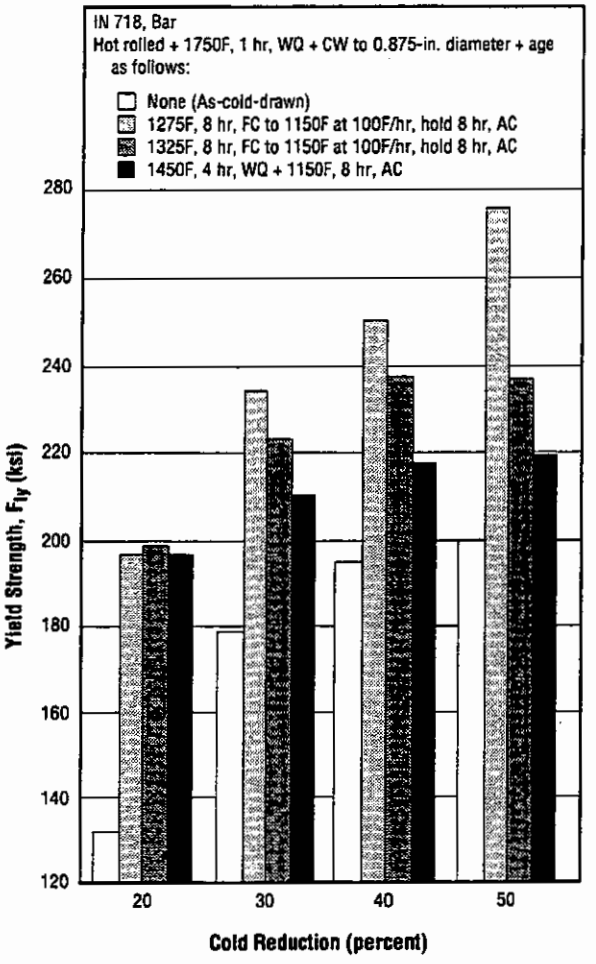

Fig. 3.2.1.11 Effects of cold drawing and various subsequent aging treatments on yield strength of bar at room temperature (Ref. 55)

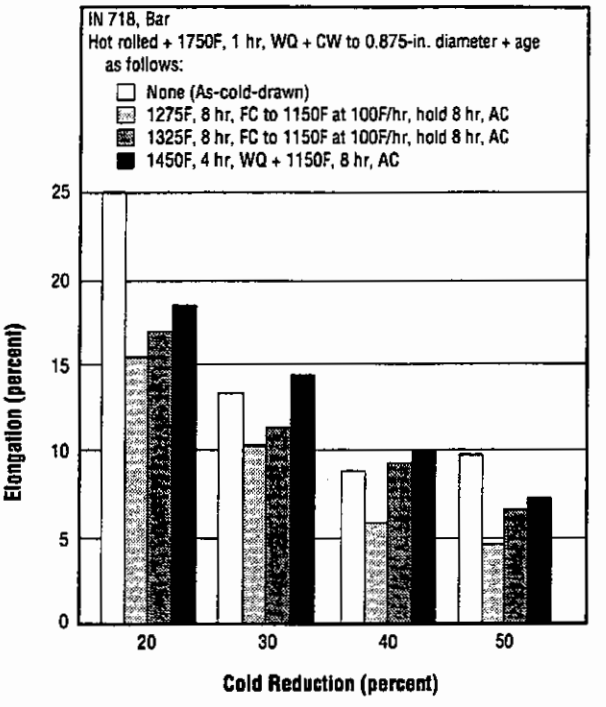

Fig. 3.2.1.12 Effects of cold drawing and various subsequent aging treatments on elongation of bar at room temperature (Ref. 55)

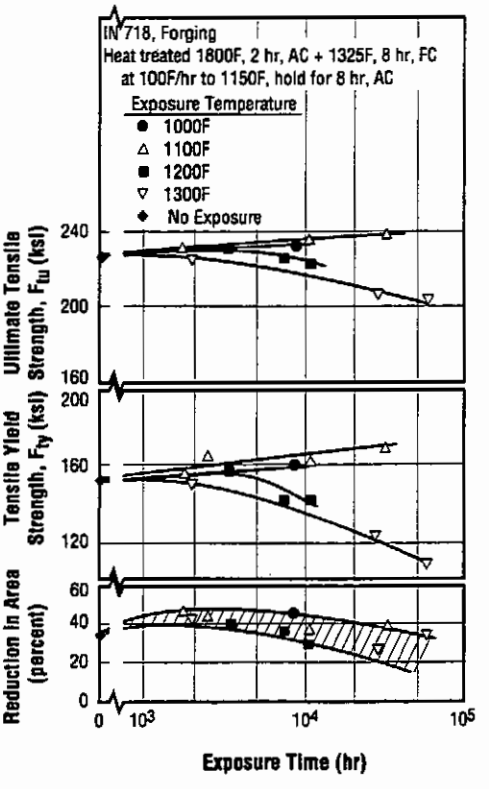

Fig. 3.2.1.13 Room-temperature tensile properties after long-time exposures to temperatures from 1000 to 1300F (Ref. 56)

Table 3.2.1.14 Effects of heat treatment and orientation on tensile properties of cast alloy at room temperature (Ref. 100)

Alloy	Inconel 718						
Ingot Number	**Ingot Condition[a]**	**Orientation**	**Aging Treatment[b]**	**F_{ty} (ksi)**	**F_{tu} (ksi)**	**e (percent)**	**RA (percent)**
1	Cast + A	T	None	95.9	100.5	1	0.5
2	As Cast	T	None	69.6	105.1	22	18
		L	None	70.8	114.0	22	20
		T	C	107.3	123.3	6	14
		L	C	110.8	134.4	7	12
3	Cast + B	T	None	100.4	135.2	22	31.4
		L	None	100.2	134.8	18	23.5
		T	C	123.3	156.1	10	17
		L	C	126.7	159.1	18	22

[a] A = 1600F, 100 hours
B = 2175F, 50 hours.

[b] C = 1325F, eight hours, FC at 180F/hour, 1150F, eight hours, AC.

Table 3.2.3.1 Charpy V-Notch impact properties at room temperature of forged and hot-rolled rounds of various sizes in two heat-treated conditions (Ref. 1)

Alloy	Inconel 718		
Form	**Diameter (in.)**	**Condition**	**Impact Energy (ft-lb)**
Forged	8	1750F, 1 hr, AC + 1325F, 8 hr, FC to 1150F, Hold for Total Age of 18 hr, AC	13
	12		24
Hot-rolled	5/8		18.5
	1		10
	1-1/2		11
Forged	8	1950F, 1 hr, AC + 1400F, 10 hr, FC to 1200F, Hold for Total Age of 20 hr, AC	35
	12		39
Hot-rolled	5/8		26
	1		33
	1-1/2		28.5

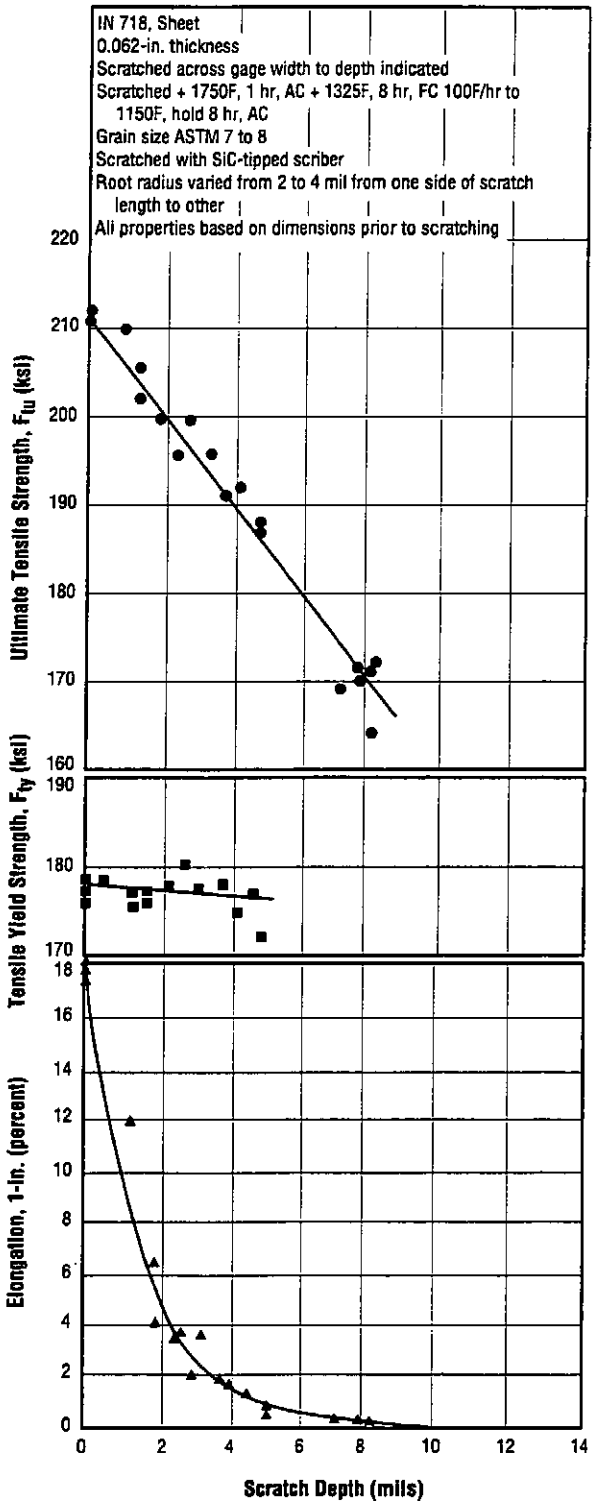

Fig. 3.2.7.1.1 Nominal tensile properties at room temperature of sheet with sharp scratches (Ref. 59)

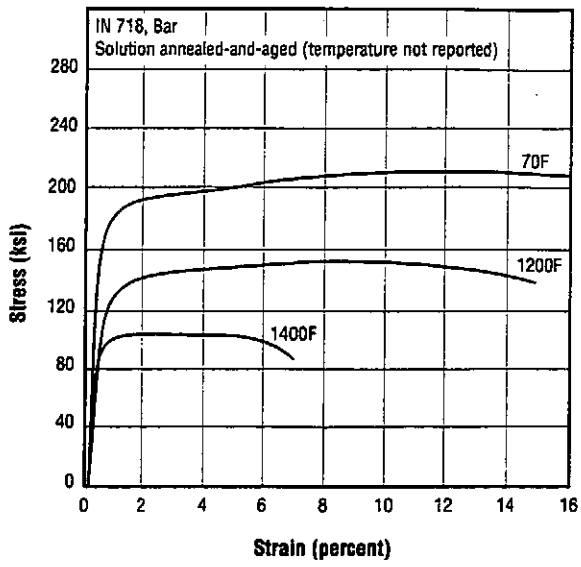

Fig. 3.3.1.1 Tensile stress-strain curves at room and elevated temperatures for solution treated-and-aged bar (Ref. 60)

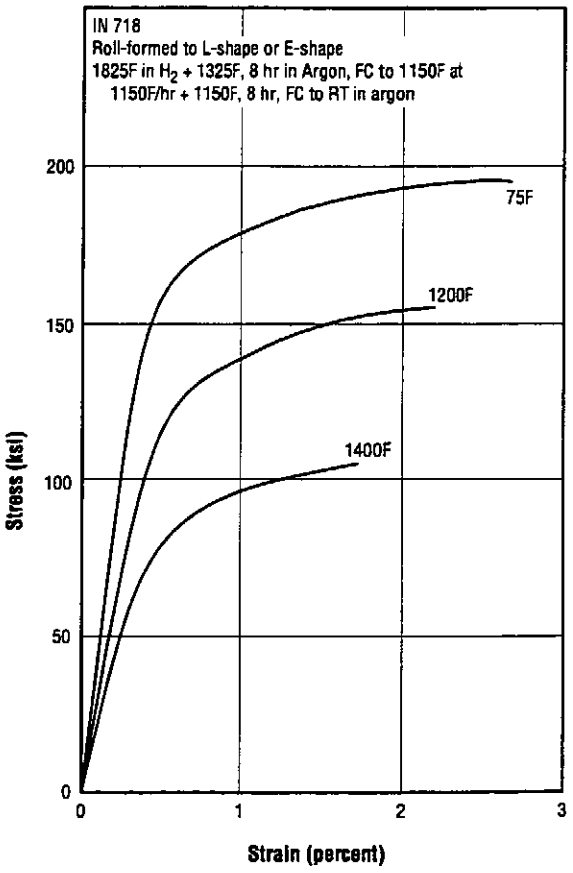

Fig. 3.3.1.2 Tensile stress-strain curves at room and elevated temperatures for specimens cut from roll-formed E and L shapes (Ref. 62)

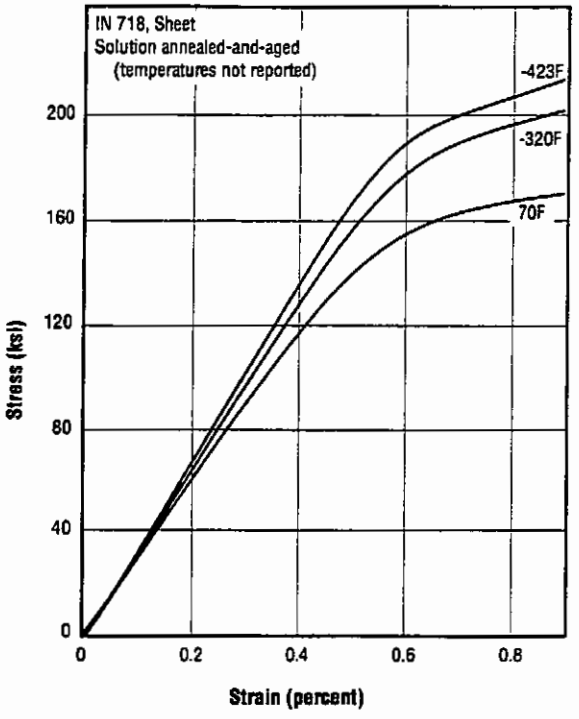

Fig. 3.3.1.3 Tensile stress-strain curves for sheet at room and low temperatures (Ref. 61)

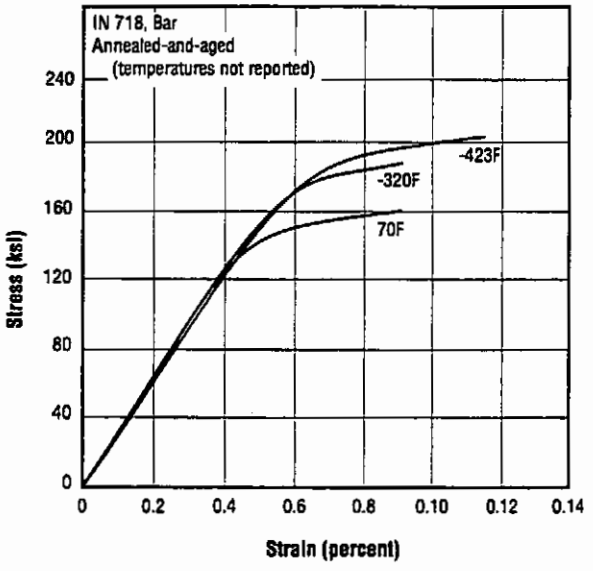

Fig. 3.3.1.4 Tensile stress-strain curves for bar at room and low temperatures (Ref. 61)

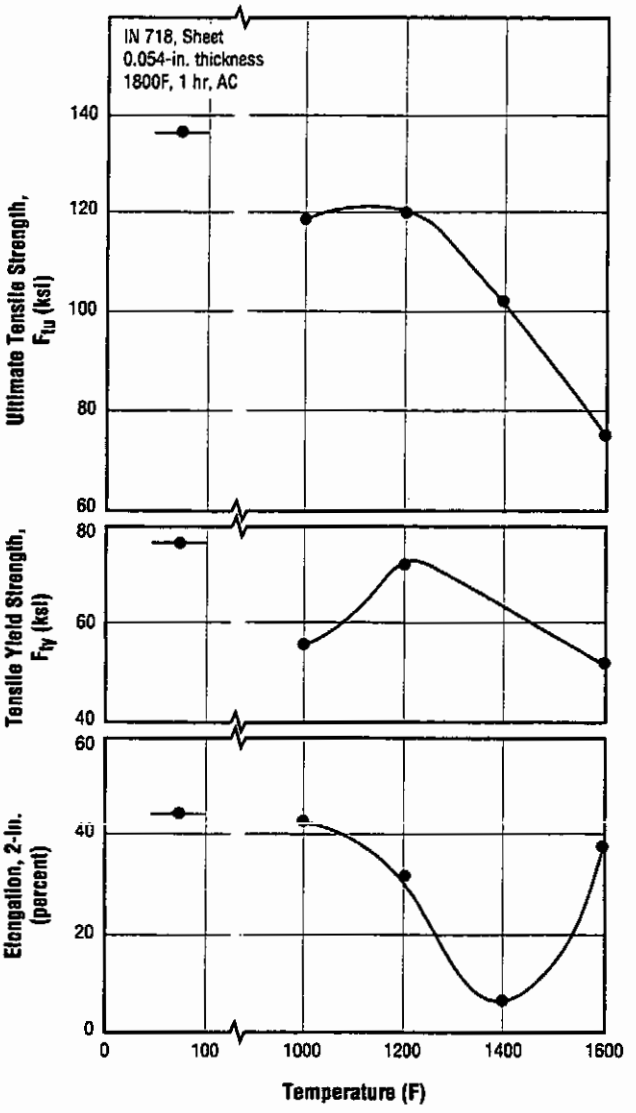

Fig. 3.3.1.5 Effect of temperature up to 1600F on tensile properties of annealed sheet (Ref. 1)

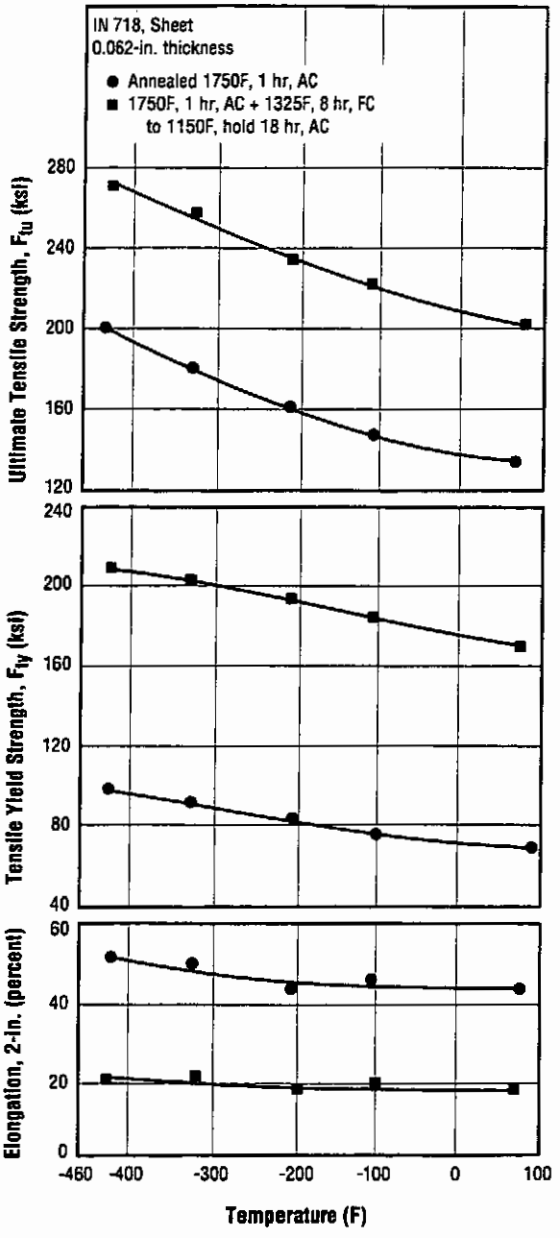

Fig. 3.3.1.6 Effects of low temperatures on the tensile properties of sheet in the annealed and annealed-and-aged conditions (Ref. 63)

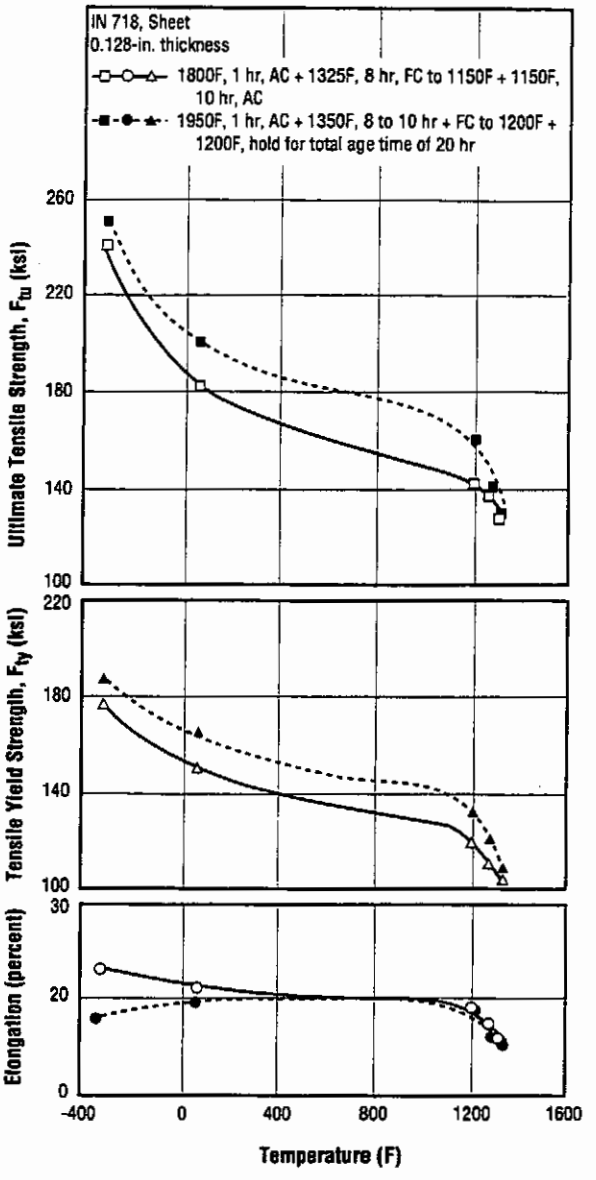

Fig. 3.3.1.7 Effects of temperatures from -320 to 1350F on tensile properties of sheet in two heat-treated conditions (Ref. 45)

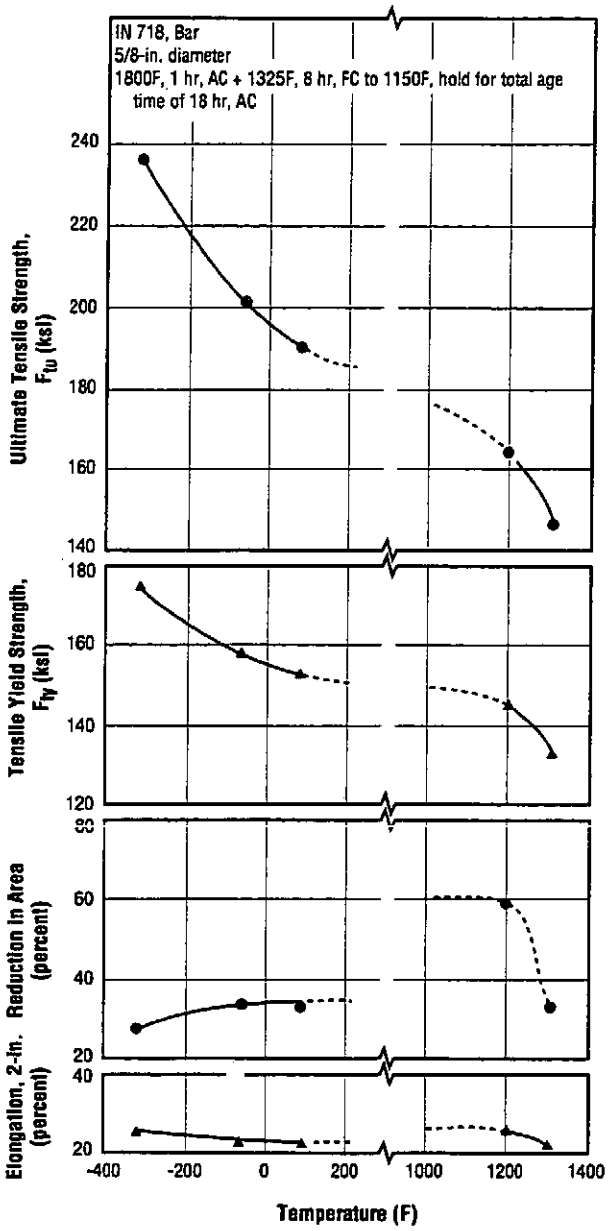

Fig. 3.3.1.8 Tensile properties of annealed-and-aged bar at temperatures from -320 to 1300F (Ref. 1)

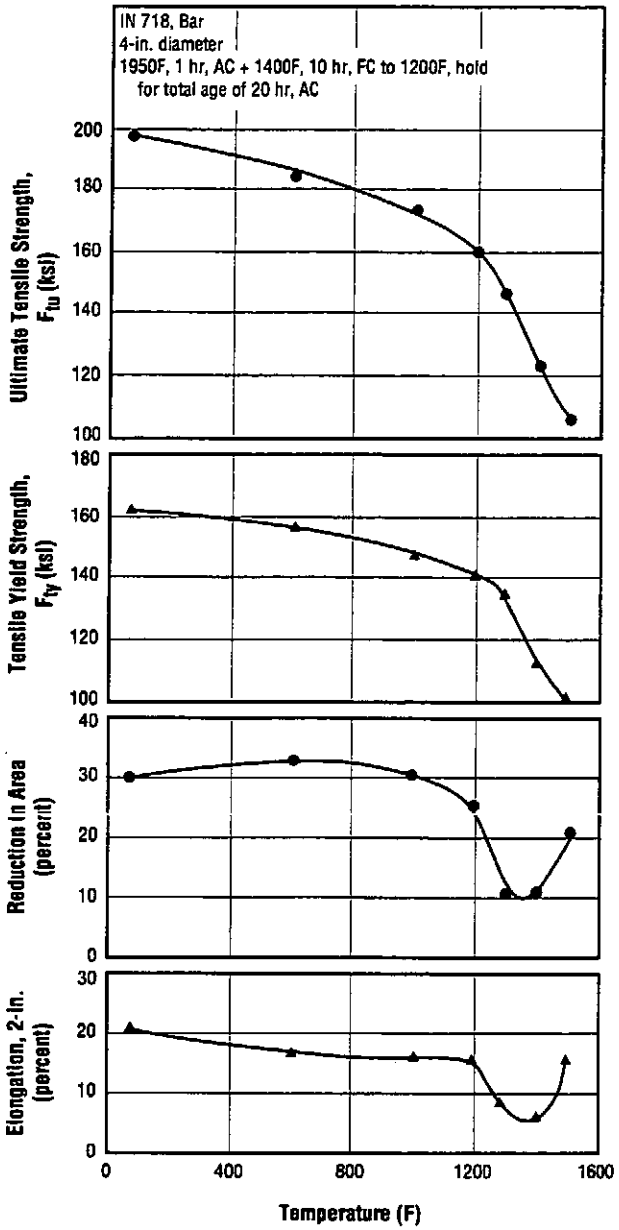

Fig. 3.3.1.9 Effect of elevated temperatures on tensile properties of annealed-and-aged bar (Ref. 1)

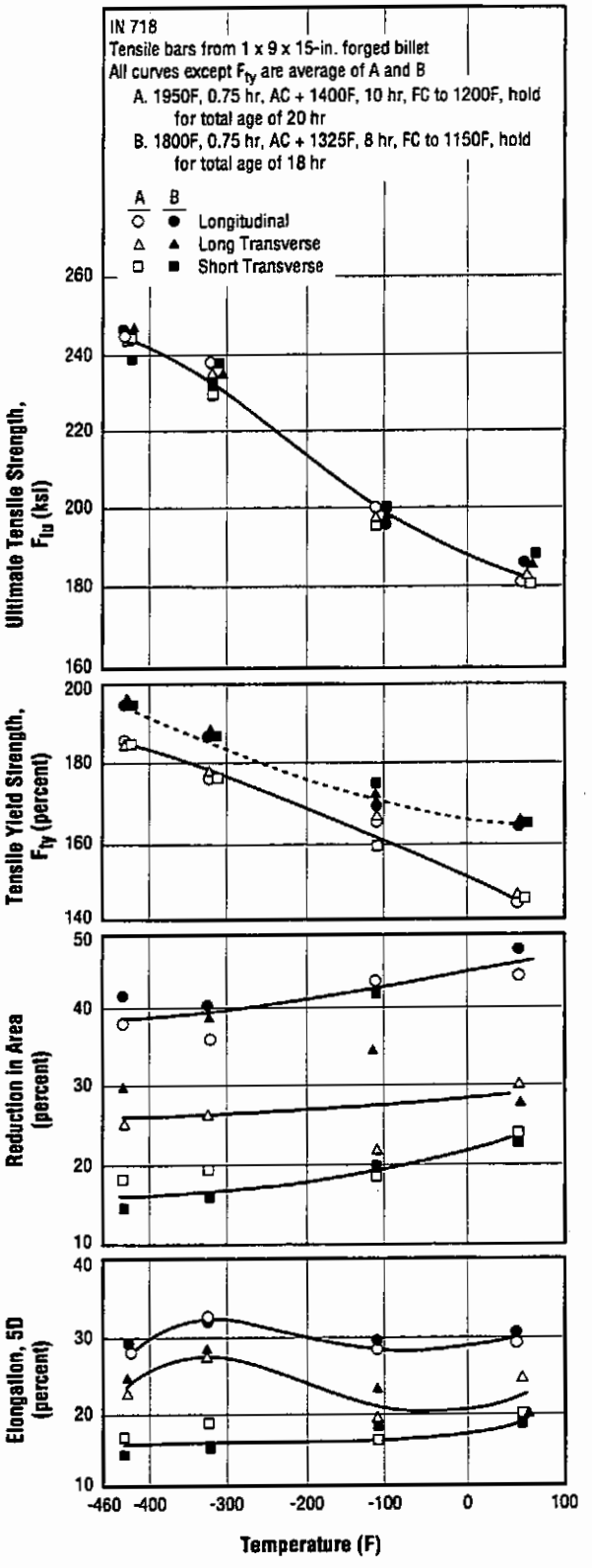

Fig. 3.3.1.10 Effects of low temperatures on tensile properties of forging in three principal orientations after two different heat treatments (Ref. 64)

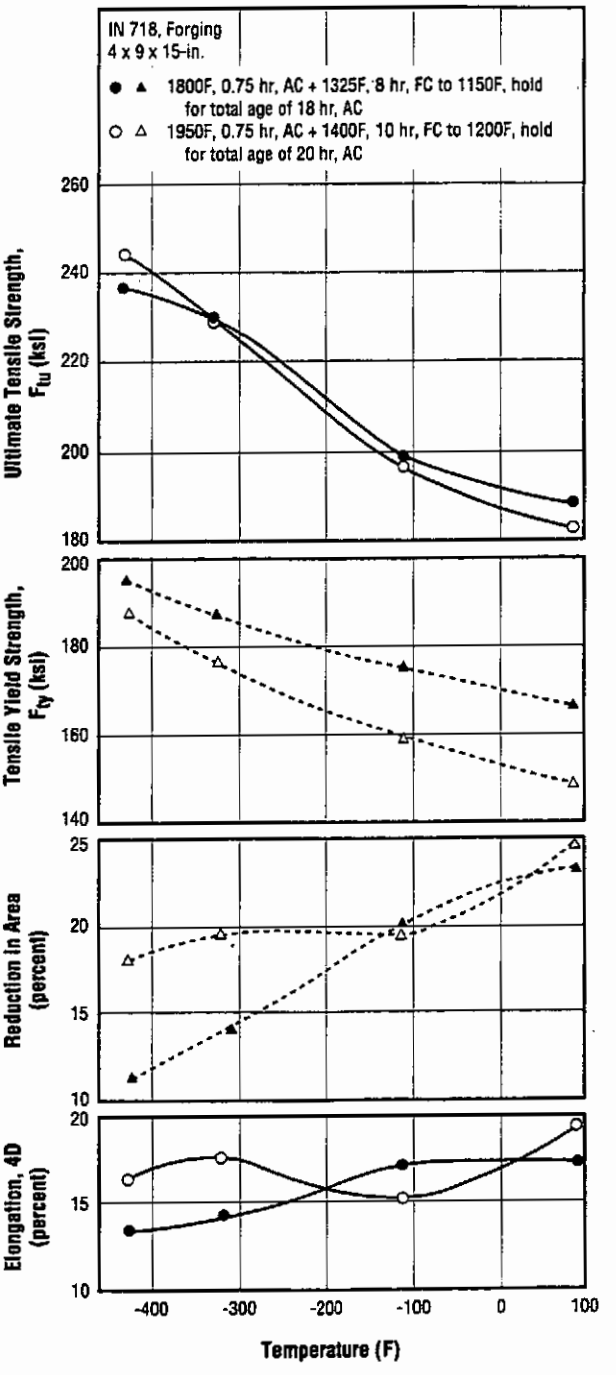

Fig. 3.3.1.11 Effects of low temperatures on short-transverse tensile properties of forging in two annealed-and-aged conditions (Ref. 1)

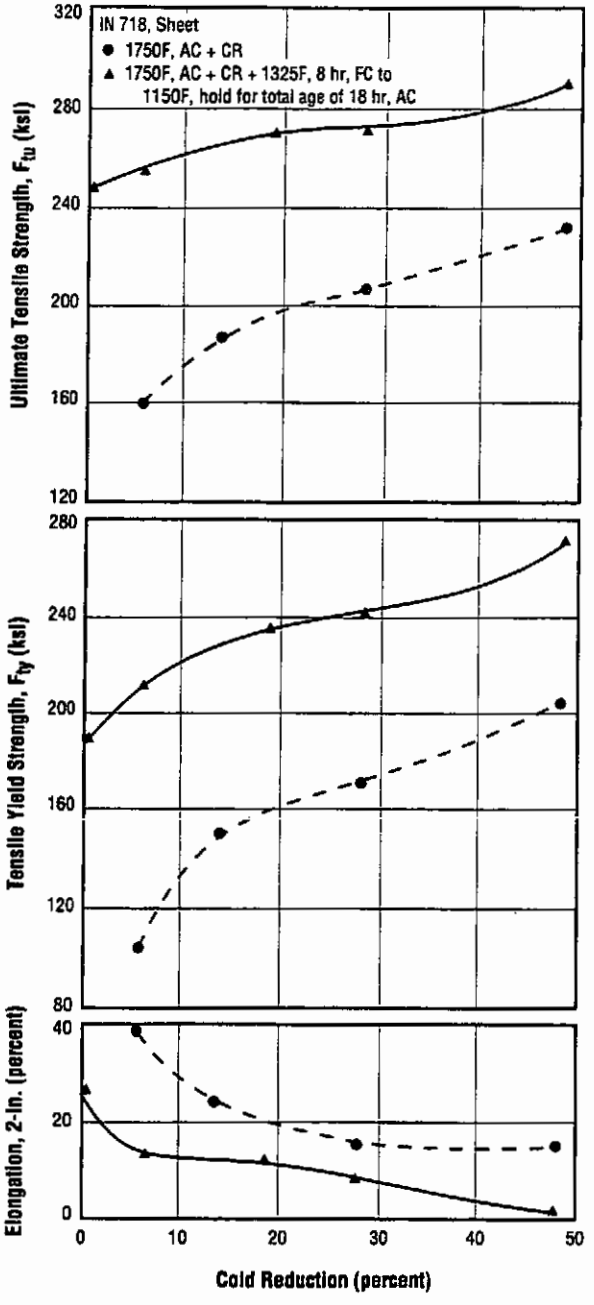

Fig. 3.3.1.12 Effects of cold rolling and aging on tensile properties of sheet at -320F (Ref. 1)

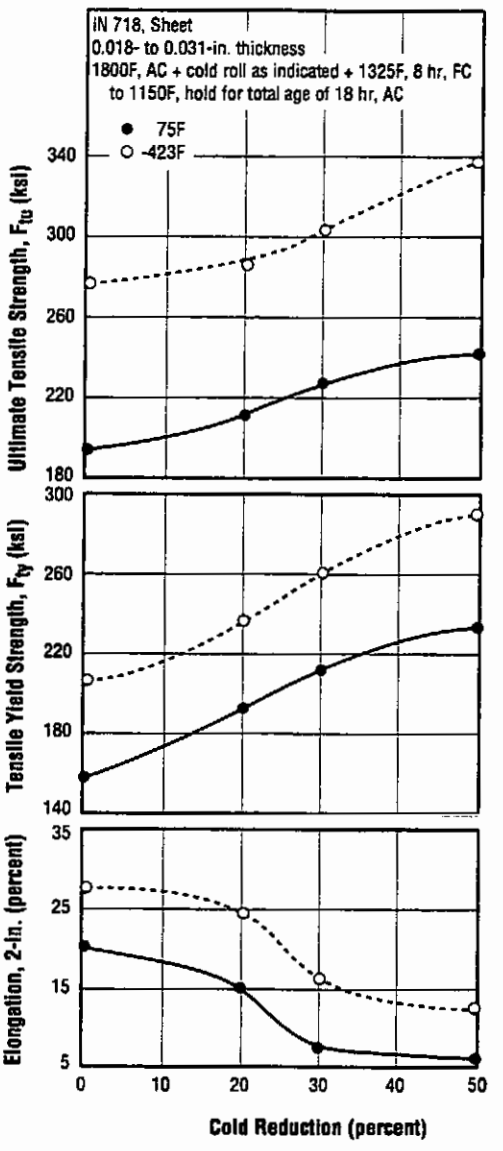

Fig. 3.3.1.13 Tensile properties at 75 and -423F of sheet cold rolled various amounts prior to aging (Ref. 1)

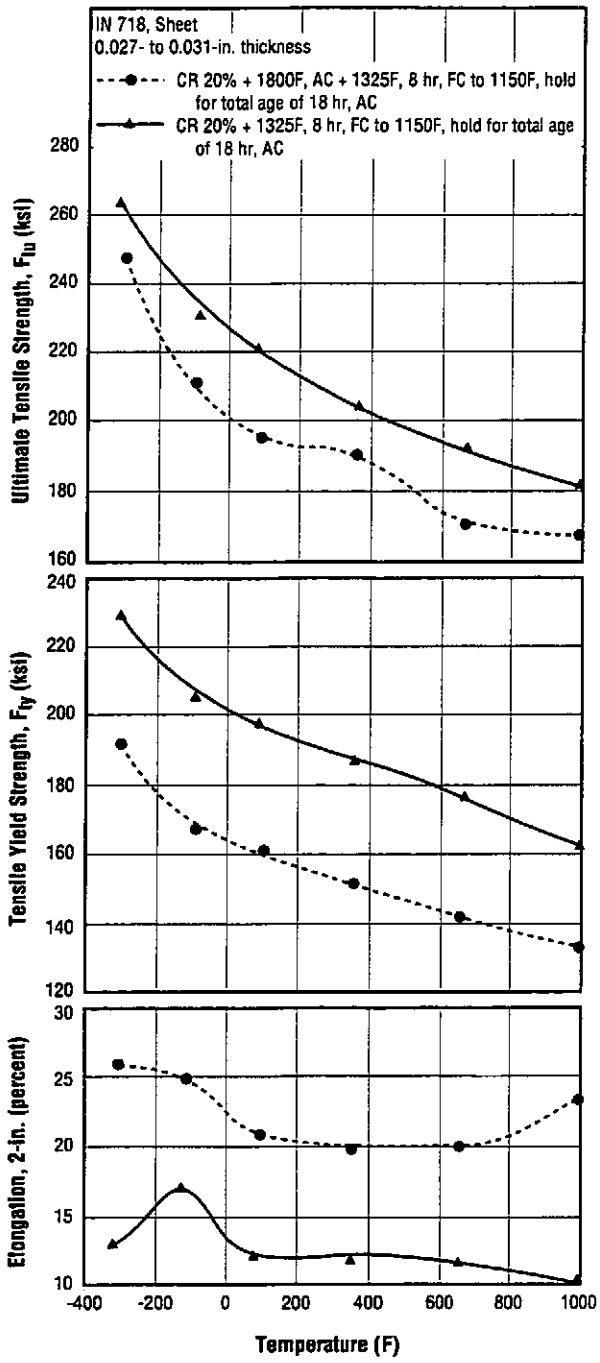

Fig. 3.3.1.14 Tensile properties at low and high temperatures of sheet cold-rolled and subsequently heat treated in two different manners (Ref. 1)

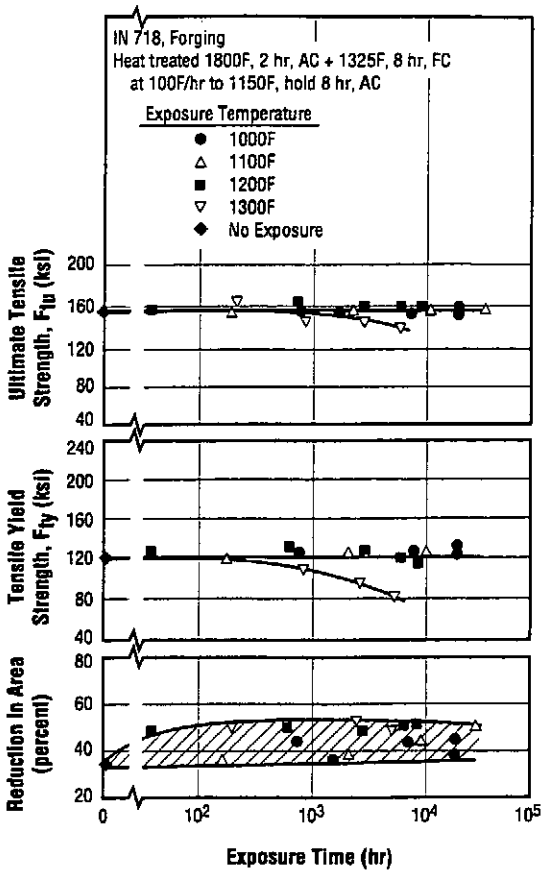

Fig. 3.3.1.15 Tensile properties of forging at 1200F after long-time exposure to temperatures from 1000 to 1300F (Ref. 56)

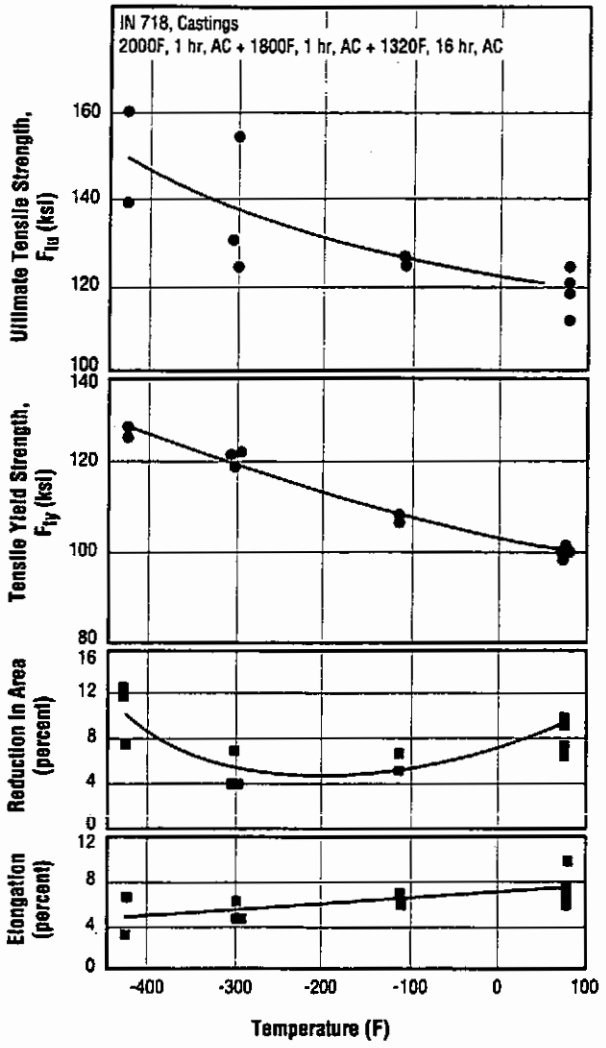

Fig. 3.3.1.16 Effect of low temperatures on the tensile properties of annealed-and-aged castings (Ref. 66)

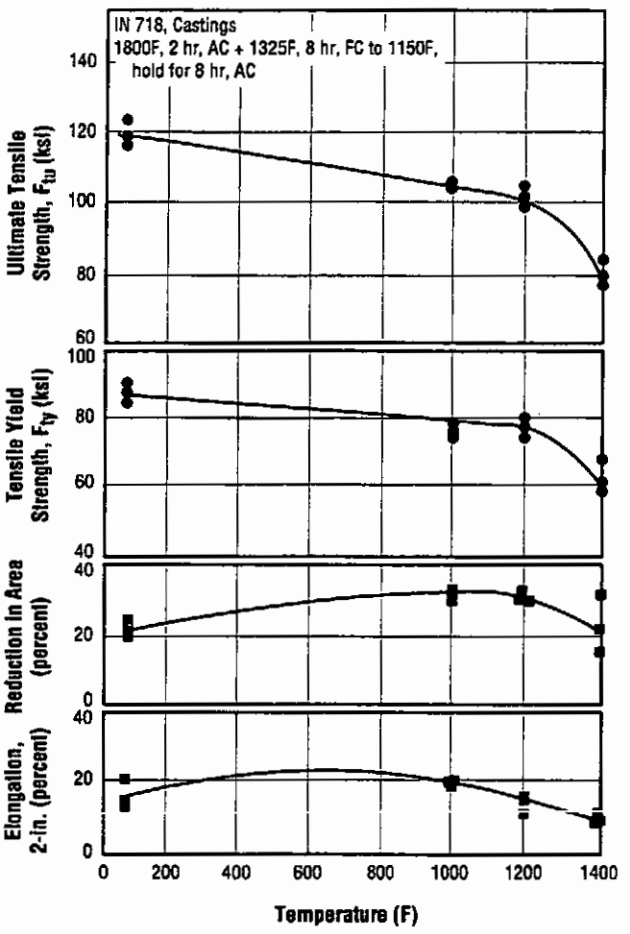

Fig. 3.3.1.17 Effect of elevated temperatures on tensile properties of annealed-and-aged castings (Ref. 67)

Table 3.3.1.18 Effect of hot-isostatic-pressing (HIP) on tensile properties of precision castings at 75 and 1100F (Ref. 24)

Alloy	Inconel 718				
Form	Castings				
Condition[a]	Test Temperature (F)	F_{ty} (ksi)	F_{tu} (ksi)	e, 2-in. (percent)	RA (percent)
HT	75	126	156	10.5	17
HIP + HT		115	147	27.5	37
HT	1100	96	116	18	28
HIP + HT		101	118	28	35

[a] HT = 2000F, one hour, AC + 1750F, one hour, AC + 1325F, eight hours, FC to 1150F, hold for total age of 18 hours, AC.
HIP = 2150F, three hours at 15,000 psi in argon.

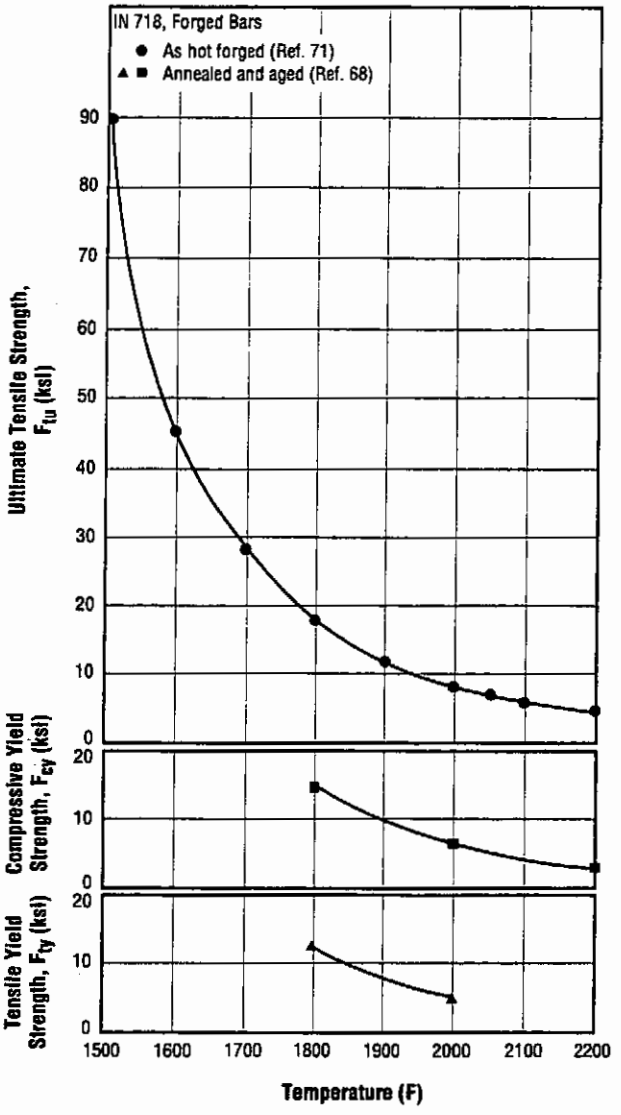

Fig. 3.3.2.1 Tensile and compressive strength properties of forged bars at high temperatures in the hot-working range (Refs. 68, 71)

Table 3.3.3.1 Impact properties of annealed-and-aged plate at room temperature and -320F (Ref. 1)

Alloy	Inconel 718	
Form	1-in. Plate	
Condition	1800F, 1 hr, AC + 1325F, 8 hr, FC to 1150F, Hold for Total Age of 18 hr, AC	
Temperature (F)	**Impact Energy (ft-lb)**	
	Charpy Keyhole	**Charpy V-Notch**
75	16.2	20.8
-320	14.0	19.0

Table 3.3.3.2 Effects of heat treatment and low temperatures on Charpy V-Notch impact properties of plate (Ref. 34)

Alloy	Inconel 718		
Form	1-in. Plate		
Condition	**Temperature (F)**	**Impact Energy (ft-lb)**	
		L	**T**
1750F, 1 hr, AC	75	—	46
	-80	—	41
1750F, 1 hr, AC + age[a]	75	22	14
	-80	18	11

[a] Age 1325F, eight hours, FC to 1150F, hold for total age of 18 hours, AC.

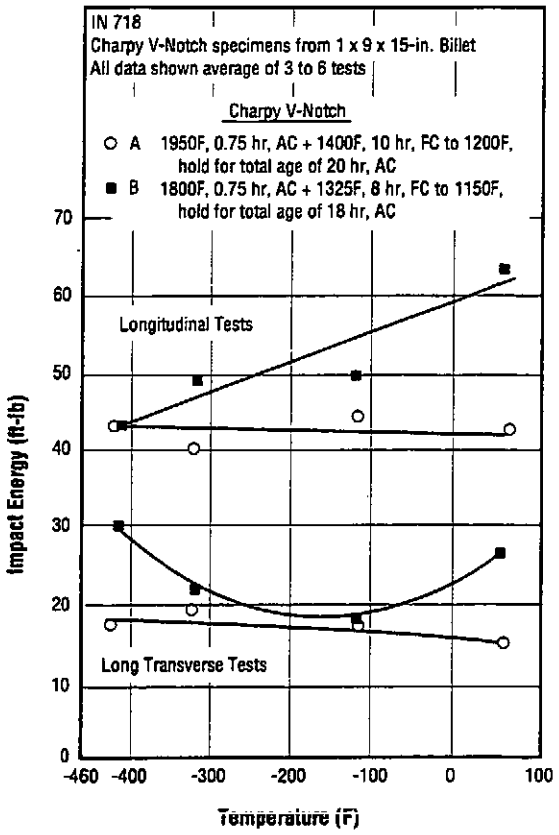

Fig. 3.3.3.3 Effects of low temperatures on longitudinal and transverse impact properties of forgings in two heat-treated conditions (Ref. 64)

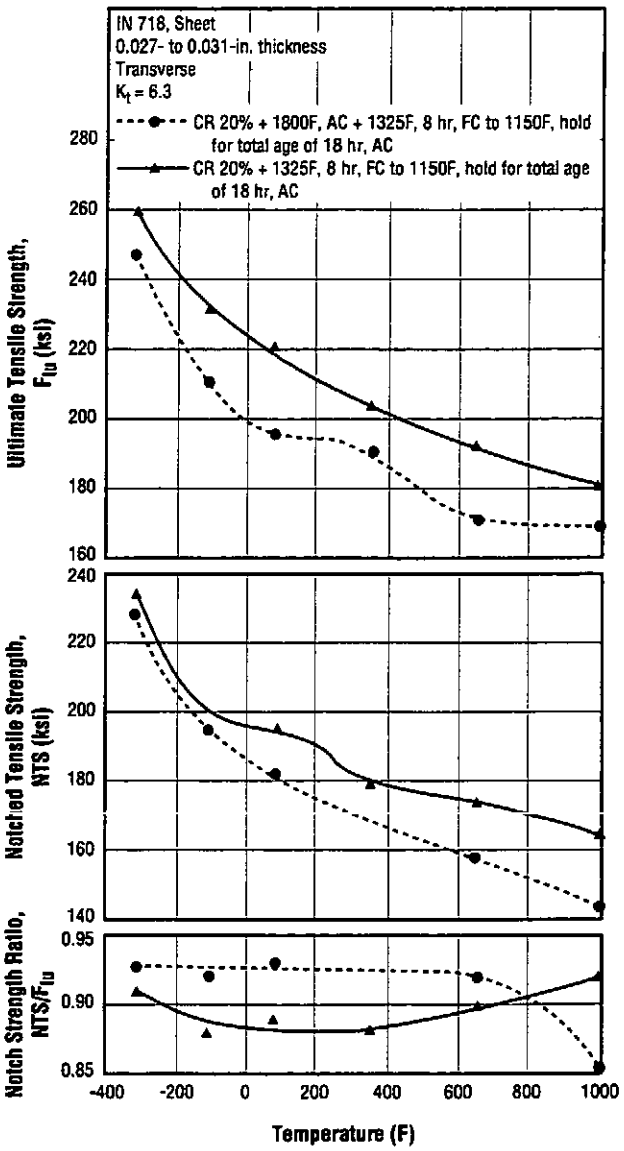

Fig. 3.3.7.1.1 Comparison of tensile strength and notched tensile strength of sheet at various temperatures after cold rolling and subsequent heat treatment in two different manners (Ref. 1)

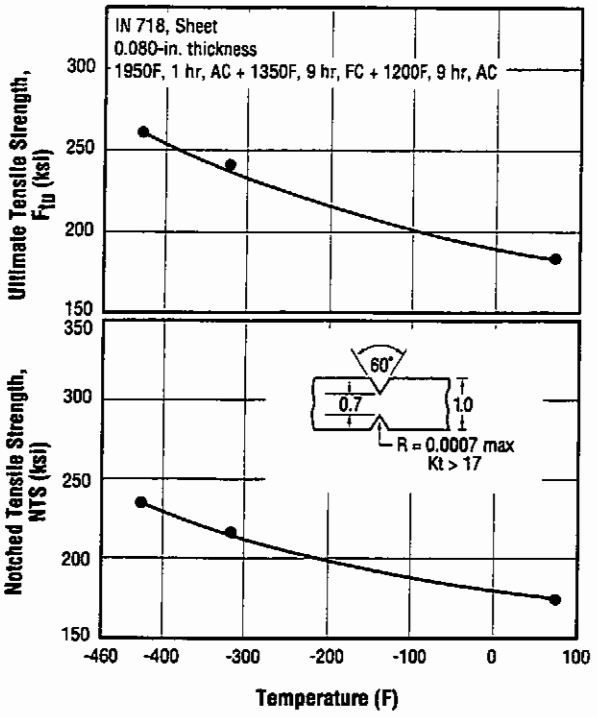

Fig. 3.3.7.1.2 Comparison of tensile strength and notched tensile strength of annealed-and-aged sheet at low temperatures (Ref. 49)

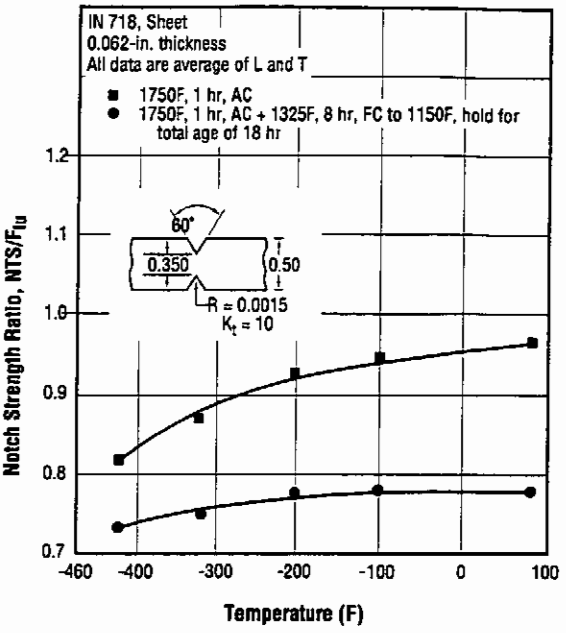

Fig. 3.3.7.1.3 Effect of low temperatures on notch strength ratio (K_t = 10) of sheet in two heat-treated conditions (Ref. 63)

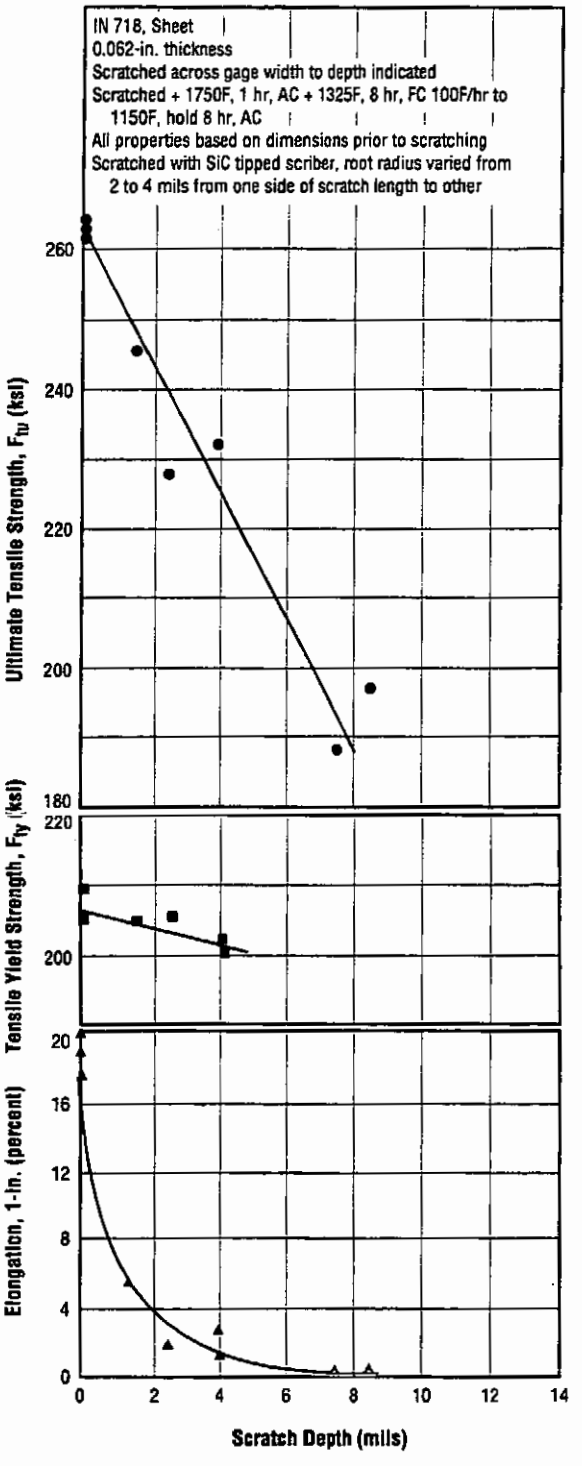

Fig. 3.3.7.1.4 Nominal tensile properties at -320F of sheet with sharp scratches (Ref. 59)

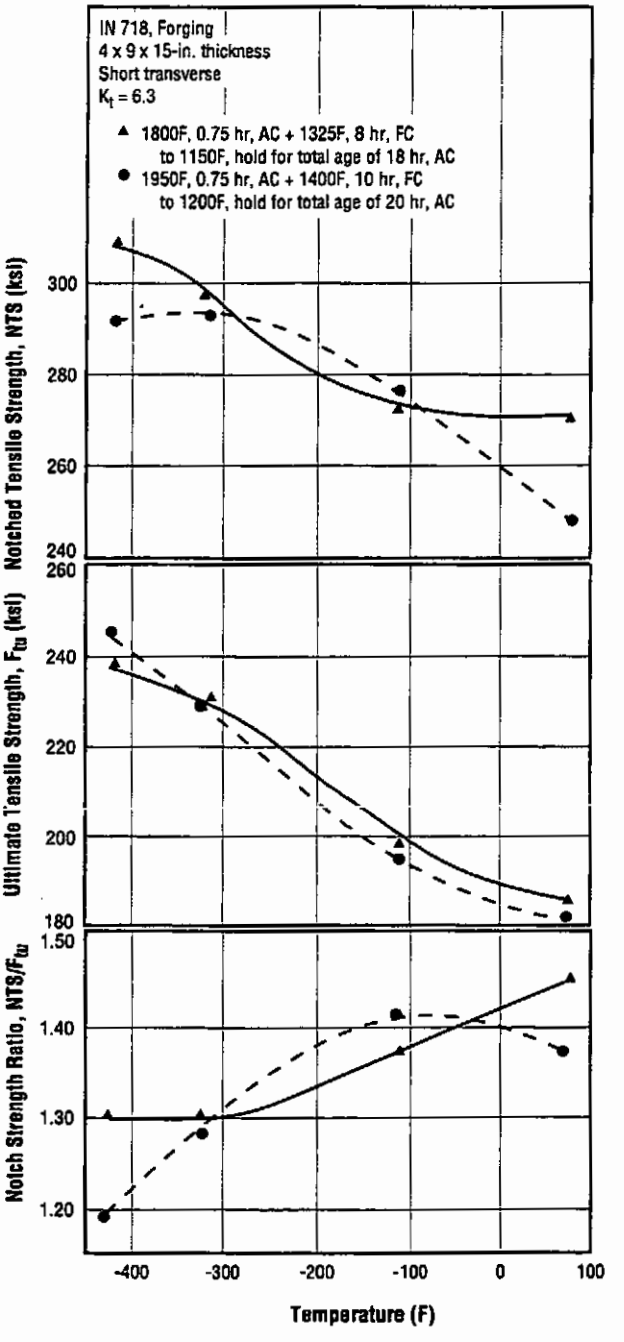

Fig. 3.3.7.1.5 Comparison of tensile strength and notch tensile strength of annealed-and-aged forging at low temperatures (Ref. 1)

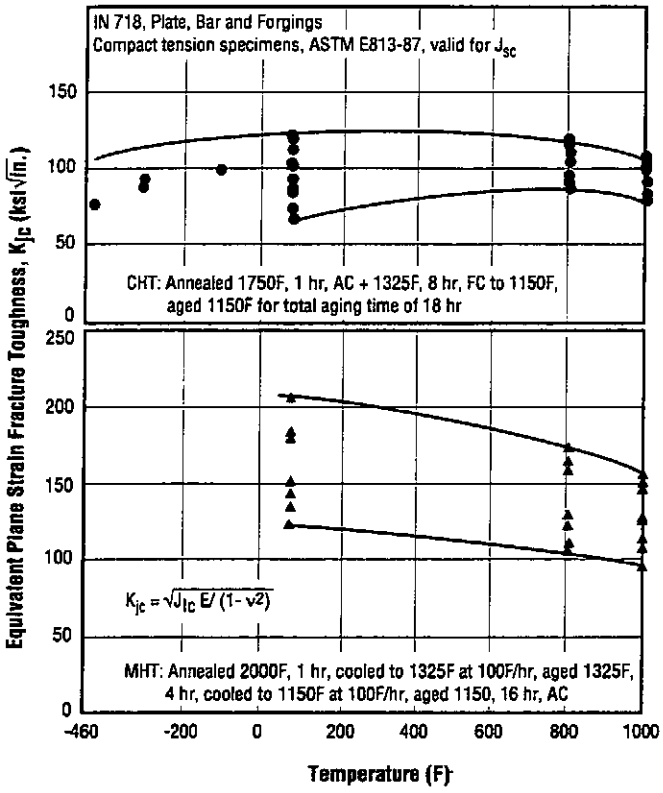

Fig. 3.3.7.2.1 Effects of heat treatment on equivalent fracture toughness at temperature to 1000F (Ref. 127)

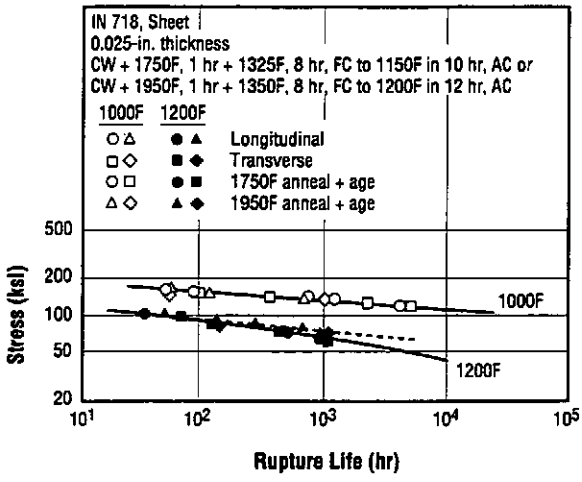

Fig. 3.4.2 Creep rupture curves for sheet at 1000 and 1200F (Ref. 44)

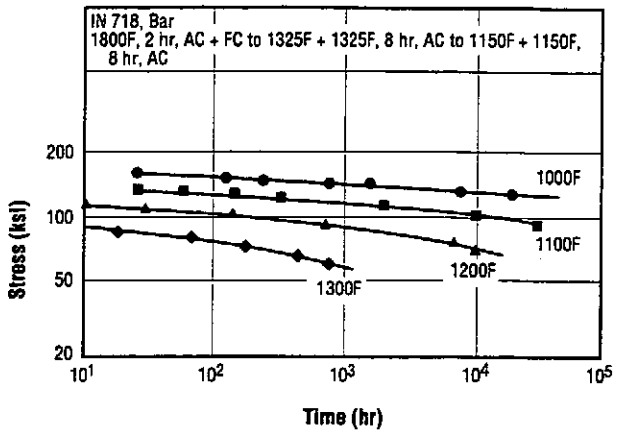

Fig. 3.4.1 Creep rupture curves for bar in the temperature range 1000 to 1300F (Ref. 41)

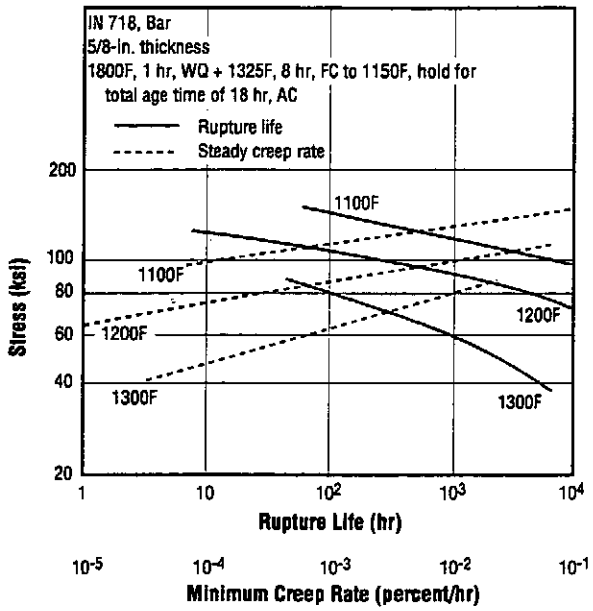

Fig. 3.4.3 Rupture life and steady creep rate of bar as functions of stress in the temperature range 1100 to 1300F (Ref. 1)

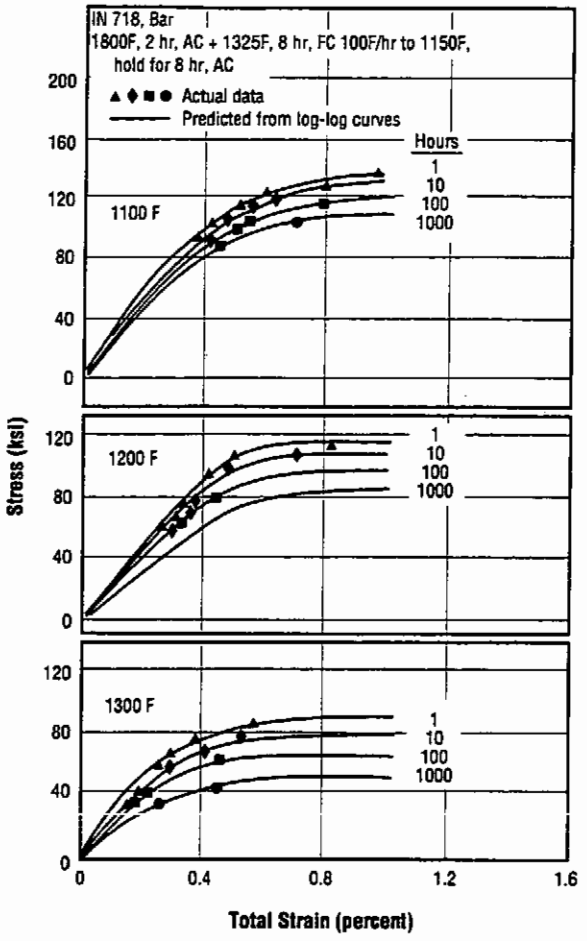

Fig. 3.4.4 Isochronous stress-strain curves at 1100, 1200, and 1300F for time range 1 to 1000 hours (Ref. 40)

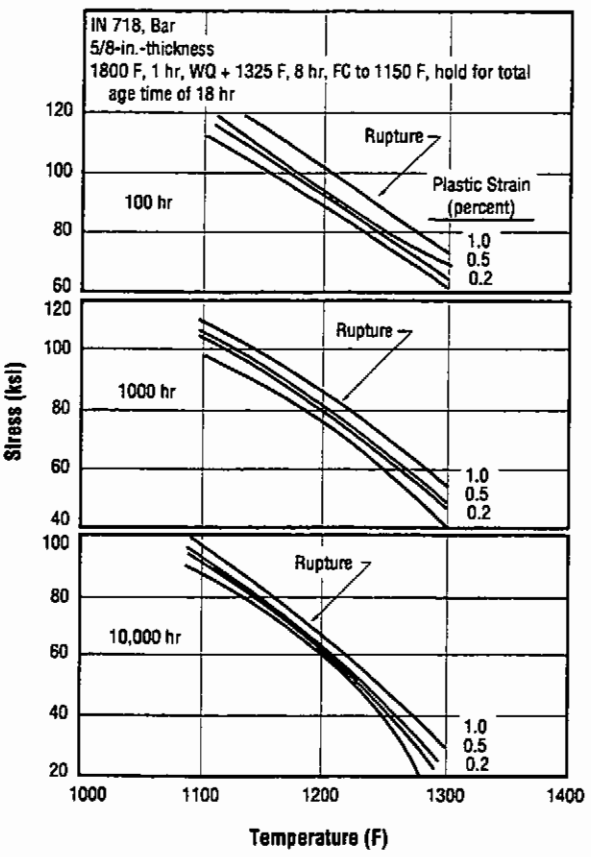

Fig. 3.4.5 Stresses required to cause various amounts of creep and rupture in 100, 1000, and 10,000 hours at temperatures from 1100 to 1300F (Ref. 1)

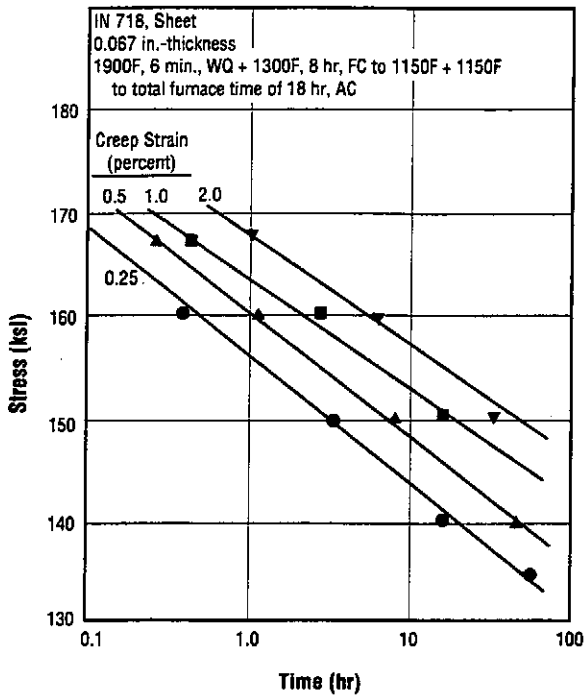

Fig. 3.4.6 Time to various amounts of creep strain as a function of stress for sheet in longitudinal orientation at 1000F (Ref. 42)

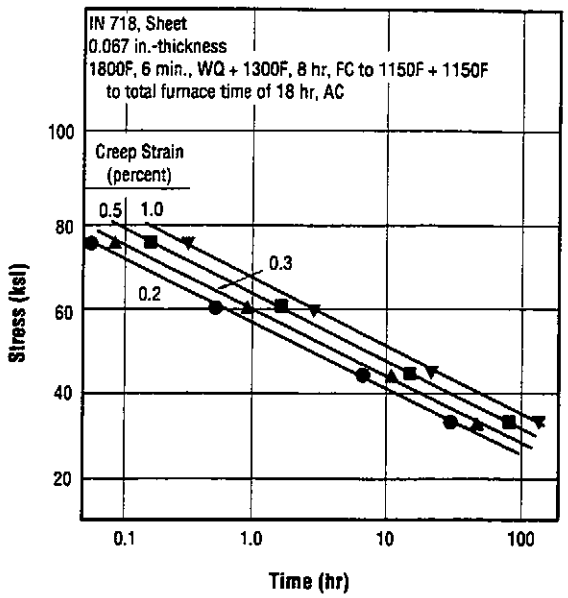

Fig. 3.4.7 Time to various amounts of creep strain as a function of stress for sheet in longitudinal orientation at 1400F (Ref. 42)

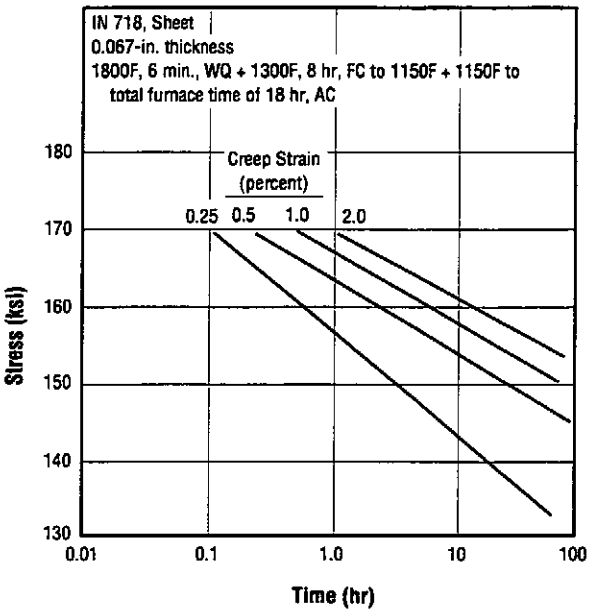

Fig. 3.4.8 Time to various amounts of creep strain as a function of stress for sheet in transverse orientation at 1000F (Ref. 42)

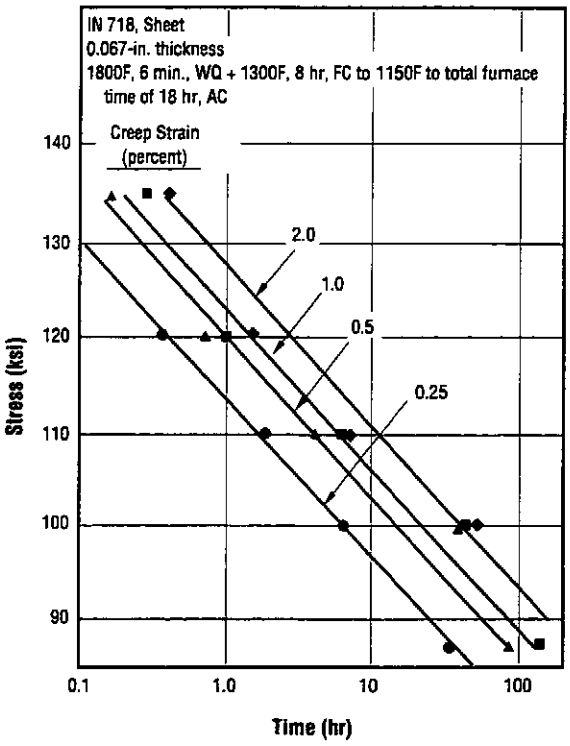

Fig. 3.4.9 Time to various amounts of creep strain as a function of stress for sheet in transverse orientation at 1200F (Ref. 42)

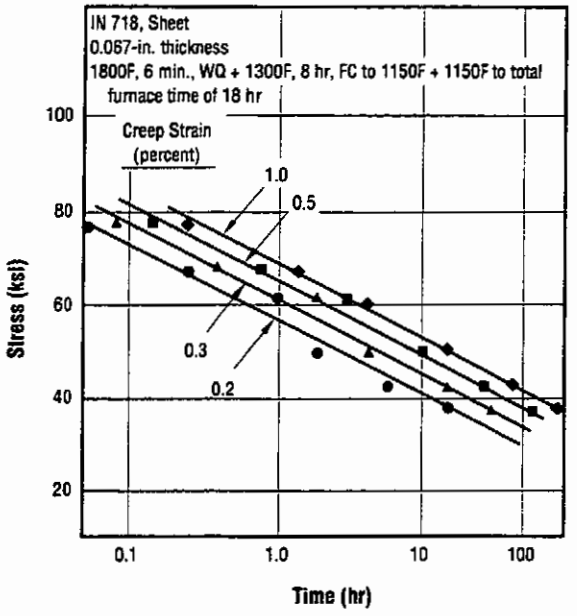

Fig. 3.4.10 Time to various amounts of creep strain as a function of stress for sheet in transverse orientation at 1400F (Ref. 42)

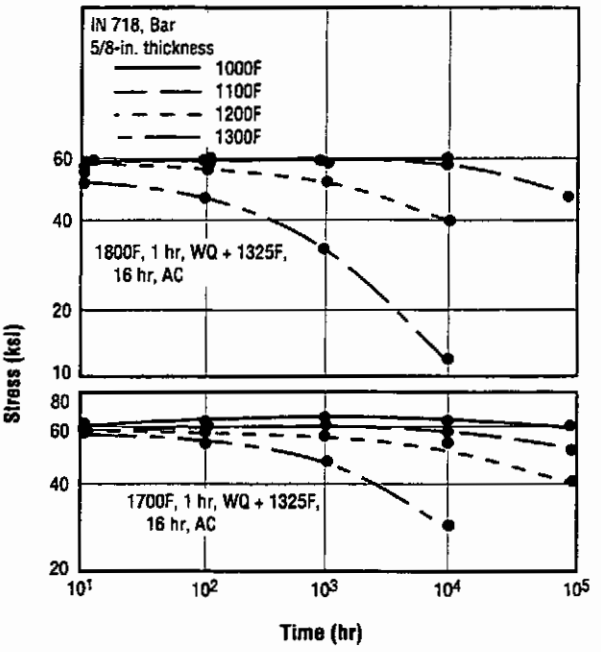

Fig. 3.4.11 Stress relaxation of bar loaded in tension to 60 ksi at various temperatures and held at constant strain for times up to 10,000 hours (Ref. 46)

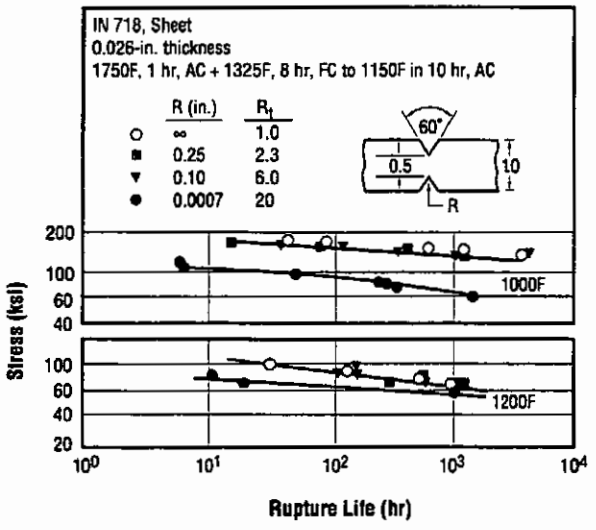

Fig. 3.4.12 Effects of notch acuity on the creep rupture properties of sheet at 1000 and 1200F (Ref. 43)

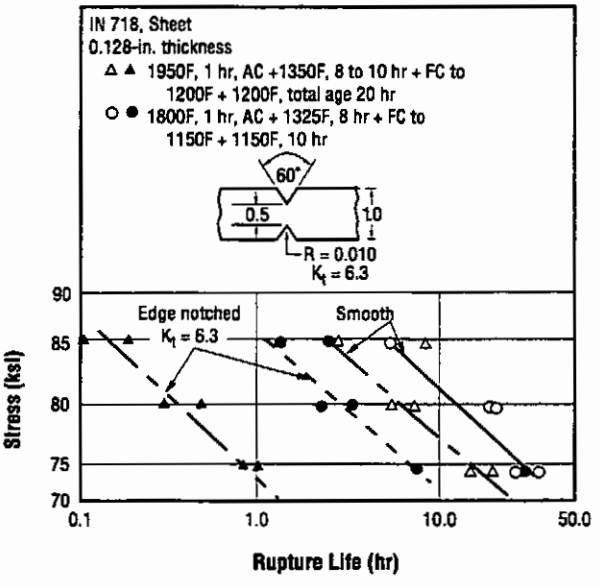

Fig. 3.4.13 Creep rupture curves for smooth and notched sheet specimens at 1350F (Ref. 45)

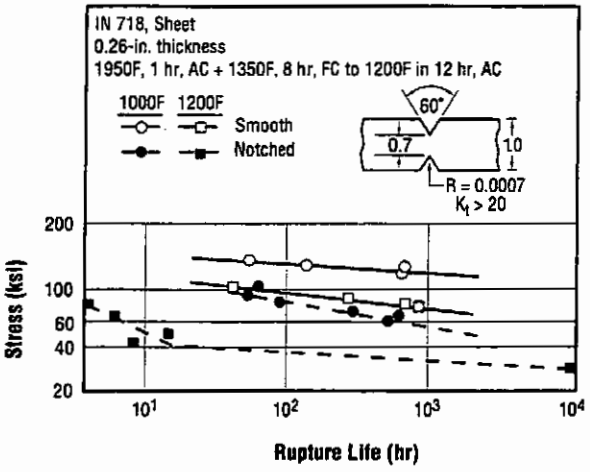

Fig. 3.4.14 Creep rupture curves at 1000 and 1200F for smooth and sharp-notched sheet specimens in the annealed-and-aged condition (Ref. 43)

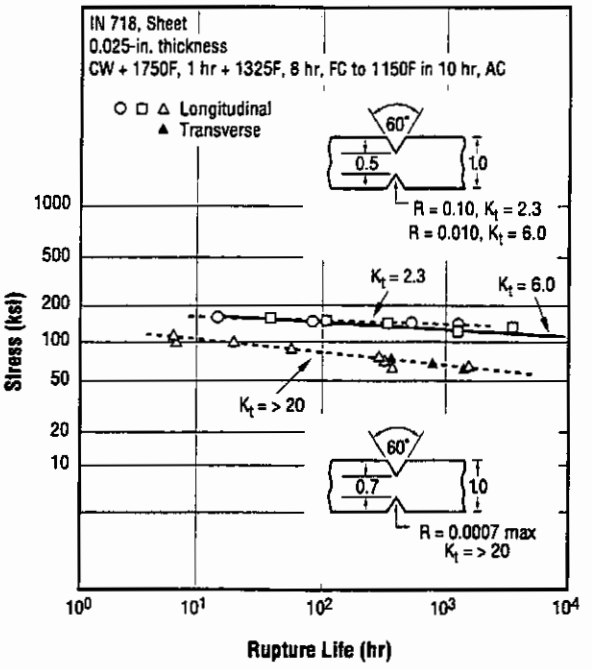

Fig. 3.4.15 Effects of notch acuity on the notched creep rupture properties of sheet at 1000F (Ref. 44)

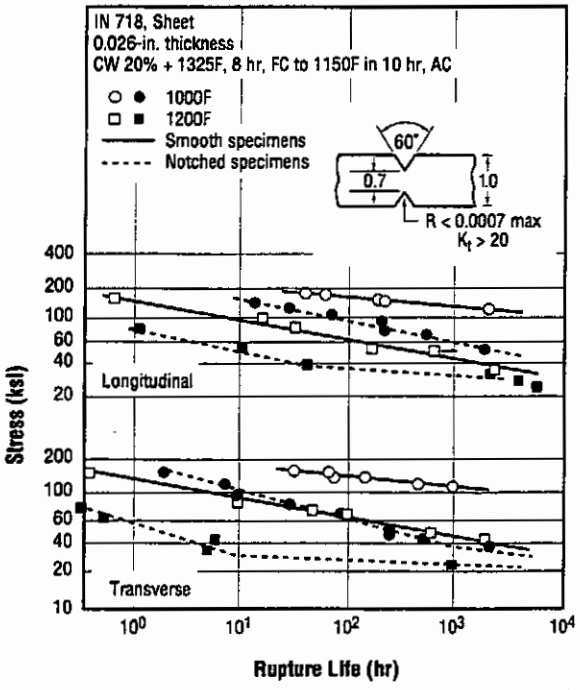

Fig. 3.4.16 Creep rupture curves at 1000 and 1200F for smooth and sharp-notched specimens in the cold-worked-and-aged condition (Ref. 43)

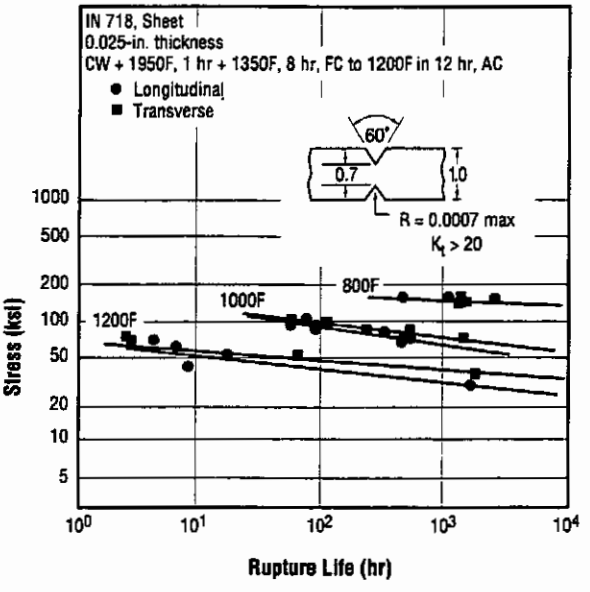

Fig. 3.4.17 Creep rupture curves for sharp-notched sheet at 800 to 1200F (Ref. 44)

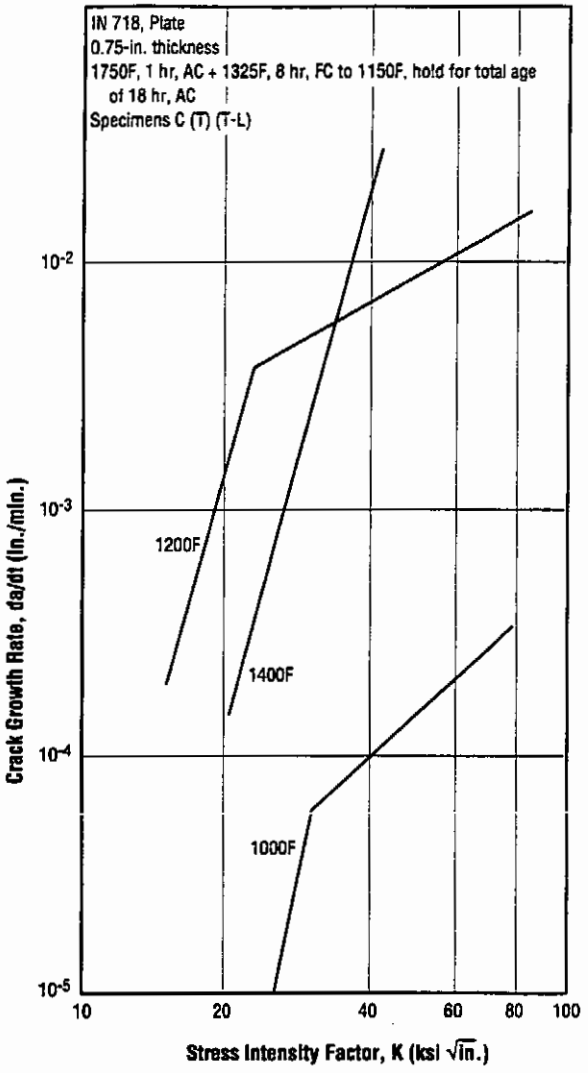

Fig. 3.4.18 Creep crack growth rates of plate at 1000, 1200, and 1400F in air (Ref. 76)

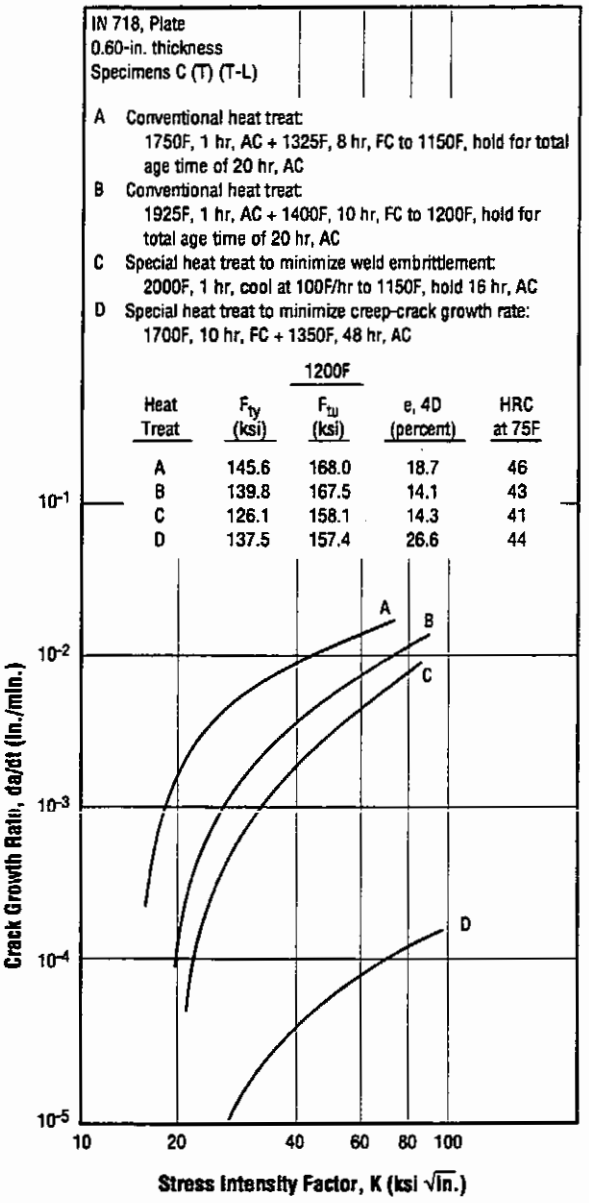

Fig. 3.4.19 Effects of various heat treatments on creep crack growth rate at 1200F in air (Ref. 33)

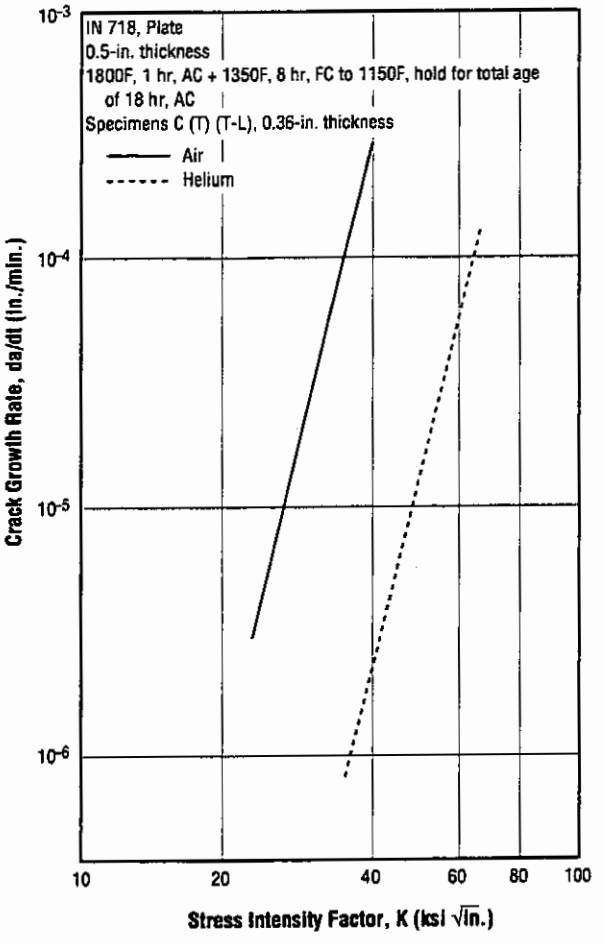

Fig. 3.4.20 Creep crack growth rates of plate at 1200F in environments of air and helium (Ref. 16)

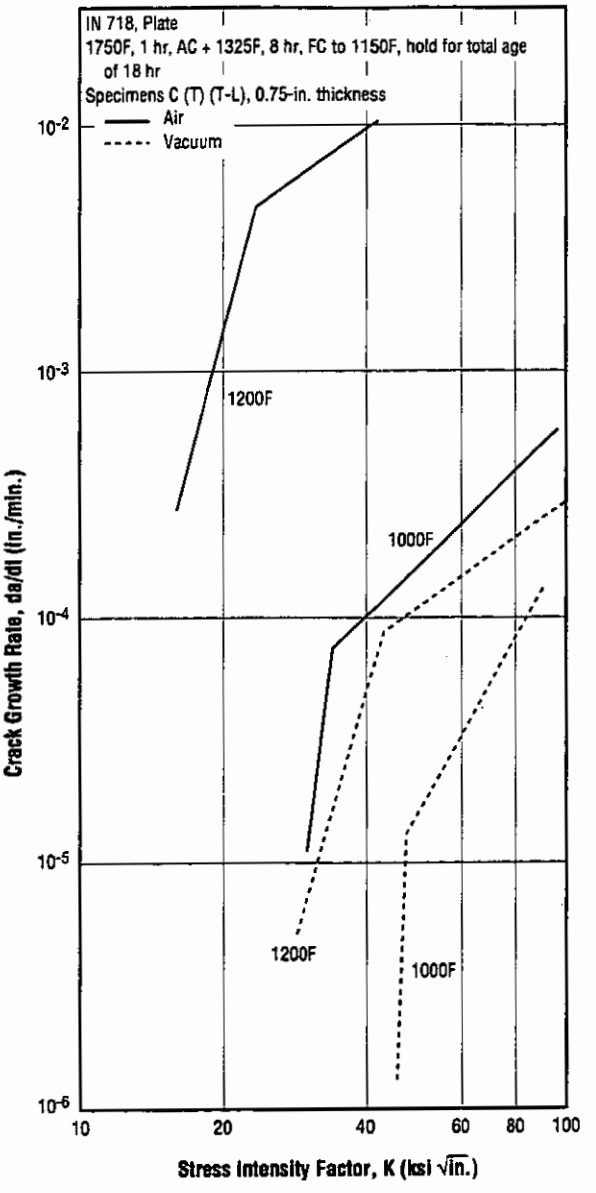

Fig. 3.4.21 Creep crack growth rates of plate at 1000 and 1200F in air and vacuum (Ref. 80)

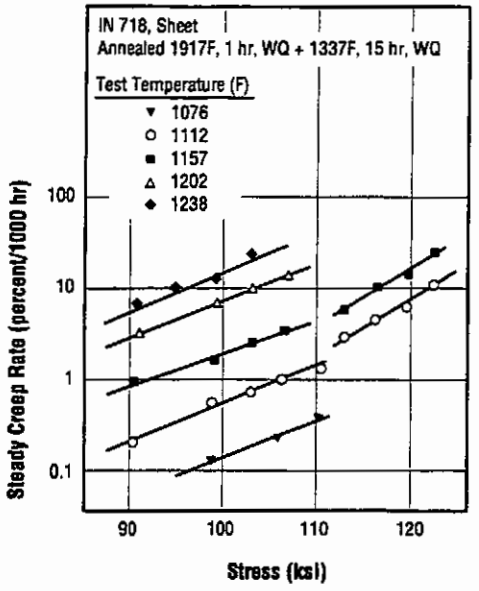

Fig. 3.4.22 Steady creep rate behavior at 1076 to 1238F in argon (Ref. 128)

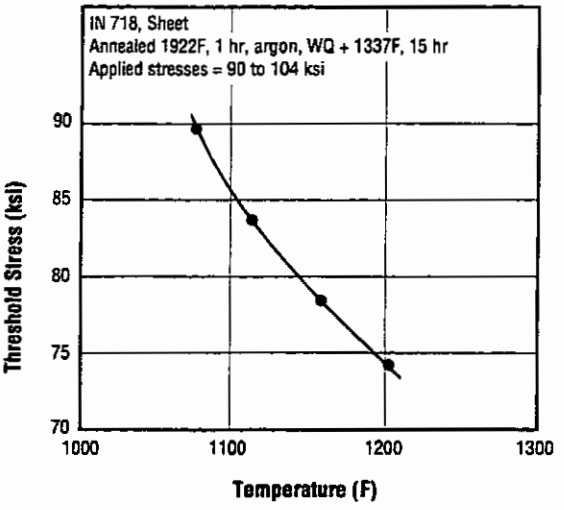

Fig. 3.4.23 Effect of temperature on threshold stress for diffusional creep in argon (Ref. 129)

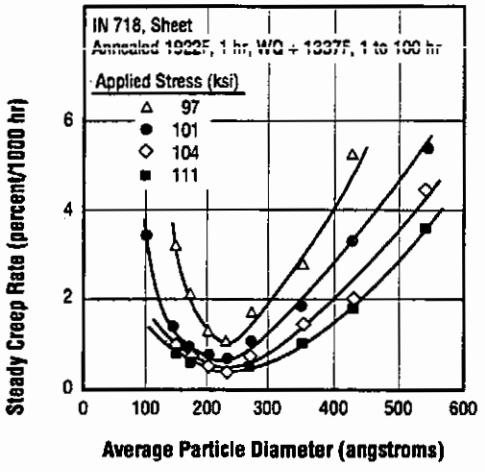

Fig. 3.4.24 Effects of gamma-double-prime particle size on steady creep rates at 1112F in argon (Ref. 130)

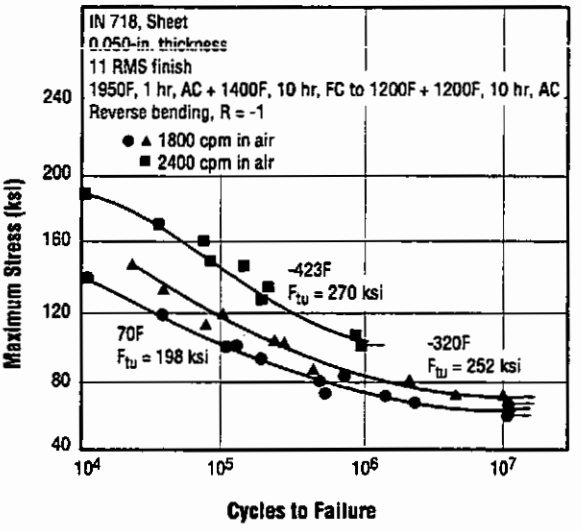

Fig. 3.5.1.1 Bending fatigue strength at room and low temperatures of sheet with 11 RMS surface finish (Ref. 47)

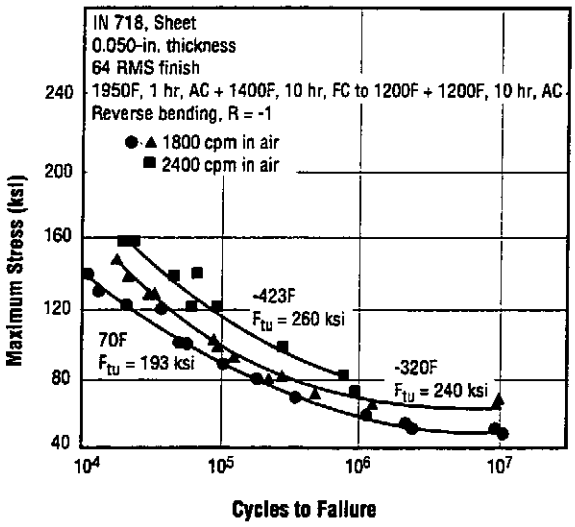

Fig. 3.5.1.2 Bending fatigue strength at room and low temperatures of sheet with 64 RMS surface finish (Ref.47)

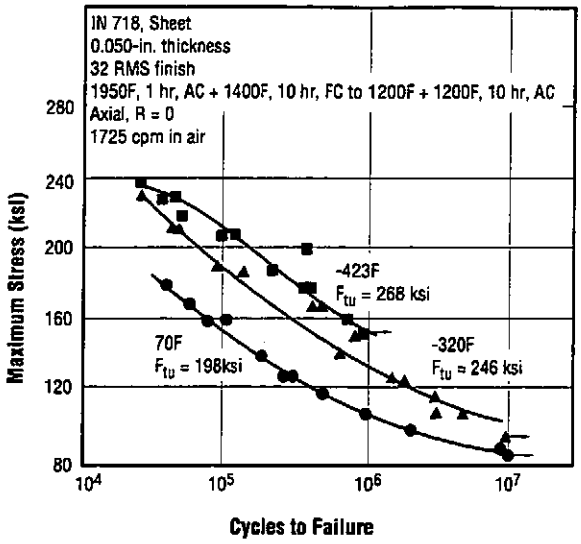

Fig. 3.5.1.3 Axial fatigue strength at room and low temperatures of sheet with 32 RMS surface finish (Ref. 47)

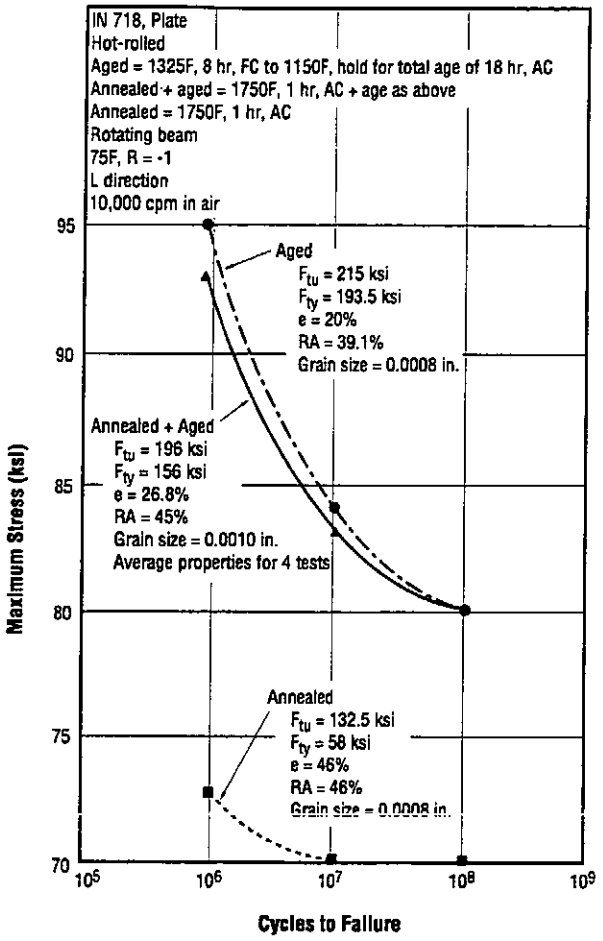

Fig. 3.5.1.4 Fatigue strength at 10^6, 10^7, and 10^8 cycles for hot-rolled plate in several heat-treated conditions (Ref. 1)

Table 3.5.1.5 Comparison of the effects of aging after annealing on tensile properties and fatigue strength of forgings at room temperature (Ref. 1)

Alloy	Inconel 718	
Form	9-in. diameter by 6-in. long Forging	
Property	**Conditions**	
	1750F, 1 hr, AC	**1750F, 1 hr, AC + 1325F, 8 hr, FC to 1150F, Hold for Total Age of 18 hr, AC**
Average Grain Size (mils)	**2.3**	**2.1**
Tensile		
F_{ty} (ksi)	99.5	169.5
F_{tu} (ksi)	143.0	191.2
e, 2-in. (percent)	32.0	10.5
RA (percent)	32.0	20.0
Fatigue Strength (ksi)		
10^6 cycles	74.0	77.5
10^7 cycles	67.5	71.0
10^8 cycles	66.5	69.5

Note: Rotating beam tests, R = -1, 75F, short-transverse specimens.

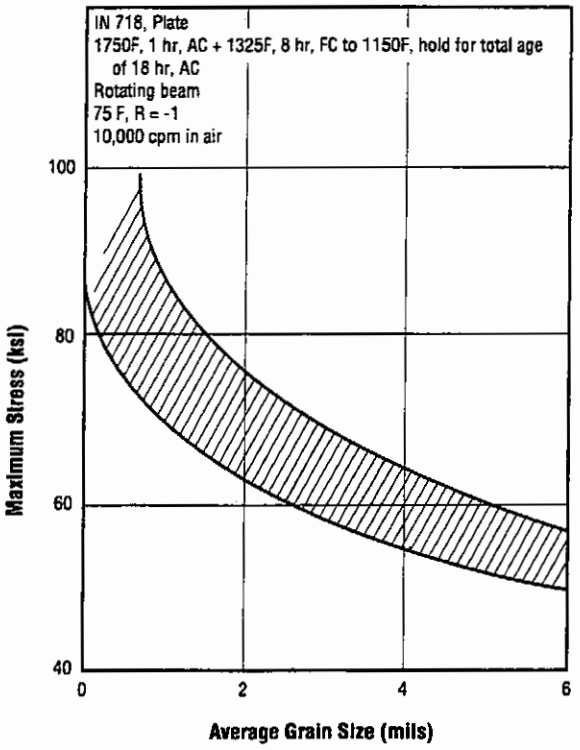

Fig. 3.5.1.6 Effect of grain size on fatigue strength of plate at 10^8 cycles (Ref. 1)

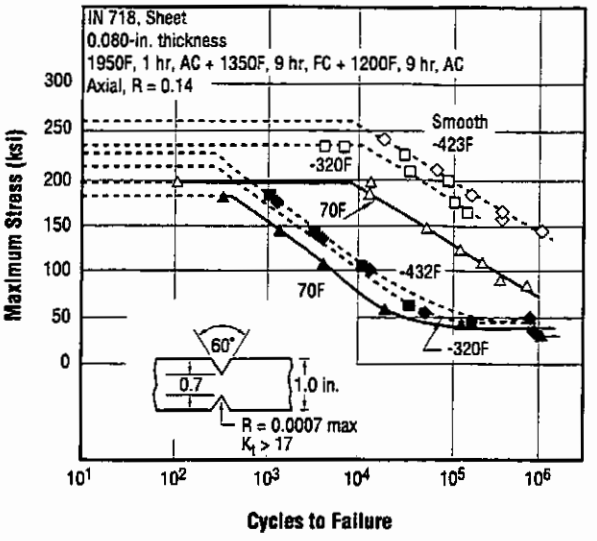

Fig. 3.5.1.7 Axial fatigue strength at room and low temperatures of both smooth and notched specimens of annealed-and-aged sheet (Ref. 49)

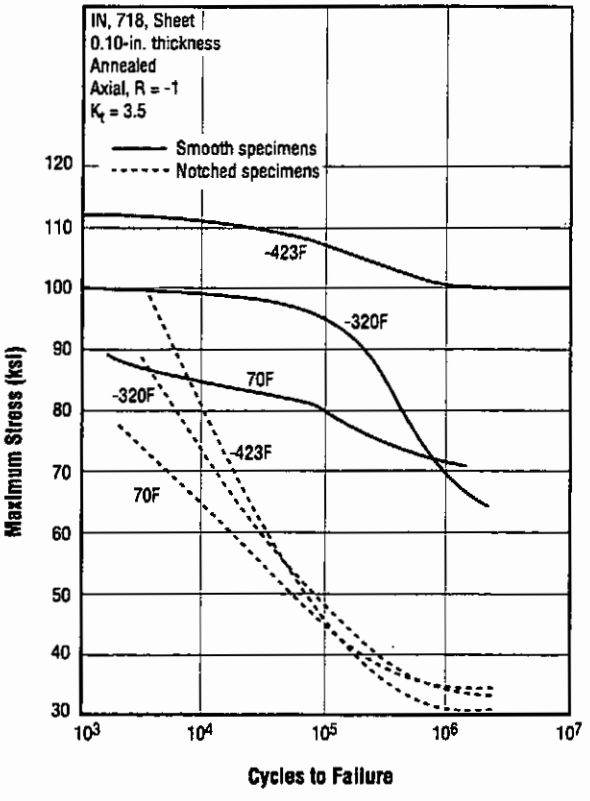

Fig. 3.5.1.8 Axial fatigue strength at room and low temperatures of both smooth and notched specimens of annealed sheet (Ref. 48)

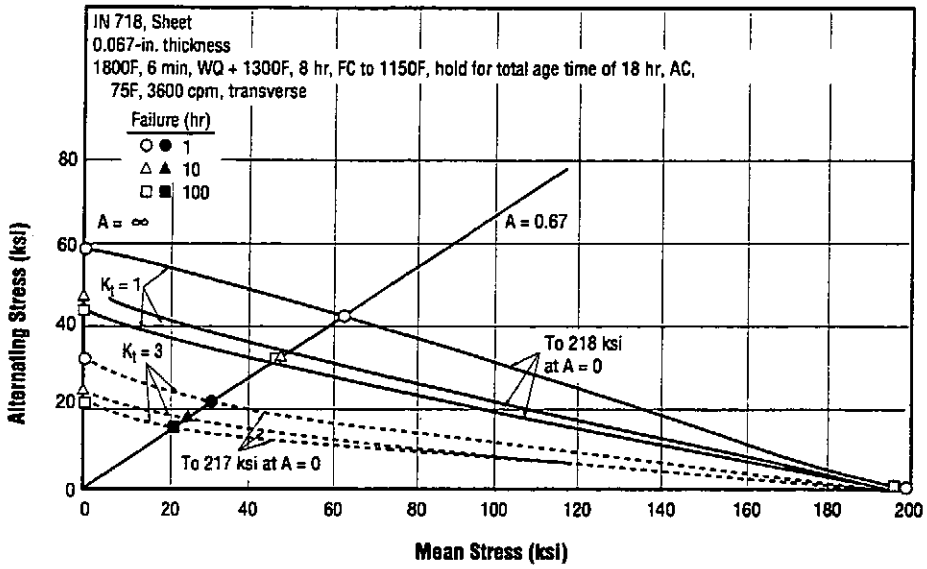

Fig. 3.5.1.9 Stress-range diagram for notched and smooth sheet at 75F (Ref. 42)

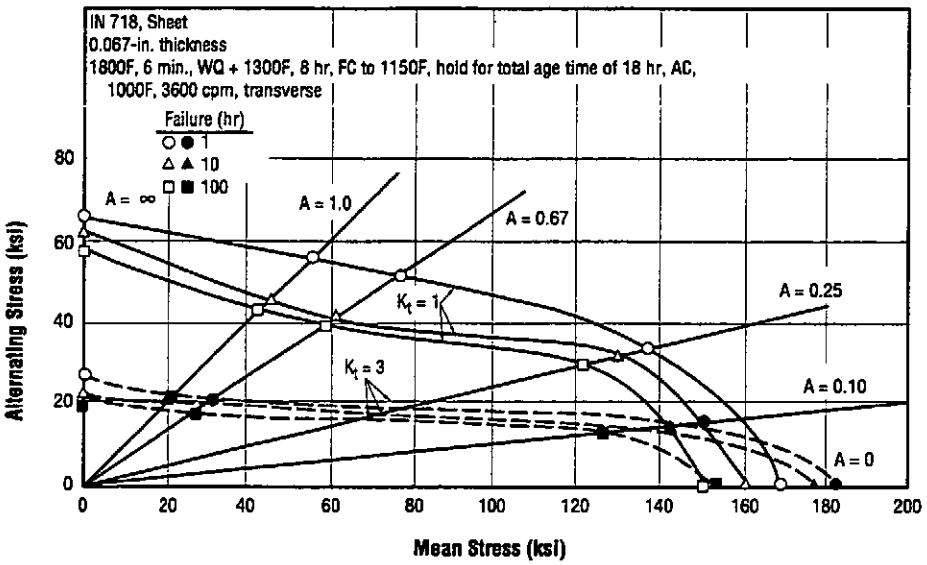

Fig. 3.5.1.10 Stress-range diagram for notched and smooth sheet at 1000F (Ref. 42)

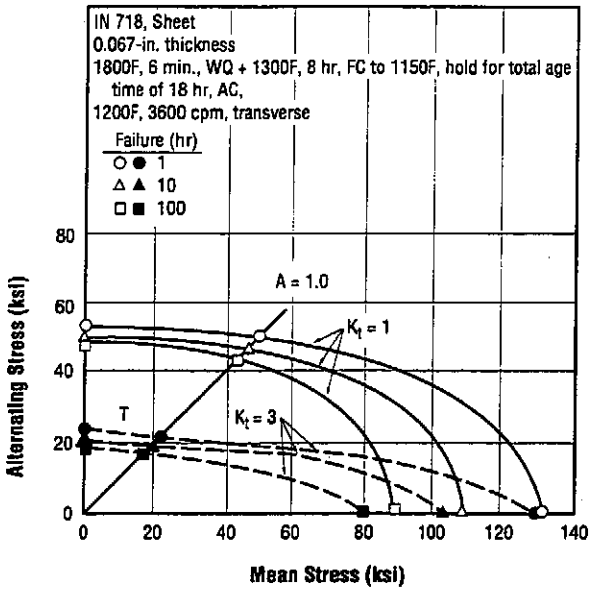

Fig. 3.5.1.11 Stress-range diagram for notched and smooth sheet at 1200F (Ref. 42)

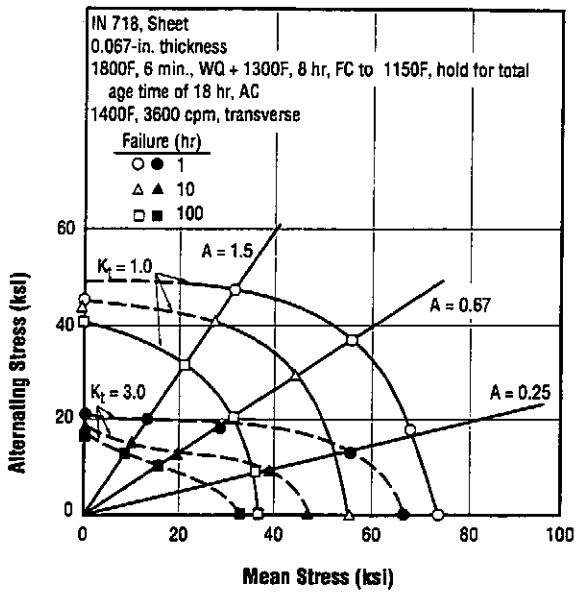

Fig. 3.5.1.12 Stress-range diagram for notched and smooth sheet at 1400F (Ref. 42)

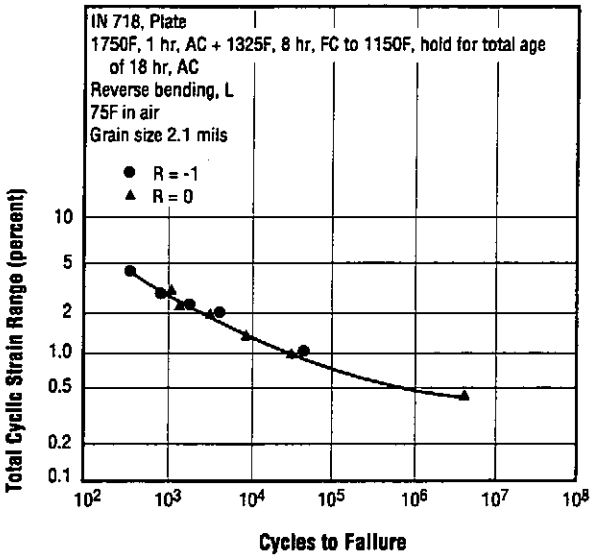

Fig. 3.5.2.1 Fatigue life of plate as a function of total cyclic strain range at room temperature (Ref. 2)

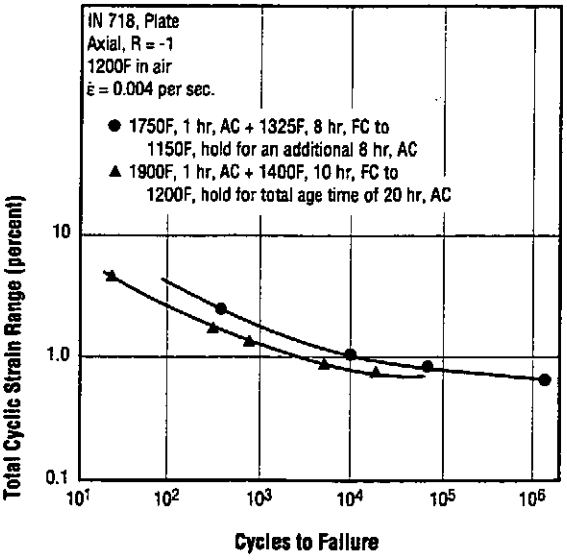

Fig. 3.5.2.2 Fatigue life of plate in two heat-treated conditions as a function of total cyclic strain range at 1200F (Ref. 29)

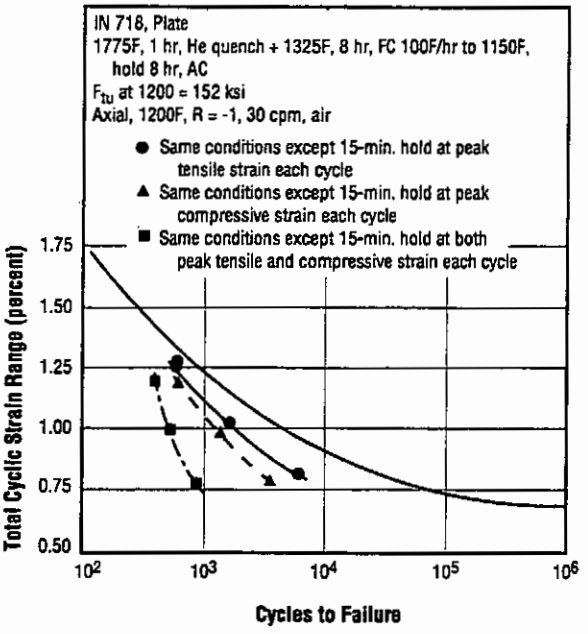

Fig. 3.5.2.3 Effects of holding at peak cyclic compressive and tensile strains on fatigue life as a function of total cyclic strain range at 1200F (Ref. 39)

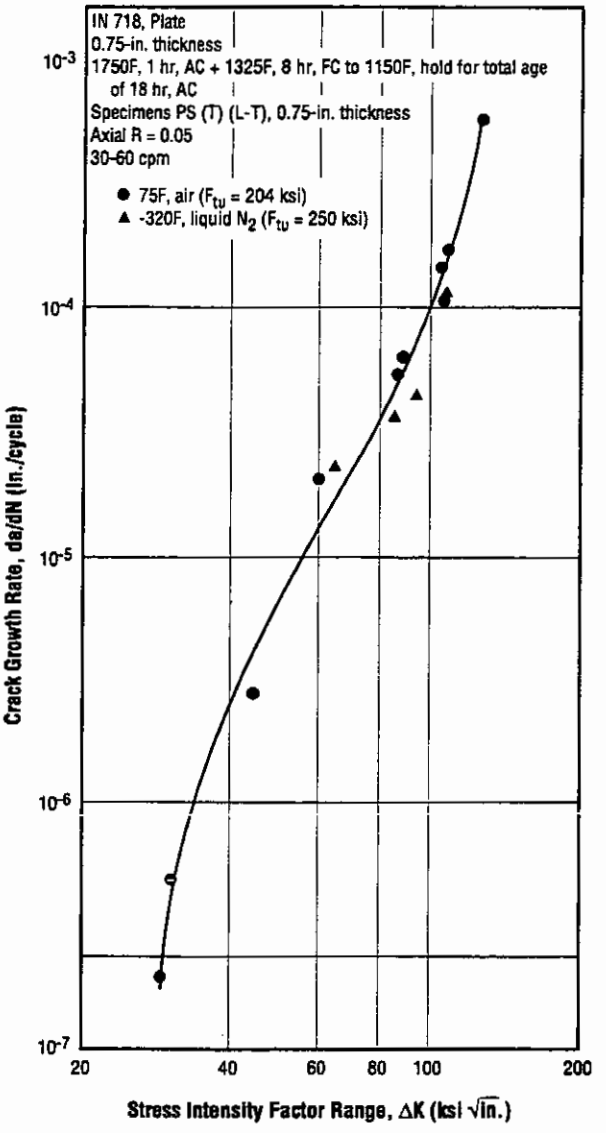

Fig. 3.5.3.1 Fatigue crack growth rate for plate tested in air and in liquid nitrogen (Ref. 15)

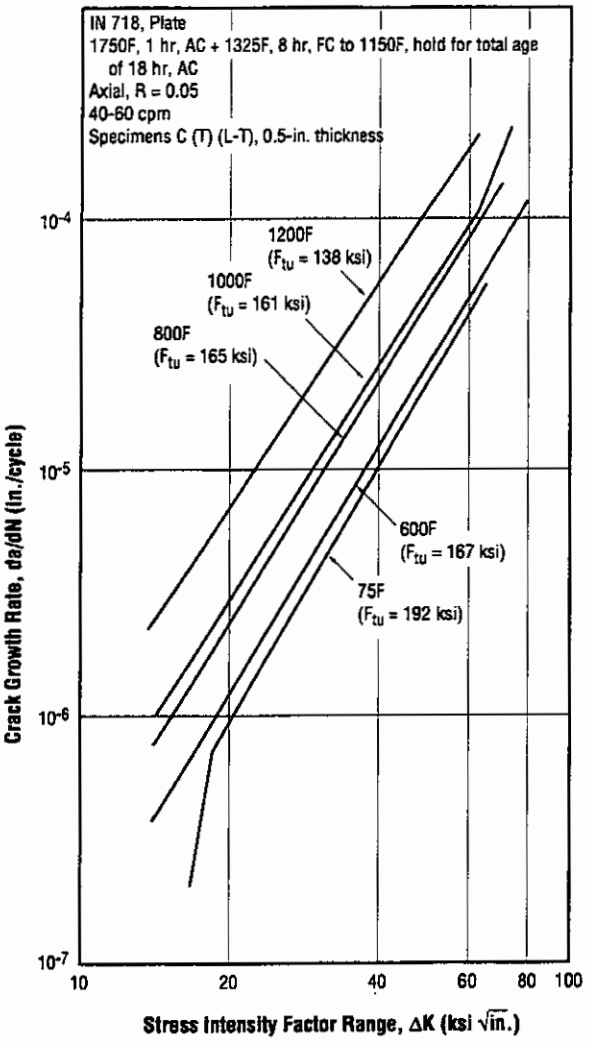

Fig. 3.5.3.2 Effects of elevated temperatures on fatigue crack growth rate of plate in air (Ref. 22)

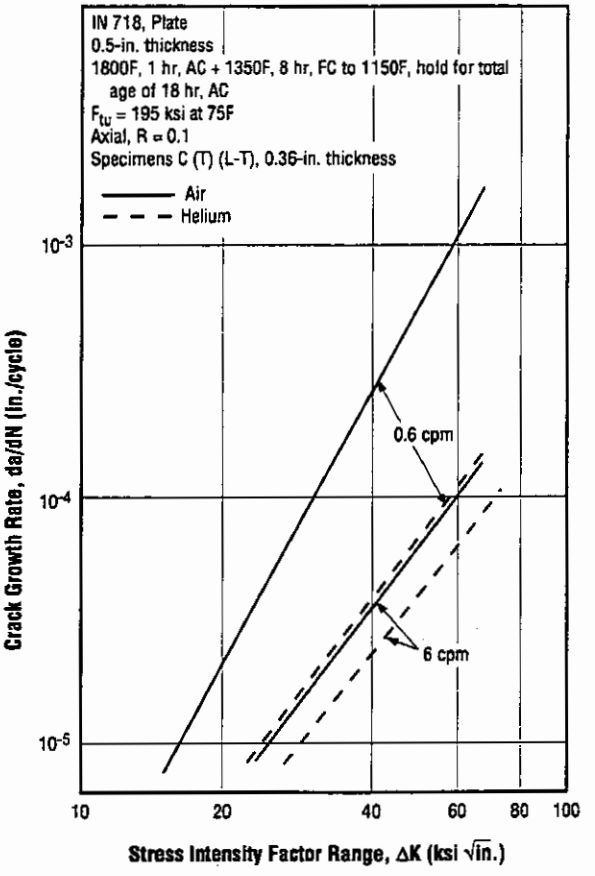

Fig. 3.5.3.3 Fatigue crack growth rates of plate at 1200F in environments of air and helium at two rates of cycling (Ref. 16)

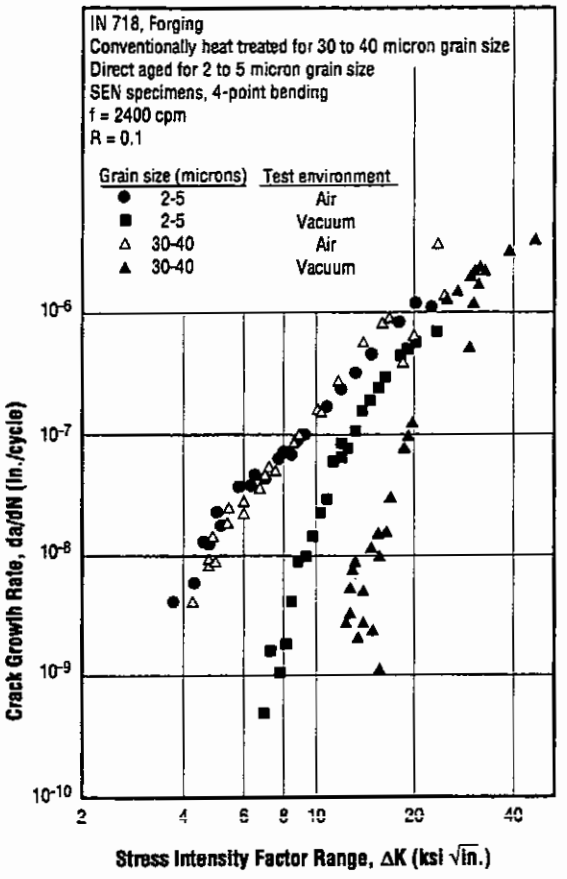

Fig. 3.5.3.4 Effects of grain size and test environment on fatigue crack growth behavior at 68F (Ref. 134)

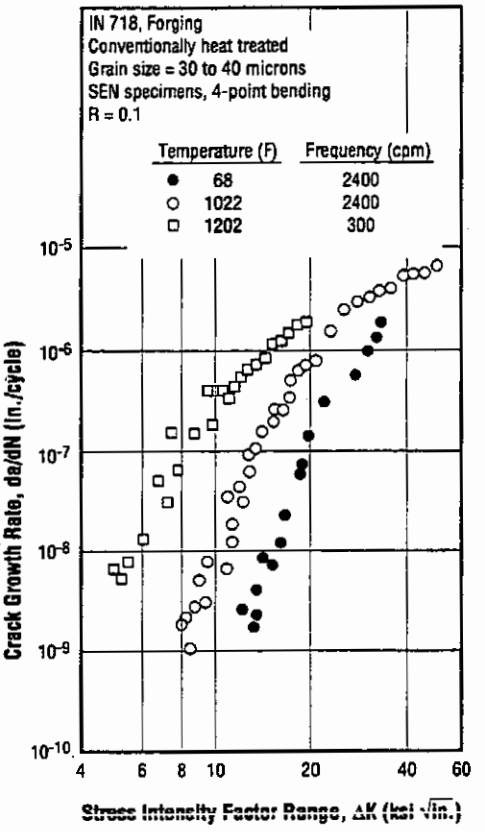

Fig. 3.5.3.5 Effect of temperature on fatigue crack growth behavior of large-grained alloy in vacuum (Ref. 134)

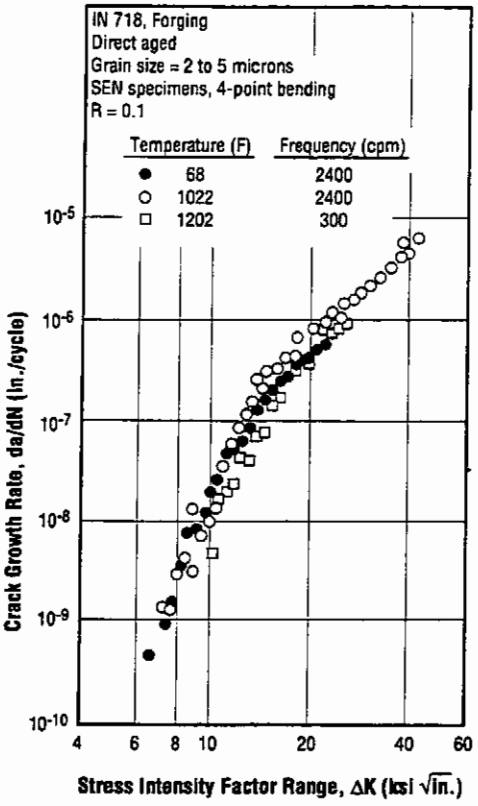

Fig. 3.5.3.6 Effect of temperature on fatigue crack growth behavior of fine-grained alloy in vacuum (Ref. 134)

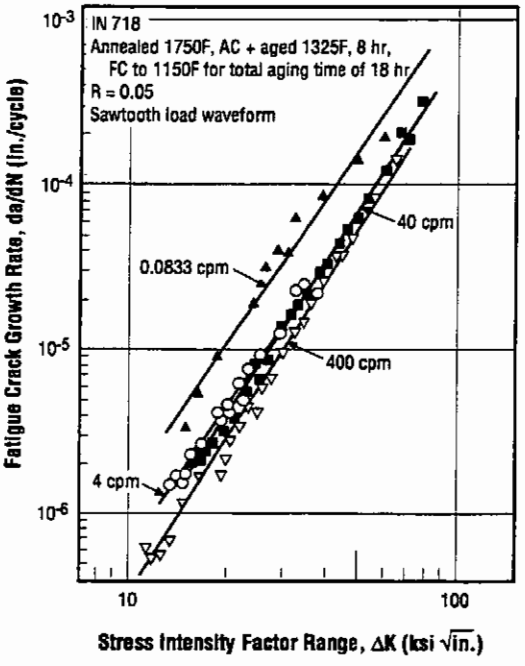

Fig. 3.5.3.8 Fatigue crack growth rates in air at 1000F and cyclic frequencies from 0.0833 to 400 cpm (Ref. 131)

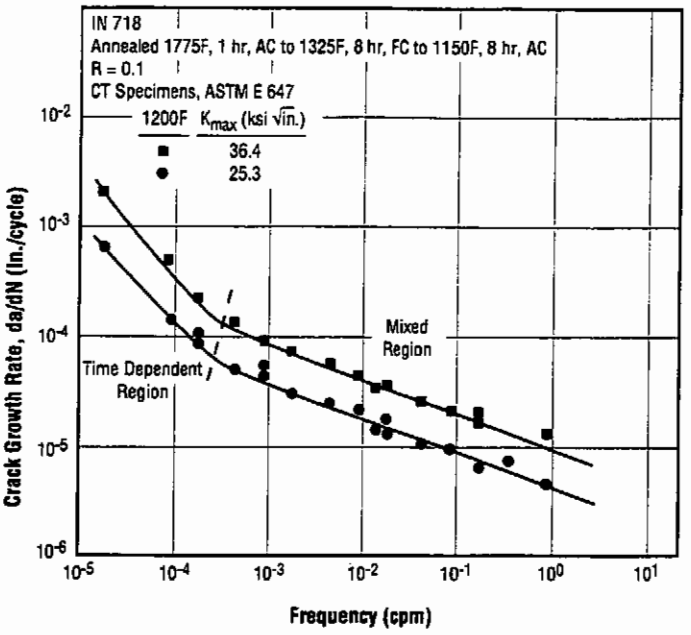

Fig. 3.5.3.7 Effect of cyclic frequency on fatigue crack growth behavior in air at 1200F (Ref. 135)

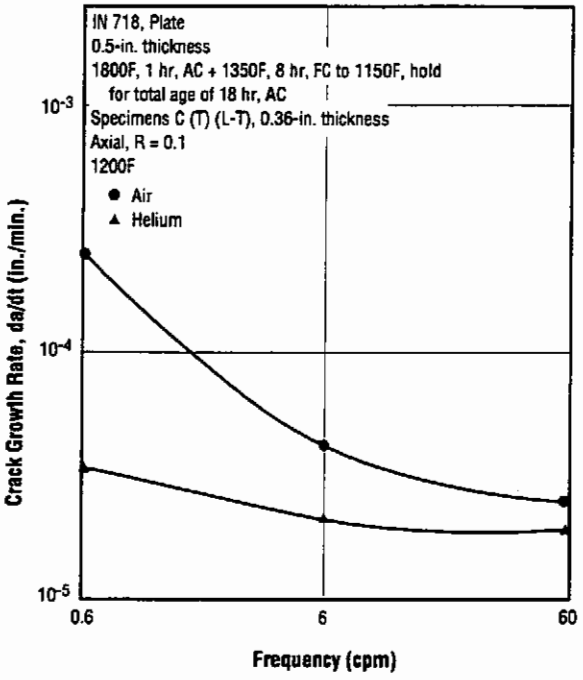

Fig. 3.5.3.9 Effect of cycle frequency on fatigue crack growth rate at ΔK = 36.4 ksi √in. and 1200F in air and helium (Ref. 16)

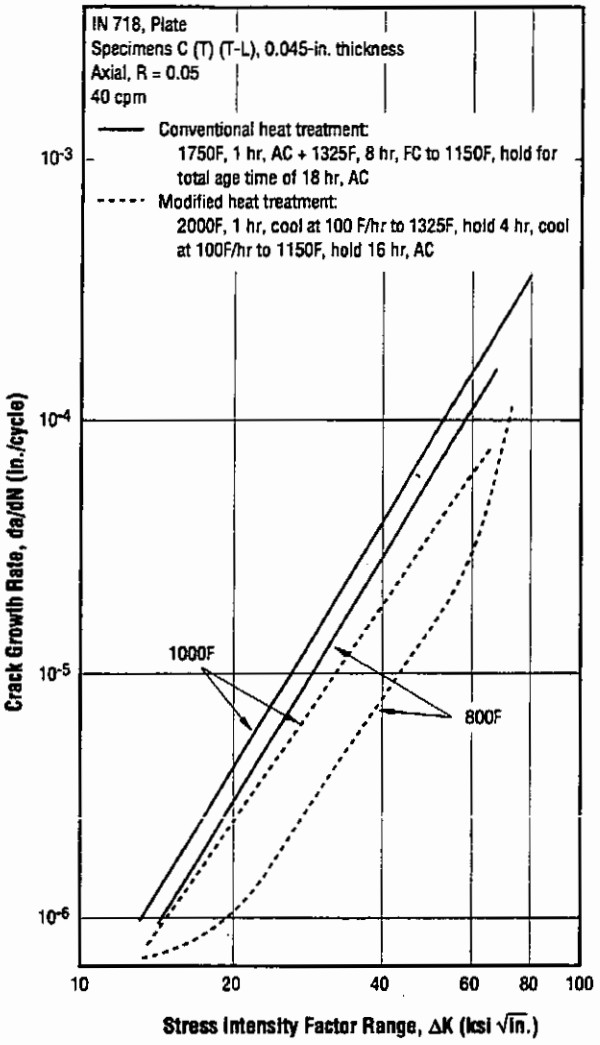

Fig. 3.5.3.10 Effects of heat treatment on fatigue crack growth rates of plate at 800 and 1000F in air (Ref. 31)

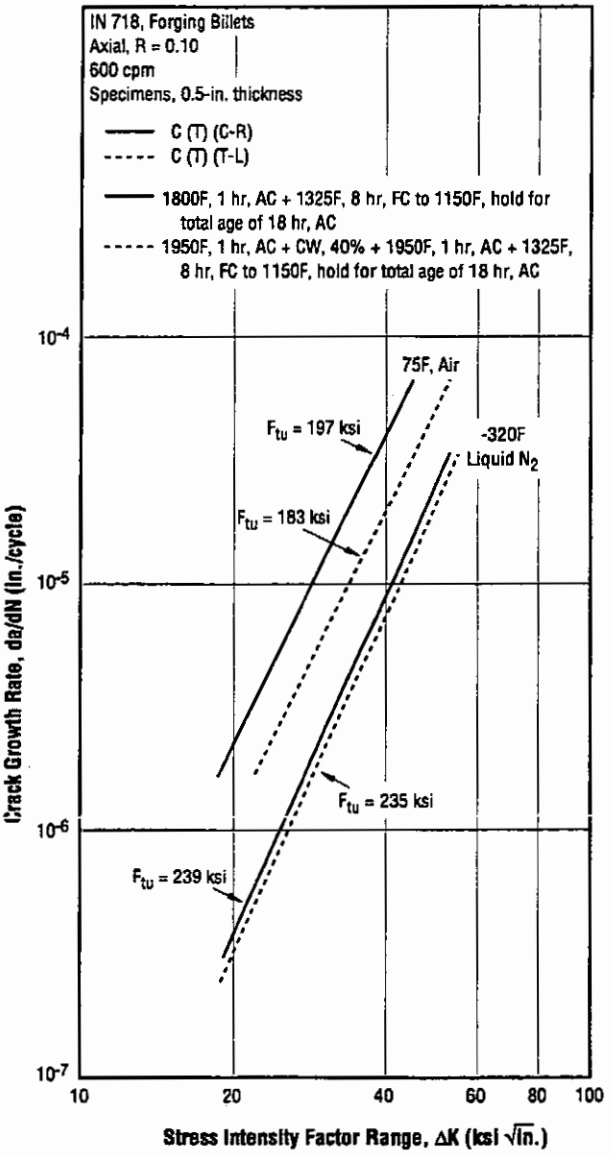

Fig. 3.5.3.11 Fatigue crack growth rate of forging billets at room temperature and -320F in two conditions of heat treatment (Ref. 20)

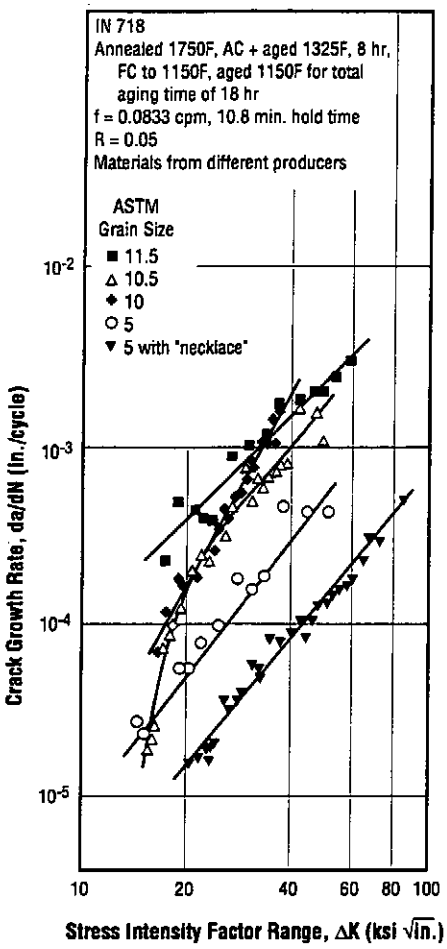

Fig. 3.5.3.12 Effects of grain size on fatigue crack growth rates in air at 1000F (Ref. 131)

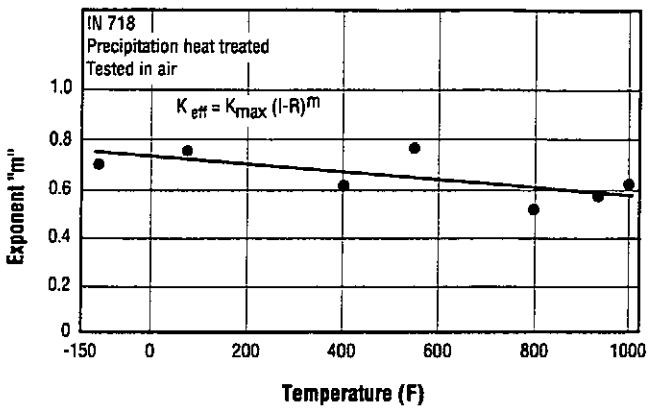

Fig. 3.5.3.13 Effects of temperature on stress ratio correlation exponent (Ref. 131)

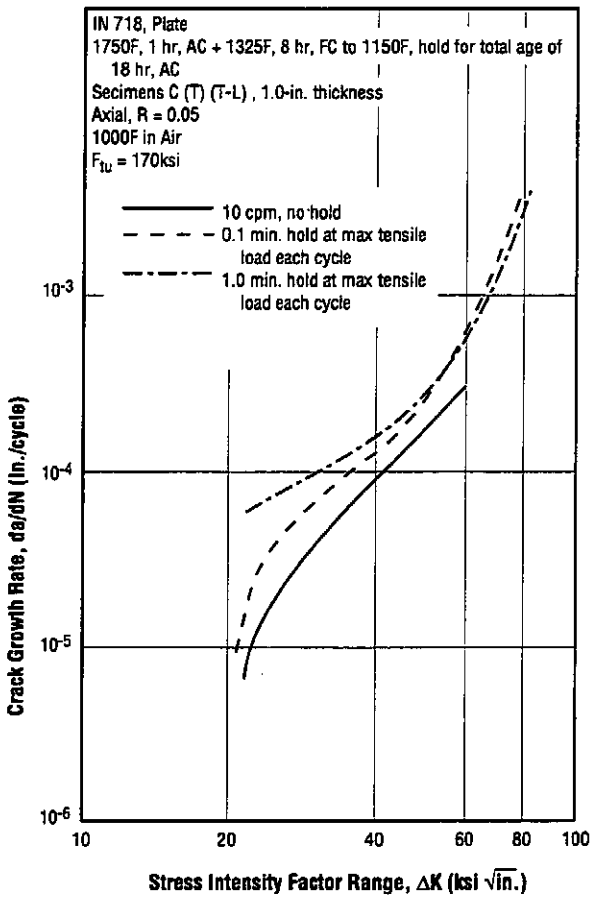

Fig. 3.5.3.14 Effects of various hold times at maximum cyclic tensile load on fatigue crack growth rate of plate at 1000F (Ref. 30)

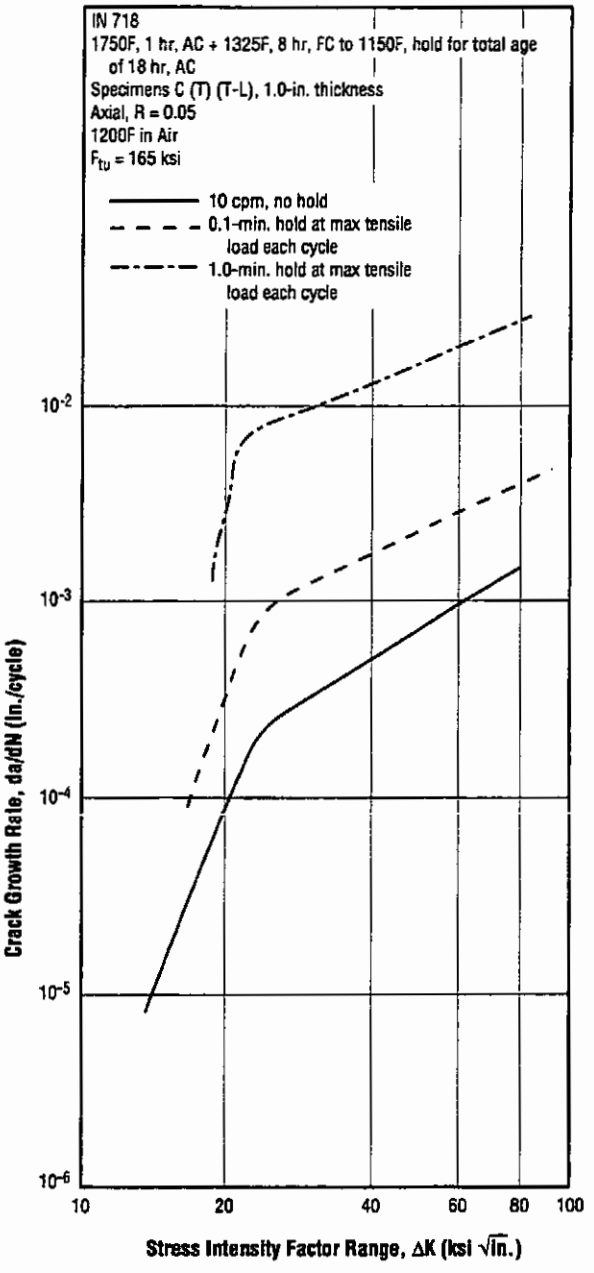

Fig. 3.5.3.15 Effects of various hold times at maximum cyclic tensile load on fatigue crack growth rate of plate at 1200F (Ref. 30)

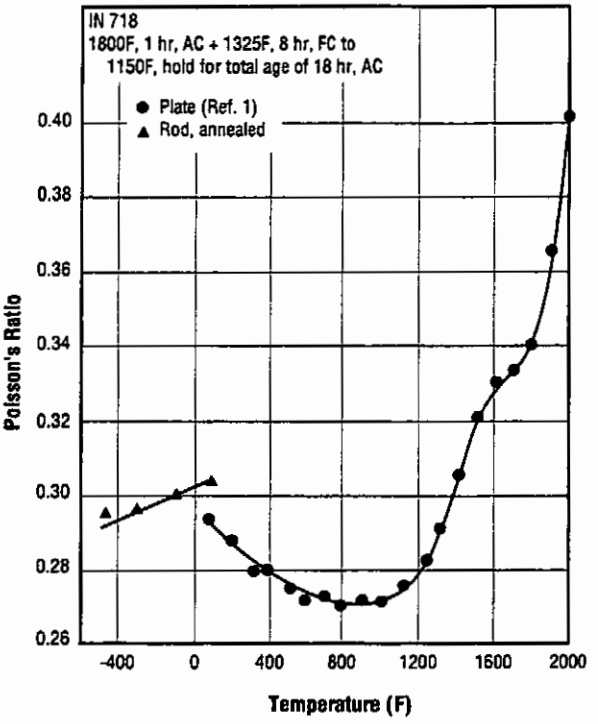

Fig. 3.6.1.1 Poisson's ratio at temperatures from -450 to 2000F (Refs. 1, 83)

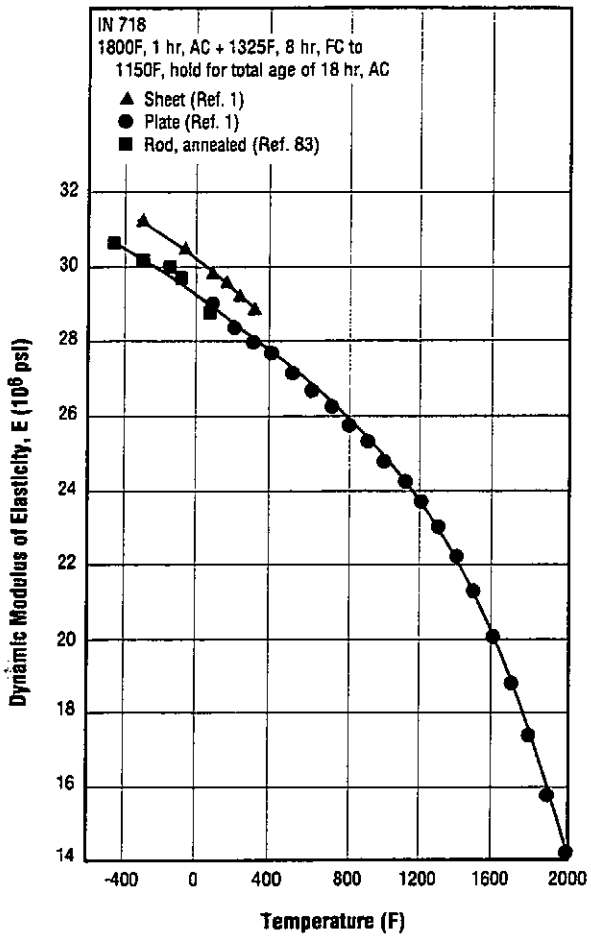

Fig. 3.6.2.1 Dynamic modulus of elasticity at temperatures from -450 to 2000F (Refs. 1, 83)

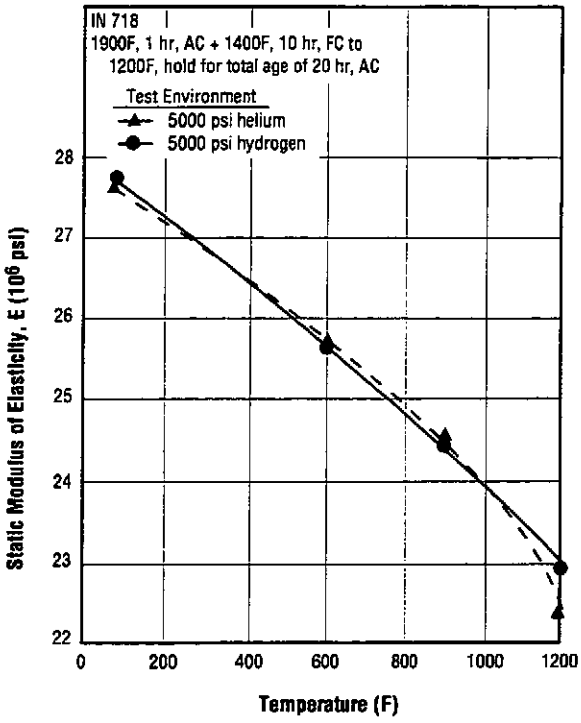

Fig. 3.6.2.2 Effects of elevated temperatures on static modulus of elasticity of plate in atmospheres of helium and hydrogen at 5000 psi (Ref. 14)

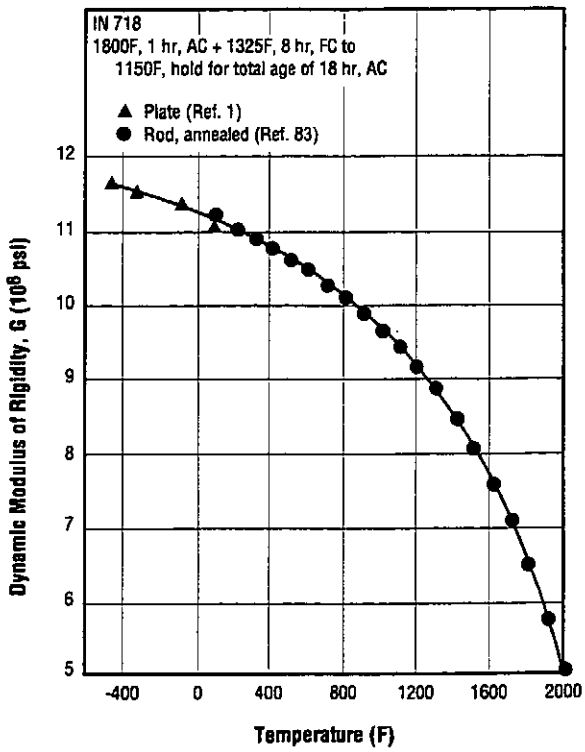

Fig. 3.6.3.1 Dynamic modulus of rigidity at temperatures from -450 to 2000F (Refs. 1, 83)

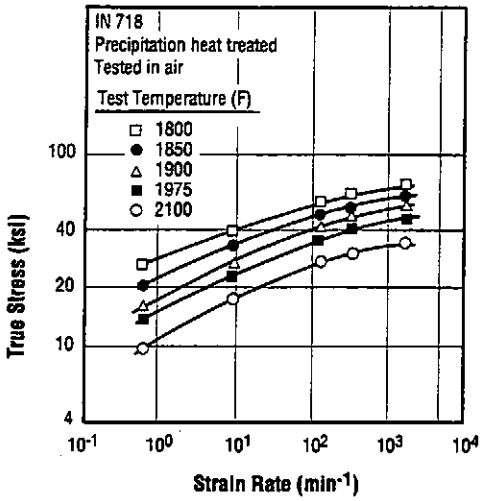

Fig. 4.1.1 Effects of strain rate and temperature on compressive flow stress at a true strain of 0.3 (Ref. 141)

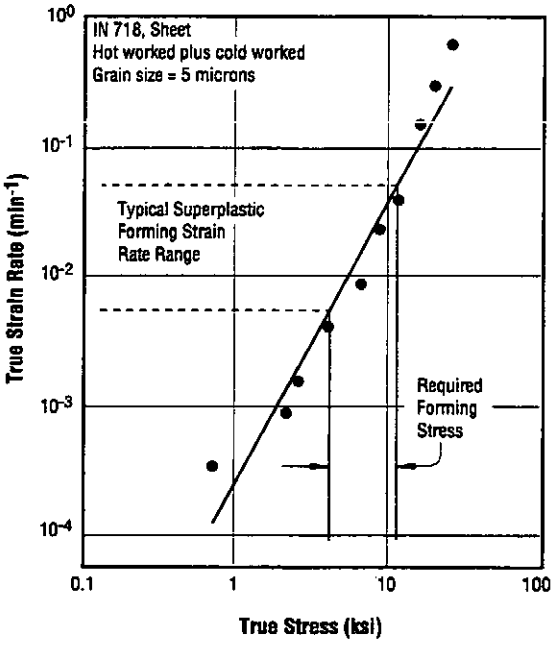

Fig. 4.1.3 Slow tensile deformation behavior of fine-grained alloy at 1750F (Ref. 142)

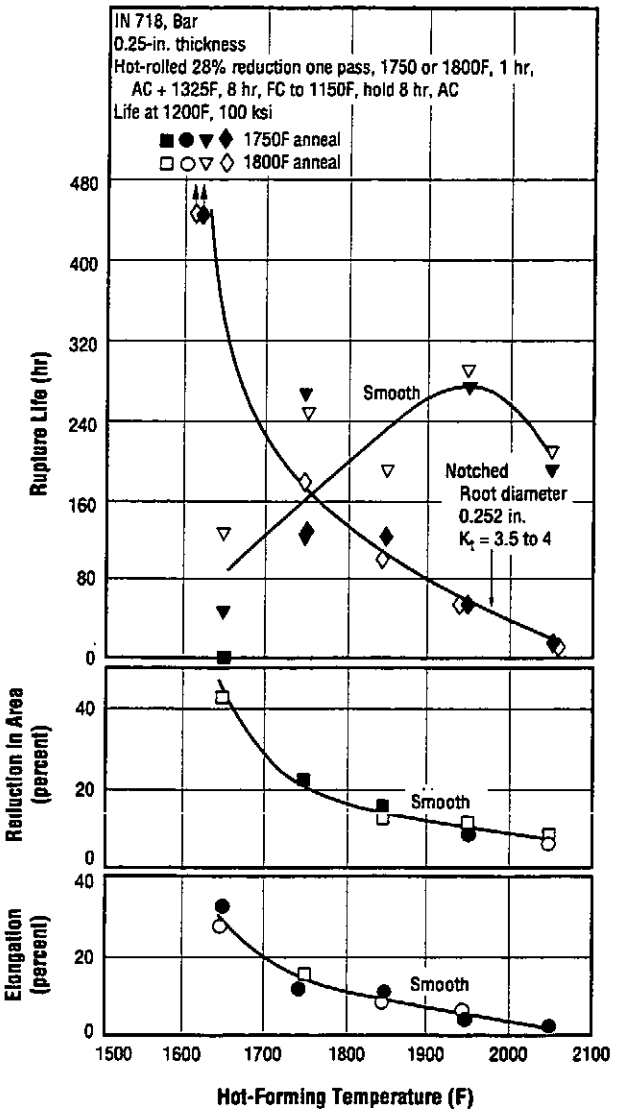

Fig. 4.1.2 Effects of hot-forming temperatures on smooth and notched creep rupture life and on creep ductility at 1200F and 100 ksi (Ref. 2)

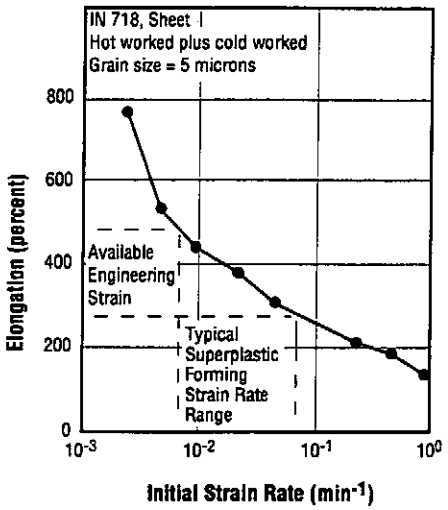

Fig. 4.1.4 Slow tensile ductility of fine-grained alloy at 1750F (Ref. 142)

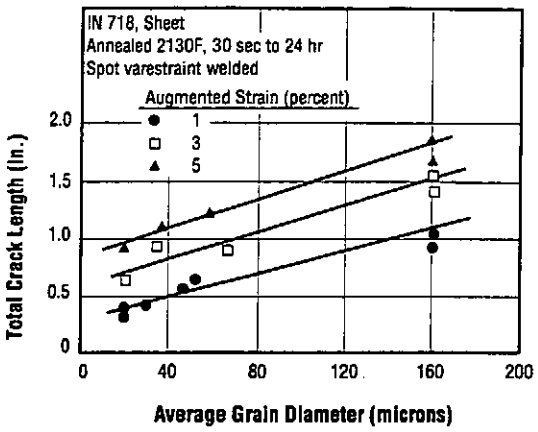

Fig. 4.3.1.1 Effect of heat-affected-zone grain size and augmented strain on GTA weld hot cracking (Ref. 150)

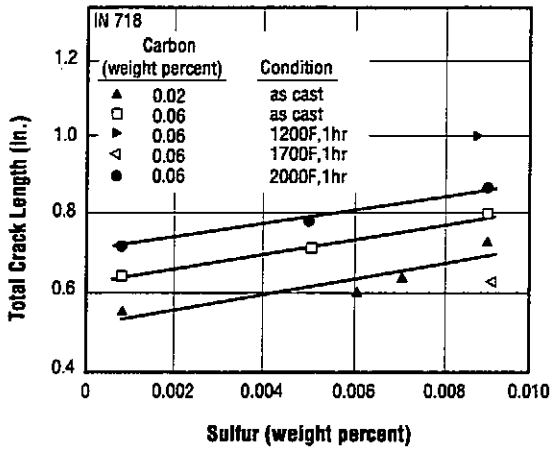

Fig. 4.3.1.2 Effects of sulfur and carbon contents and heat treatment on heat-affected-zone crack length in welded cast alloy (Ref. 146)

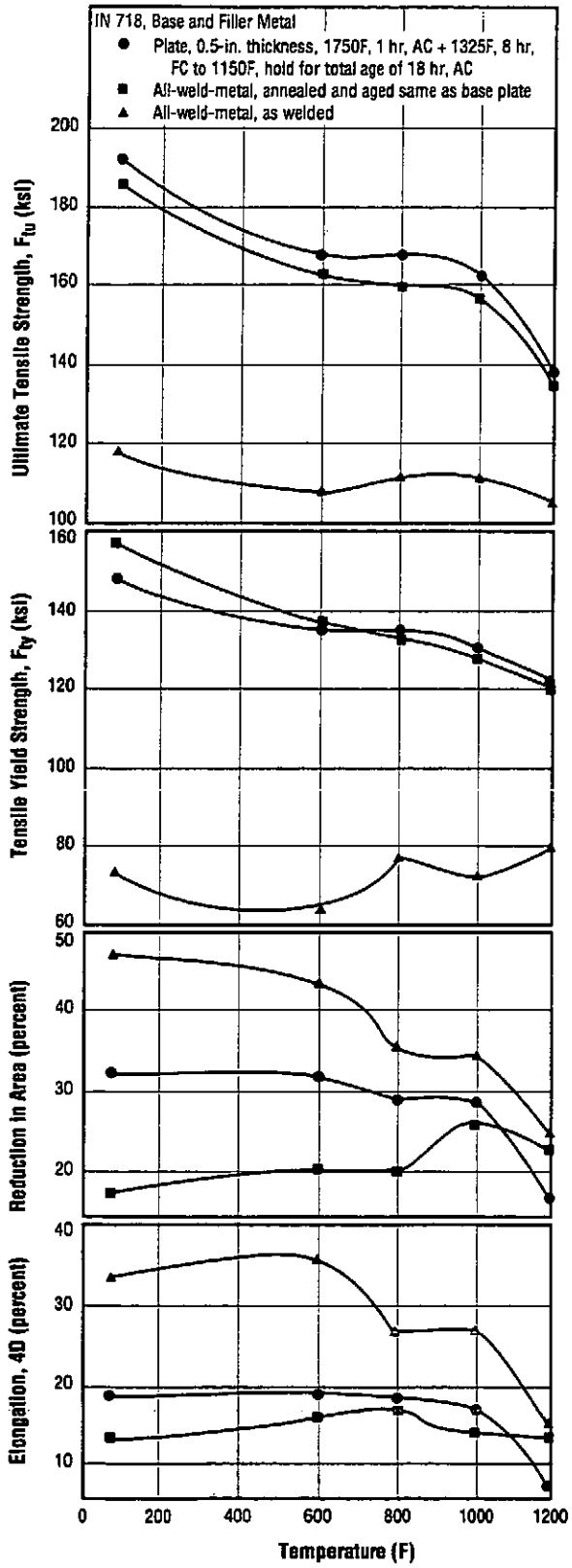

Fig. 4.3.1.3 Effects of elevated temperatures on base plate and on IN 718 GTA deposit that formed butt joint between two segments of base plate (Ref. 17)

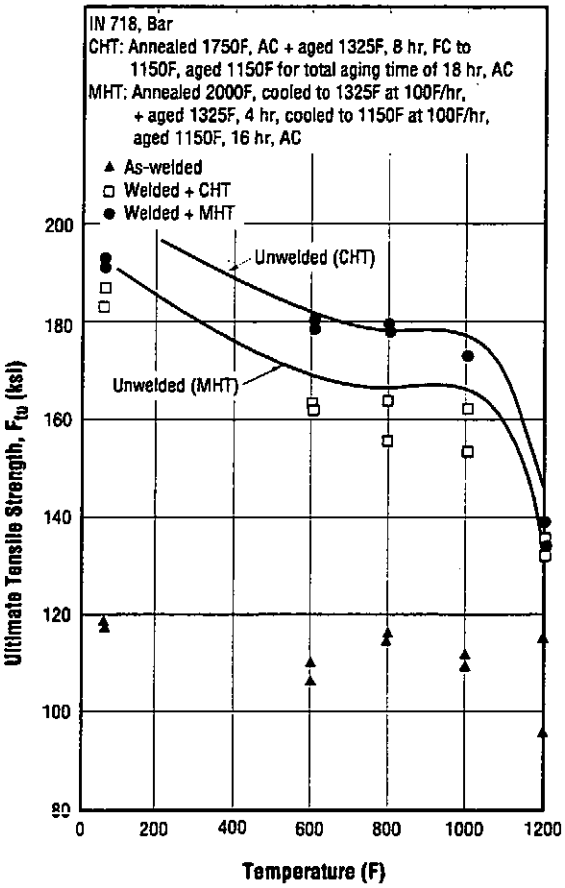

Fig. 4.3.1.4 Effects of heat treatment on ultimate tensile strength of GTA weld metal at room temperature to 1200F (Ref. 89)

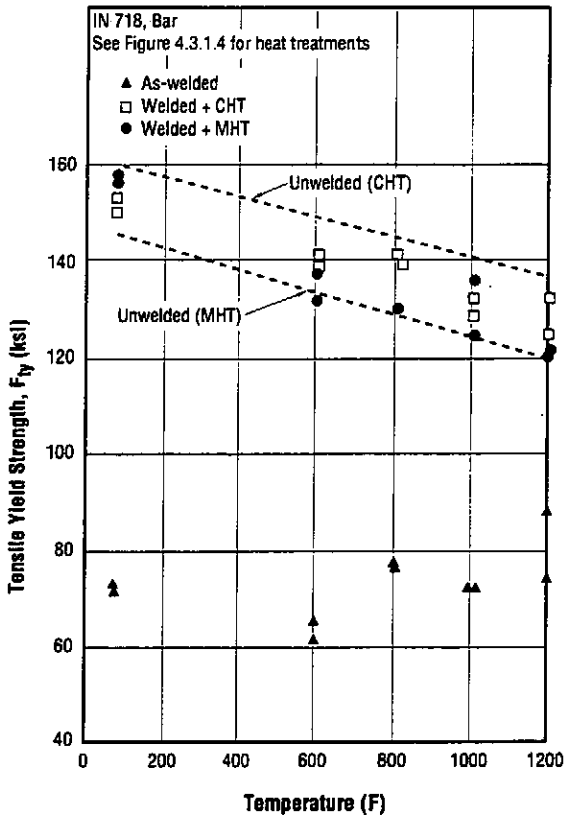

Fig. 4.3.1.5 Effects of heat treatment on tensile yield strength of GTA weld metal at room temperature to 1200F (Ref. 89)

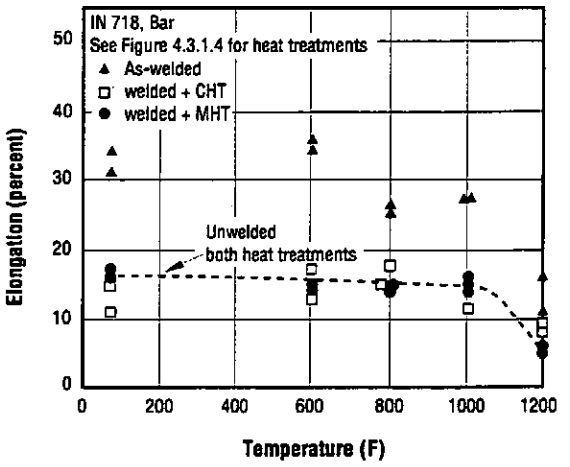

Fig. 4.3.1.6 Effects of heat treatment on elongation of GTA weld metal at room temperature to 1200F (Ref. 89)

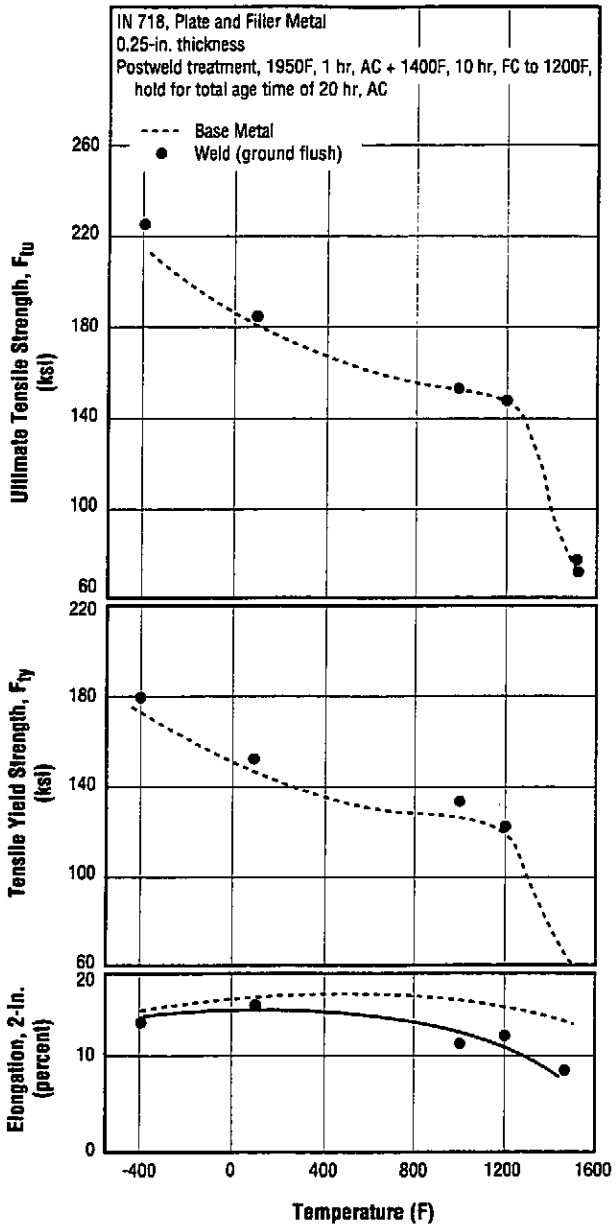

Fig. 4.3.1.7 Effects of low and high temperatures on tensile properties of GTA butt-weld joints in 0.25-in. plate (Ref. 51)

Table 4.3.1.8 Tensile properties at room temperature of all-weld-metal deposited by the GTA technique and subjected to various post-weld treatments (Ref. 1)

Alloy	Inconel 718				
Form	GTAW, All-Weld-Metal				
Filler Wire Diameter (in.)	**Postweld Treatment**	**F_{ty} (ksi)**	**F_{tu} (ksi)**	**e, 2-in. (percent)**	**RA (percent)**
0.045	As-Welded	83.3	123.1	28.0	30.2
	1750F, 1 hr, AC + age[a]	146.2	174.8	7.8	12.2
	1950F, 1 hr, AC + age[b]	163.8	195.3	16.0	21.8
	Age[a]	150.6	183.2	9.4	11.9
0.062	As-Welded	79.2	124.2	31.2	36.4
	1750F, 1 hr, AC + age[a]	148.0	177.2	8.8	12.7
	1950F, 1 hr, AC + age[b]	170.0	197.2	14.9	26.2
	Age[a]	145.5	176.1	9.8	15.0
0.094	As-Welded	84.0	123.8	28.0	31.3
	1750F, 1 hr, AC + age[a]	145.2	174.5	7.7	12.5
	1950F, 1 hr, AC + age[b]	168.5	197.0	10.0	18.0
	Age[a]	150.5	166.5	4.0	4.0

[a] Age 1325F, eight hours, FC to 1150F, hold for total age of 18 hours, AC.

[b] Age 1400F, 10 hours, FC to 1200F, hold for total age of 20 hours, AC.

Table 4.3.1.9 Tensile properties at room temperature of all-weld-metal and of butt-welded joint in 0.5-inch plate after two post-weld treatments (Ref. 1)

Alloy	Inconel 718 Base and Filler Metal				
Form	GTAW Butt-Weld Joint in 1/2-in. Plate				
Specimen	**Postweld Treatment**	**F_{ty} (ksi)**	**F_{tu} (ksi)**	**e, 0.5-in. (percent)**	**RA (percent)**
All-weld-metal	1950F, 1 hr, AC + age[a]	155.5	185.8	22.0	31.8
	Age[a]	139.2	174.5	18.3	21.5
Across weld	1950F, 1 hr, AC + age[a]	160.8	192.2	17.3	23.5
	Age[a]	149.5	183.5	12.0	24.8

[a] Age consists of 1400F, 10 hours, FC to 1200F, hold for total age of 20 hours, AC.

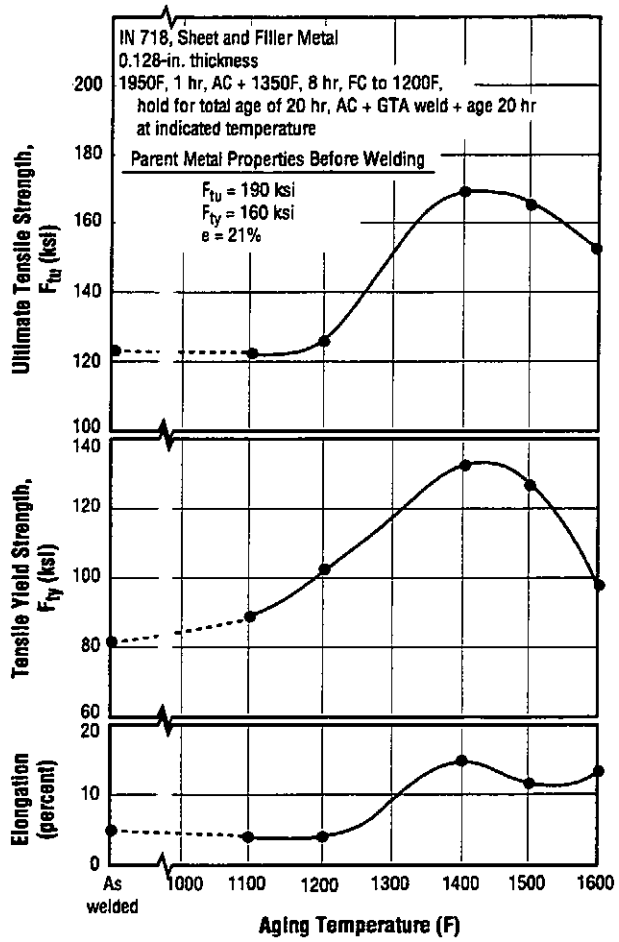

Fig. 4.3.1.10 Effect of post-weld aging for 20 hours at various temperatures on room-temperature tensile properties of GTA butt join in sheet (Ref. 45)

Table 4.3.1.11 Comparison at various temperatures of tensile and notched-tensile properties of parent metal and of butt-welded joints in forgings (Ref. 1)

Alloy	Inconel 718 Base and Filler Metal						
Form	GTA Weld Joint in Forging						
Condition	Weld + 1950F, 1 hr, AC + 1400F, 10 hr, FC + 1200F, Hold for Total Age of 20 hr						
Specimen	**Temperature (F)**	**F_{ty} (ksi)**	**F_{tu} (ksi)**	**e, 2-in. (percent)**	**RA (percent)**	**NTS [a] (ksi)**	**NSR (NTS/F_{tu})**
Parent Metal	-423	203.6	245.9	22.5	33.1	323.8	1.32
Across Weld		201.0	237.9	19.7	30.7	308.7	1.30
Parent Metal	75	163.8	197.5	25.5	38.5	272.8	1.38
Across Weld		165.6	189.7	19.3	38.1	263.1	1.39
Parent Metal	1200	125.7	143.8	21.1	40.7	207.4	1.44
Across Weld		127.3	147.3	11.9	30.2	204.2	1.39

[a] Notched tensile strength, K_t = 6.3.

Table 4.3.1.12 Tensile and shear properties of GTA weld deposit in the as-welded condition (Ref. 1)

Alloy	Inconel 718
Form	All GTA Weld Metal
Condition	**As Welded**
F_{ty} (ksi)	73.0
F_{tu} (ksi)	120.3
e, 4D (percent)	28.3
RA (percent)	30.1
F_{su} (ksi)	84.2

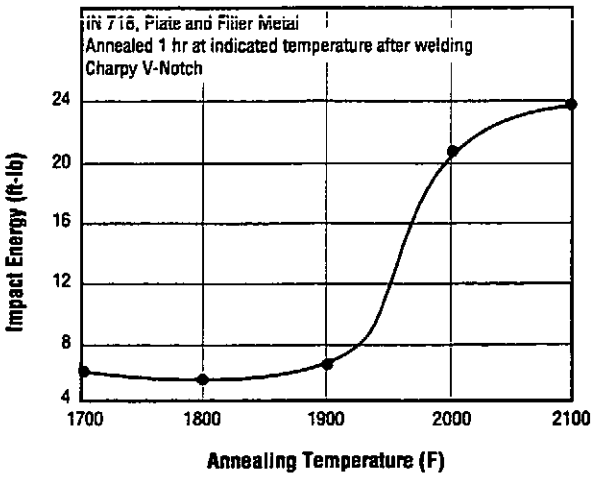

Fig. 4.3.1.13 Effect of post-weld annealing temperature on the impact strength of the heat-affected zones of GTA welds (Ref. 77)

Table 4.3.1.14 Effects of aging before and after welding on tensile and impact properties of GTA butt-welded joints in 1.0-inch plate (Ref. 34)

Alloy	Inconel 718 Base and Filler Metal		
Form	1.0-in. Plate with GTA Butt Weld		
Condition	**Temperature (F)**	**1750F, 8 hr, AC + Age[a] + Weld (As Welded)**	**1750F, 8 hr, AC + Weld + Age[a] (Postweld Aged)**
F_{tu} (ksi)	75	141	182
e, 2-in. (percent)		8	4
RA (percent)		25	4
Charpy V (ft-lb)	75	32	9
	-80	25	6

[a] Age 1325F, eight hours, FC to 1150F, hold for total age of 18 hours, AC.

Table 4.3.1.15 Effects of heat treatment and test temperature on fracture toughness of welded bar (Ref. 89)

Alloy	Inconel 718	
Condition	**Temperature (F)**	**Fracture Toughness, K_{Ic} (ksi $\sqrt{in.}$)[a]**
As-welded[b]	75	170
	800	170
	1000	187
Welded + CHT[c]	75	62
	800	71
	1000	69
Welded + MHT[d]	75	160
	800	137
	1000	124

[a] Valid K_{Ic} using ASTM E 399-81 compact tension specimens obtained only for CHT at 75F. All others used elastic-plastic procedure to obtain J_{Ic} (ASTM E 813-81). K_{Ic} values obtained by conversion from J_{Ic} (see Figure 3.3.7.2.1).

[b] GTA welded using Inconel 718 filler rod.

[c] CHT - Annealed 1750F, AC + aged 1325F, eight hours, FC to 1150F, held for total aging time of 18 hours, AC.

[d] MHT - Annealed 2000F, cooled to 1325F at 100F/hour, aged 1325F, four hours, cooled to 1150F at 100F/hour, aged 1150F, 16 hours, AC.

Table 4.3.1.16 Tensile strength and fracture toughness of base metal and weld metal at 75 and -320F for butt joints produced by various welding methods in plate (Ref. 15)

Alloy	Inconel 718				
Form	Plate				
Weld Method[a]	**Postweld Treatment**	F_{tu} (ksi)		K_{Ic} (ksi $\sqrt{in.}$)[e]	
		75F[c]	320F[d]	75F[c]	-320F[d]
Base Metal	1750F, 1 hr, AC + age[b]	204	250	146	153
GTAW	1750F, 1 hr, AC + age[b]	187	222	93	87
	age[b]	188	224	73	69
EBW	age[b]	200	224	49	45
PAW-GTAW	age[b]	195	225	53	48

[a] GTAW = Gas tungsten arc weld, Inconel 718 filler.
EBW = Electron beam weld (no filler).
PAW-GTAW = Root pass made by plasma-arc welding and remaining passes by GTAW, Inconel 718 filler.

[b] 1325F, eight hours, FC to 1150F, hold for total age of 18 hours, AC.

[c] Air environment.

[d] Liquid nitrogen environment.

[e] Specimen PS (T) (L-T), 0.50- to 0.75-inch thickness, K_{Ic} values should be regarded as approximations (see Section 3.3.7.2).

Table 4.3.1.17 Comparison of creep rupture properties of parent metal and weld joints in GTA butt-welded sheet (Ref. 1)

Alloy	Inconel 718 Base and Filler Metal				
Form	GTAW Butt-Weld Joint in 0.060-in. Sheet				
Specimen	**Condition**	**Temperature (F)**	**Stress (ksi)**	**Rupture Life (hr)**	**e, 2-in. (percent)**
Parent Metal	1750F, 1 hr, AC + age[a]	1200	100	47.3	8.0
		1300	72.5	26.1	11.0
Across Weld	1750F, 1 hr, AC + age[a] (postweld)	1200	100	10.8	1.0
		1300	72.5	9.4	1.0
Across Weld	Age[a] (postweld)	1200	100	16.4	1.0
		1300	72.5	15.8	2.0

[a] Age consists of 1325F, eight hours, FC to 1150F, hold for total age of 18 hours, AC.

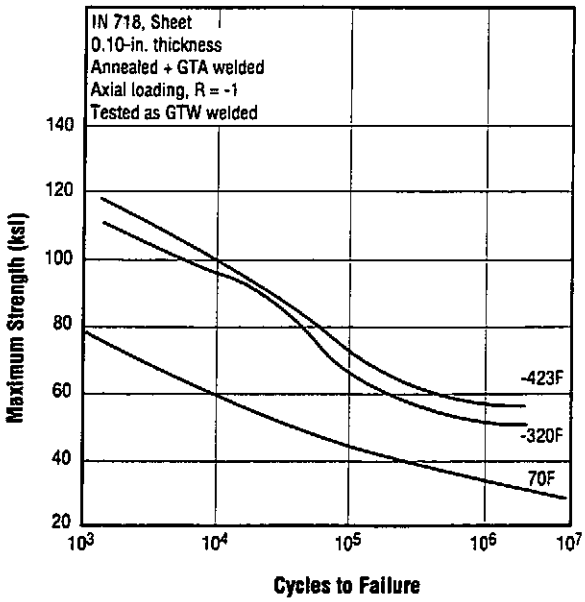

Fig. 4.3.1.18 Fatigue strength of GTA as-welded butt joints in annealed sheet at room and low temperatures (Ref. 48)

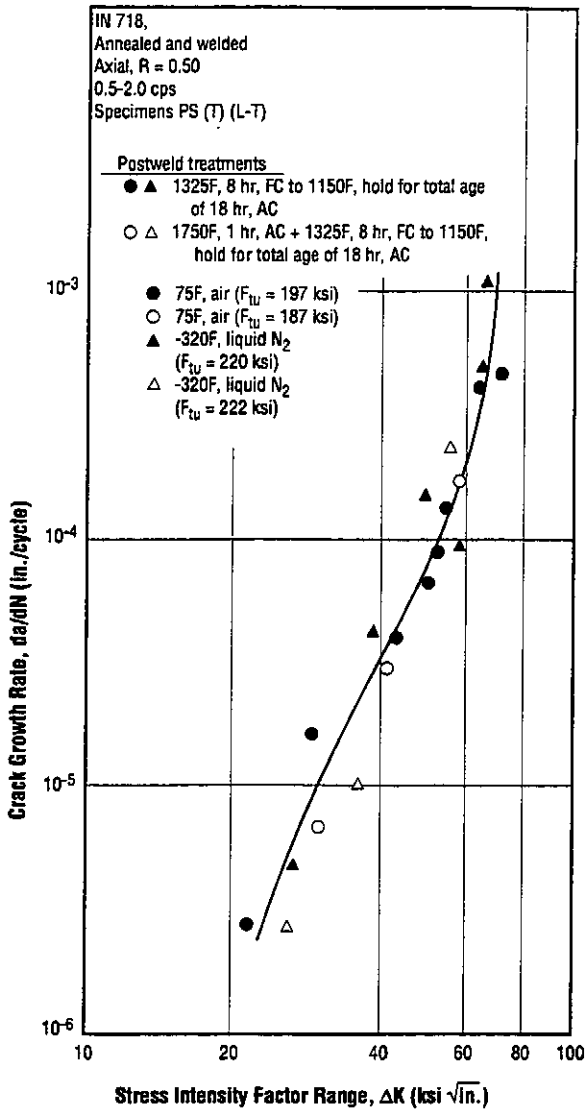

Fig. 4.3.1.19 Fatigue crack growth rates of Inconel 718 weld deposit in butt-welded joint produced by GTA method (Ref. 15)

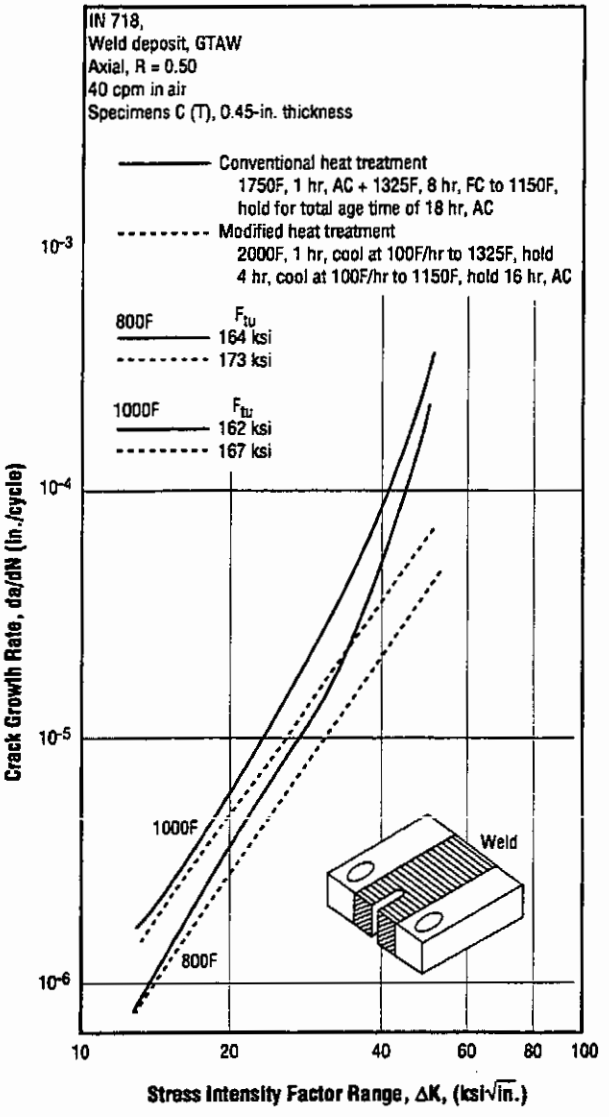

Fig. 4.3.1.20 Fatigue crack growth rate at 800 and 1000 F of GTA weld deposit after conventional heat treatment and modified postweld heat treatment (Ref. 31)

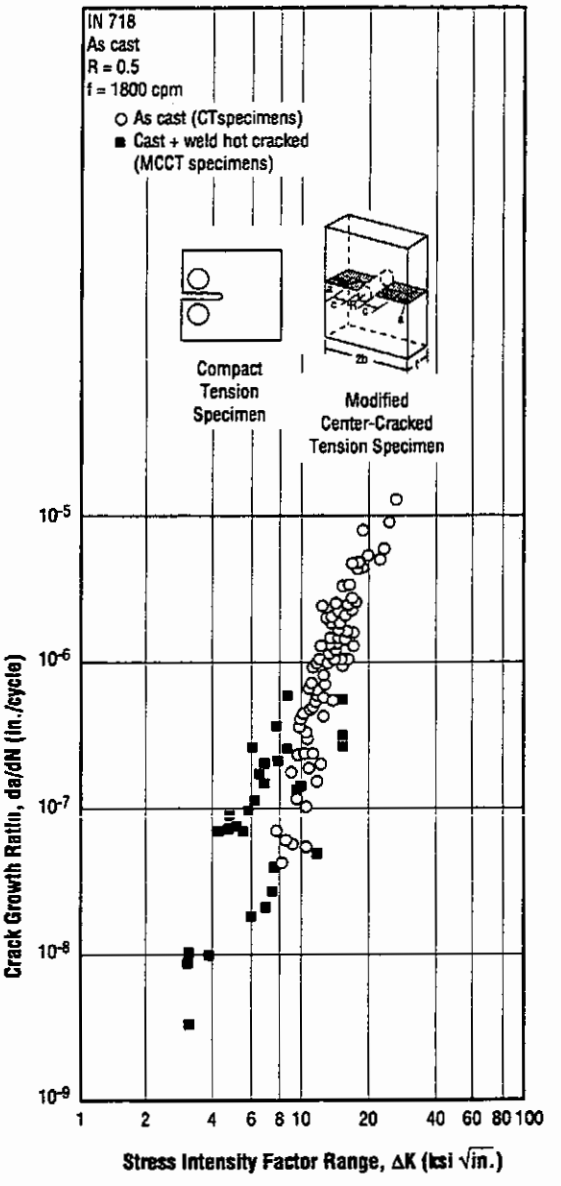

Fig. 4.3.1.21 Fatigue crack growth behavior at room temperature in the cast condition and after weld hot cracking (Ref. 148)

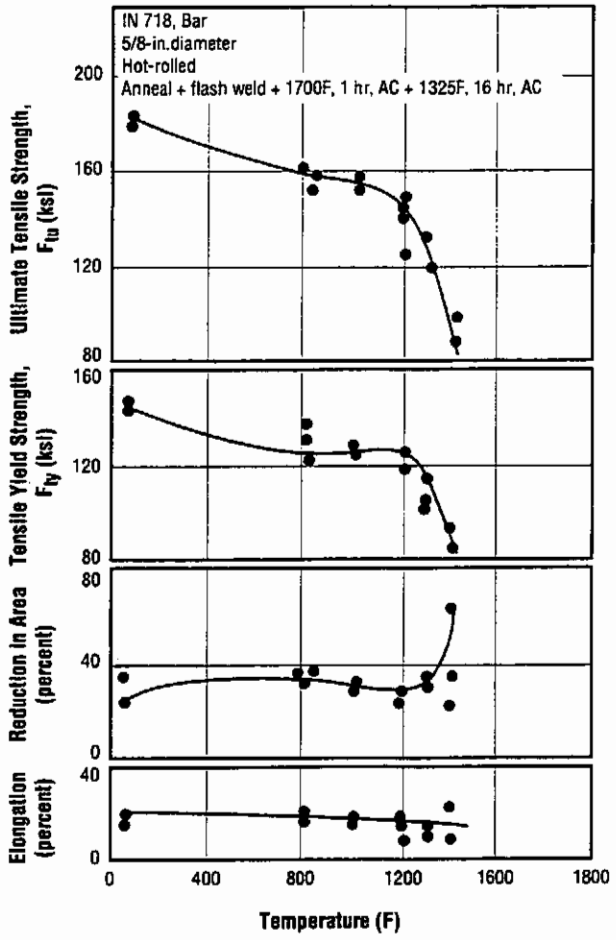

Fig. 4.3.2.1 Effects of temperatures up to 1400F on tensile properties of annealed-and-aged resistance-flash-welded joints in 5/8-in. bar (Ref. 50)

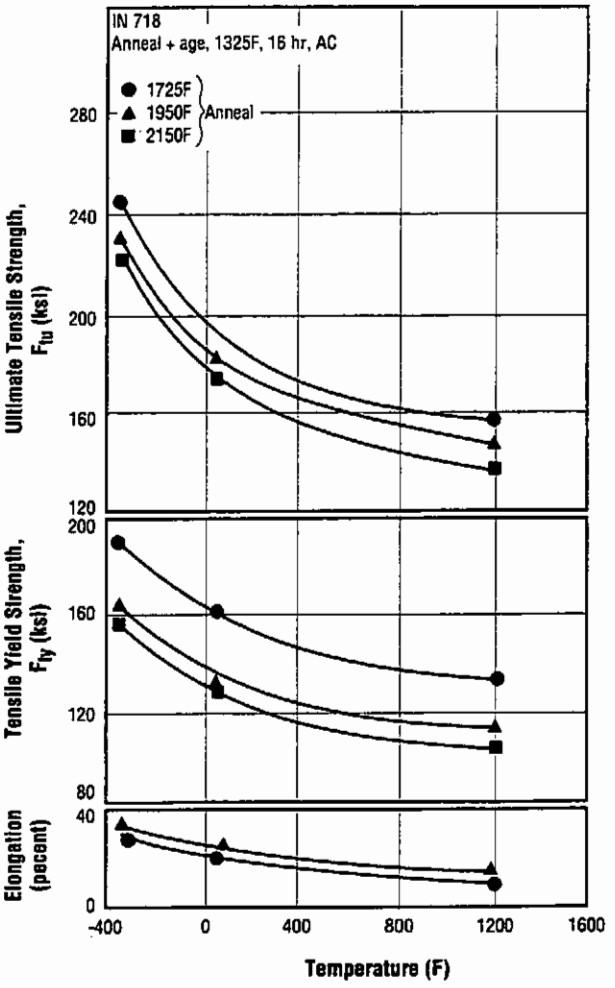

Fig. 4.3.3.1 Effects of various annealing temperatures, representing brazing exposures, on tensile properties of annealed-and-aged alloy at various temperatures (Ref. 50)

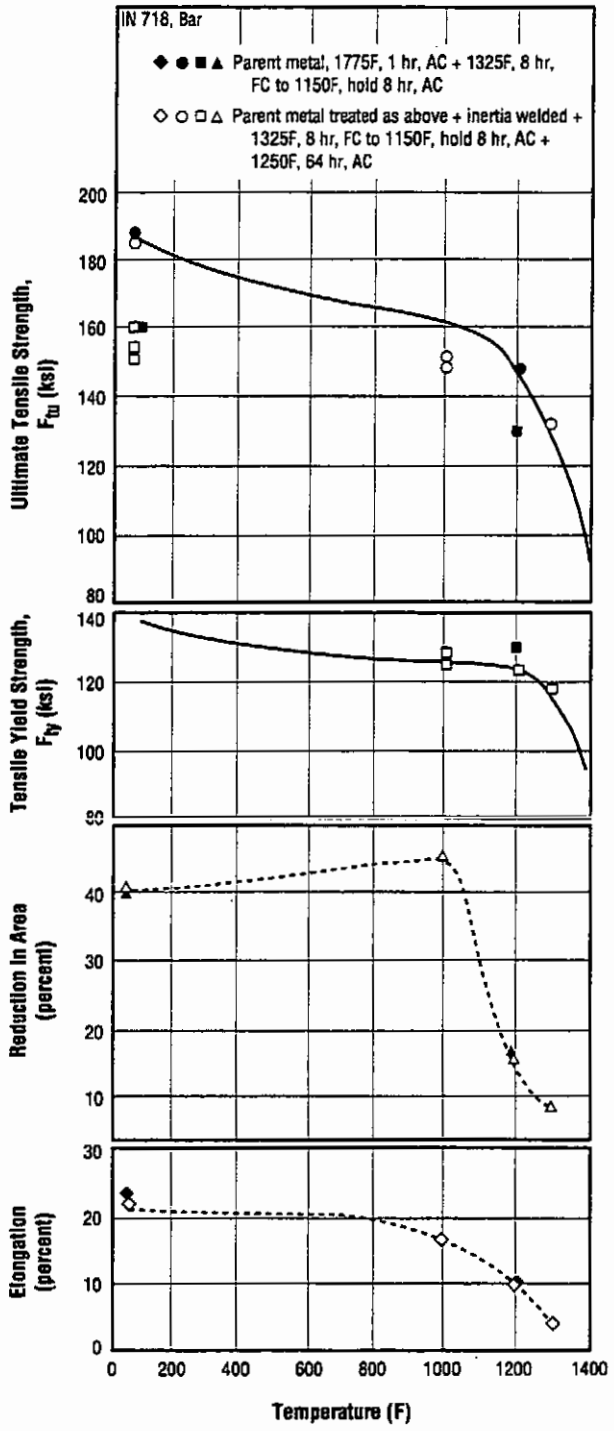

Fig. 4.3.4.1 Effects of elevated temperatures on tensile properties of annealed-and-aged inertia welds and base metal (Ref. 70)

References

1. "Inconel Alloy 718," Huntington Alloys, Inc. 10M 7-78 T-39 (1978).
2. "Inconel Alloy 718," International Nickel Company (1972).
3. Clark, A. F.; Childs, G. E.; and Wallace, G. H., "Electrical Resistivity of Some Engineering Alloys at Low Temperatures," *Cryogenics*, pp. 295-305 (August 1970)
4. AMS 5596G, Society of Automotive Engineers (April 1, 1987).
5. AMS 5597D, Society of Automotive Engineers (August 1994).
6. AMS 5589C, Society of Automotive Engineers (August 1994).
7. AMS 5590C, Society of Automotive Engineers (April 1, 1993).
8. AMS 5383D, Society of Automotive Engineers (April 1, 1993).
9. AMS 5662J, Society of Automotive Engineers (September 1994).
10. AMS 5663F, Society of Automotive Engineers (January 1, 1989).
11. AMS 5664D, Society of Automotive Engineers (July 1994).
12. AMS 5832D, Society of Automotive Engineers (January 1, 1991).
13. Walter, R. J., and Chandler, W. T., "Influence of Gaseous Hydrogen on Inconel 718," Hydrogen in Metals, ASM (1973).
14. Mucci, J., and Harris, J. A., Sr., "Influence of Gaseous Hydrogen on Mechanical Properties of High Temperature Alloys," Pratt & Whitney Aircraft Group, FR-7746 (July 1976).
15. Forman, R. G., "Crack-Growth Behavior in Thick Welded Plates of Inconel 718 at Room and Cryogenic Temperatures," Johnson Space Center, NASA TN D-7665 (May 1974).
16. Floreen, S., and Kane, R. H., "An Investigation of the Creep-Fatigue Environment Interaction in a Ni-Base Superalloy," Fatigue of Engineering Materials and Structures, Vol. 2, Pergamon Press (1979).
17. Mills, W. J., "The Influence of Heat Treatment on the Microstructure and Mechanical Properties of Alloy 718 Base Metal and Weldments," Hanford Engineering Development Laboratory, HEDL-TME 78-54, UC-79, b, h (1979).
18. Gilbreath, W. P., and Adamson, M. J., "The Stress Corrosion Susceptibility of Several Alloys in Hydrazine," NASA Technical Note D-7604 (February 1974).
19. Hall, A. M., and Beuharig, V. F., "Thermal and Mechanical Treatments for Nickel and Some Nickel-Base Alloys: Effects on Mechanical Properties," NASA SP-5106 (1972).
20. Logsdon, W. A., and Wells, J. M., "Influence of Processing and Heat Treatment on the Cryogenic Fracture Mechanics Properties of Inconel 718," Westinghouse Research Labs, Scientific Paper 77-9E7-CRYMT-P2 (March 31, 1977).
21. Ward, A. L.; Steichen, J. M.; and Knecht, R. L., "Irradiation and Thermal Effects on Tensile Properties of Inconel 718," ASTM STP 611, pp. 156-170 (1976).
22. James, L. A., "Fatigue-Crack Propagation Behavior of Inconel 718," Hanford Engineering Development Laboratory, HEDL-TME 75-80, UC-79, b, h (September 1975).
23. Schwartzberg, F. R., and Shepic, J. A., "Effect of High-Pressure Oxygen on the Mechanical Properties of Alloys," Martin Marietta Corp., Denver, CO (February 1977).
24. Nagan, R. M., "Precision Castings State-of-the-Art," *SAMPE Quarterly* (July 1975).
25. Jewett, R. P.; Walter, R. J.; and Chandler, W. T., "Influence of High-Pressure Hydrogen on Cyclic Load Crack Growth in Metals," ASTM STP 642 (November 1976).
26. Muzyka, D. R., "Physical Metallurgy and Effects of Process Variables on the Microstructure of Wrought Superalloys," ASTM STP 672 (April 1978).
27. Kolts, J., "Temperature Limits for Stress Corrosion Cracking of Selected Stainless Steels and Nickel-Base Alloys in Chloride-Containing Environments," NACE, Paper No. 241 (March 1982).
28. Franklin, D. B., and Nelson, E. F., "Corrosion Fatigue of Inconel 718 and Incoloy 903," Marshall Space Flight Center, NASA TM-82426 (June 1981).
29. Smolik, G. R., and Korth, G. E., "Evaluation of Roll-Extruded Alloy 718 Tubing," DOE, Idaho National Engineering Laboratory, TREE-1255 (May 1978).
30. Shahinian, P., and Sadananda, K., "Crack Growth Behavior Under Creep-Fatigue Conditions in Alloy 718," *Proceedings from the 1976 ASME-MPC Symposium on Creep-Fatigue Interactions* (December 1976).
31. James, L. A., "Fatigue-Crack Growth in Inconel 718 Weldments at Elevated Temperatures," *Welding Journal Research Supplement*, Vol. 57, pp. 175-235 (January 1978).

32. Smith, H. H., and Mickel, D. J., "Effect of Heat Treatment on Fatigue Crack Propagation and Deformation Mode in Alloy 718 at Elevated Temperatures," NRL Memorandum Report 3810 (July 1978).

33. Sadananda, K., and Shahinian, P., "Effect of Heat Treatment on High Temperature Crack-Growth Under Static Load in Alloy 718," NRL Memorandum Report 3727 (February 1978).

34. Hack, H. P., "Mechanical, Corrosion and Fatigue Properties of 15-5 PH, Inconel 718, and René 41 Weldments," Naval Ship Research and Development Center, Report 4528 (May 1975).

35. Vanderham, M. C., and Harris, J. A., Jr., "Properties of Materials in High Pressure Hydrogen at Cryogenic, Room, and Elevated Temperatures," Pratt & Whitney Aircraft, FR5768 (July 31, 1973).

36. Royster, D. M., and Lisagor, W. B., "The Effect of High-Temperature Creep and Oxidation on the Residual Room-Temperature Properties of Several Thin-Sheet Superalloys," NASA TN D-6893 (November 1972).

37. Hust, J. G.; Weitzel, D. H.; and Powell, R. L., "Thermal Conductivity, Electrical Resistivity, and Thermopower of Aerospace Alloys from 4 to 300 K," *Journal of Research NBS*, Vol. 75A (July-August 1971).

38. Gray, H. R., "Embrittlement of Nickel-, Cobalt-, and Iron-Base Superalloys by Exposure to Hydrogen," NASA TN D-7805 (January 1975).

39. Thakker, A. B., and Cowles, B. A., "Low-Strain Long-Life Creep-Fatigue of AF2-1DA and Inco 718," NASA CR-167989, United Technologies Corporation (April 1983).

40. Goldhoff, R. M., "Methods for Constructing Isochronous Creep Curves," ASME Pamphlet, The Generation of Isochronous Stress-Strain Curves, pp. 67-85 (November 1972).

41. Goldhoff, R. M., and Hahn, G. J., "Correlation and Extrapolation of Creep-Rupture Data of Several Steels and Superalloys Using Time-Temperature Parameters," ASM Publication D8-100, pp. 199-246 (1969).

42. Blatherwick, A. A., and Cers, A., "Fatigue, Creep, and Stress-Rupture Properties of Nicrotung, Super A-286, and Inconel 718," AFML TR65-447 (June 1966).

43. Wilson, D. J.; Freeman, J. W.; and Goodell, P. D., "Sensitivity of the Creep Rupture Properties of Nickel Base Superalloys to Sharp Edge Notches in the Temperature Range of 1000 to 1400F," Paper presented at 97th AIME Annual Meeting, New York, NY (February 25-28, 1968).

44. Cullen, T. M., and Freeman, J. W., "The Mechanical Properties of Inconel 718 Sheet Alloy at 800, 1000, and 1200F," NASA CR-268 (July 1965).

45. Inouye, F. T.; Hunt, V.; Janser, F. R.; and Frick, V., "Application of Alloy 718 in M-1 Engine Components," NASA CR-788 (June 1967).

46. "Inconel 718, Age Hardenable Nickel Base Alloy," *Alloy Digest*, Filing Code: Ni-65 (April 1961).

47. Malin, C. O., and Schmidt, E. F., "Tensile and Fatigue Properties of Alloy 718 at Cryogenic Temperatures," Report of Rocketdyne Corporation, presented at ASM, Cleveland, OH (October 1967).

48. Kiefer, T. F., et al, "Determination of Low-Temperature Fatigue Properties of Structural Metal Alloys," Final Report, Martin Company NASA Contract NAS-8-11300 (October 1965).

49. Nachtigall, A. J.; Klima, S. J.; and Frecke, J. C., "Fatigue Behavior of Rocket Engine Materials to -452F (4K)," NASA article for *ASTM Materials Research and Standards* (June 1967).

50. Evans, R. M., "The Welding and Brazing of Alloy 718," DMIC Report 204 (June 1, 1964).

51. Betts, R. D., et al, "Weld Efficiencies of Inconel 718 Gas Turbine Arc Welds in the -423 to 1500F Temperature Range," Report MPR5-175-363 North American Aviation, Inc. (July 1965).

52. Anon., "Metallurgy – a Compilation," NASA S.P. 5940(01) (1970).

53. Anon., "Effect of Heat Treatment and Surface Oxidation on the Low-Cycle Fatigue Life of Alloy 718," Rocketdyne Report MPR No. 9-176A-77 (May 1969).

54. Masteller, R. D.; Brown, H. J.; Herzog, R. G.; and Osgood, S. H., "Properties of Cryogenically Worked Materials," NASA CR-72638 (May 1, 1970).

55. Heacox, R. A., "Influence of Cold Reduction and Heat Treatment on the Properties and Microstructure of Alloy 718 Fastener Stock," AIME Report MCIC-72-10, *Superalloy Processing Procedings of Second International Conference* (September 1972).

56. Barker, J. F.; Ross, E. W.; and Radavick, J. R., "Long-Time Stability of Inconel 718," *Journal of Metals* (January 1970).

57. Walter, R. J., and Chandler, W. T., "Effect of High-Pressure Hydrogen on Metals," ASM Report D8-142 (1968).

58. Keiser, D. D., "Heat-Treat Cracking in Inconel 718, Its Cause and Prevention," Technical Report No. 606, Aerojet Nuclear Company (April 4, 1975).

59. Shogan, R. P., "Tensile Properties of Irradiated Inconel 718 and Inconel X750 at Cryogenic Temperatures," WANL Report TME-1922 (August 1969).

60. Heslington, G. L., and Foster, S. D., "Stress-Strain Diagrams in the Elastic and Plastic Regions at Elevated

Temperatures," Rocketdyne Report MPR 8-176A-37 (October 17, 1968).

61. Schmidt, E. H., "Fatigue Properties of Sheet, Bar, and Cast Metallic Materials for Cryogenic Applications," NASA CR-111396 (August 30, 1968).
62. Wassil, G. N.; Makepeace, D. E.; et al, "Form Rolling Close Tolerance Shapes of Superalloys," A. F. Contract No. AF33(615)-3545.
63. Martin, H. L.; Miller, P. C.; Ingram, A. G.; and Campbell, J. E., "Effects of Low Temperatures on the Mechanical Properties of Structural Metals," NASA SP 5012(01) (1968).
64. Anon., "Low-Temperature Mechanical Properties of Various Alloys," NASA S.P.-592(01) (1970).
65. Frick, V.; Janser, G. R.; and Brown, J. A., "Enhanced Flaw Growth in SSE Main Engine Alloys in High-Pressure Gaseous Hydrogen," Space Shuttle Materials, *SAMPE*, Vol. 3, pp. 597-634 (1971).
66. Moon, D. P.; Simon, R. C.; and Favor, R. J., "The Elevated Temperature Properties of Selected Superalloys," ASTM Data Series DS 7-S1 (1968).
67. Heyer, B. A., "Manufacturing Process for Superalloy Cast Parts: Phase 1 – Fundamentals," Interim Progress Report to AFML, R&T Division (June 15, 1968).
68. Hoegfeldt, J. M., "Manufacturing Technology for the Extrusion of Superalloy Structural Shapes," Phase II Engineering Report IR 8-301(V), Report from TRW to AFML.
69. Boeing-North American Aviation (Joint Venture) "Thick-Section Fracture Toughness," ML-TDR-64-326 (October 1964).
70. Korton, G., and Stalker, K. W., "Improved Fabrication Methods of Jet Engine Rotors," AFML-TR-70-101 (May 1970).
71. "Udimet 718," Special Metals, Inc.
72. "Pyromet Alloy 718," Carpenter Technology Corporation (July 1981).
73. "Allvac 718 – Technical Data," Teledyne Allvac Corporation.
74. "Haynes Alloy No. 718," High Technology Materials Division, Cabot Corporation (1975).
75. ASM Handbook, "Heat Treating," Ninth Edition, Vol. 4 (1981).
76. Sadananda, K., and Shahinian, P., "Creep Crack Growth in Alloy 718," *Metallurgical Transactions*, Vol. 8A (March 1977).
77. Gordine, J., "Some Problems with Welding Inconel 718," *Welding Journal*, Vol. 50, pp. 480s-484s (November 1971).
78. Wilson, D. J., "Relationship of Mechanical Characteristics and Microstructural Features to the Time-Dependent Edge-Notch Sensitivity of Inconel 718 Sheet," *Journal of Engineering Materials and Technology*, pp. 112-123 (April 1973).
79. Beltram, A. M., and Saeguse, F., "Fused Salt Corrosion Resistance of Water Cooled Gas Turbine Alloys," *Materials Performance*, Vol. 21 (December 1982).
80. Sadananda, K., and Shahinian, P., "The Effect of Environment on Creep Crack Growth Behavior of Several Structural Alloys," *Materials Science and Engineering*, Vol. 43, pp. 159-168 (1980).
81. Mills, W. J., "The Effect of Heat Treatment on the Room Temperature and Elevated Temperature Fracture Toughness Response of Alloy 718," *Journal of Engineering Materials and Technology*, Vol. 102, pp. 118-126 (January 1980).
82. Rice, P. W., "Evaluating Nickel Base and Stainless Alloys for Subsurface H_2S Service," *Materials Performance*, Vol. 17, pp. 16-25 (September 1978).
83. Weston, W. F., and Ledbetter, "Low-Temperature Elastic Properties of a Nickel-Chromium-Iron-Molybdenum Alloy," *Materials Science and Engineering*, Vol. 29, pp. 287-290 (1975).
84. "Observations on Intermetallic Compound and Carbide Precipitation in Two Commercial Nickel-Base Alloys," *Journal of Less-Common Metals*, Vol. 27, pp. 17-26 (1972).
85. Rizzo, F. J., and Buzzanell, J. D., "Effect of Chemistry Variations on the Structural Stability of Alloy 718," International Symposium on the Structural Stability in Superalloys, pp. 501-543, Symposium sponsored by ASM, ASME, AIME, and ASTM (September 4-6, 1968).
86. "Joining Huntington Alloys," Huntington Alloys, Inc., Third Edition, pp. 33-34 (1978).
87. Gordine, J., "Some Problems in Welding Inconel 718," *Welding Research Supplement*, pp. 480s-484s (November 1971).
88. Mills, W. J., "The Effect of Heat Treatment on the Room Temperature and Elevated Temperature Fracture Toughness Response of Alloy 718," *Journal of Engineering Materials and Technology*, Vol. 102, pp. 118-126 (1980).
89. Mills, W. J., "Effect of Heat Treatment on the Tensile and Fracture Toughness Behavior of Alloy 718 Weldments," *Welding Reserach Supplement*, pp. 237s-245s (August 1984).
90. Thompson, R. G.; Dobbs, J. R.; and Mayo, D. E., "The Effect of Heat Treatment on Microfissuring in Alloy 718," *Welding Research Supplement*, pp. 299s-304s (November 1986).

91. *Metals Handbook*, 10th Edition, Vol. 4, American Society for Metals, p. 800 (1991).

92. Barker, J. F.; Kreuger, D. D.; and Chang, D. R., "Thermomechanical Processing of Inconel 718 and Its Effect on Properties," *Advanced High-Temperature Alloys: Processing and Properties*, held in Cambridge, MA, June 16-18, 1985, American Society for Metals, Metals Park, OH, pp. 125-137 (1986).

93. *Metals Handbook*, 10th Edition, Vol. 1, American Society for Metals, pp. 950-956 (1990).

94. Fox, S.; Brooks, J. W.; Loretto, M. H.; and Smallman, R. E., "Influence of Carbides on the Mechanical Properties of Inconel 718," *Proceedings, 7th International Conference on the Strength of Metals and Alloys*, held at Montreal, Canada, August 12-16, 1985, Pergammon Press, Elmsford, NY, pp. 399-404 (1986).

95. Loria, E. A., "The Status and Prospects of Alloy 718," *Journal of Metals*, Vol. 40, No. 7, pp. 36-41 (July 1988).

96. *Metals Handbook*, 10th Edition, Vol. 4, American Society for Metals, pp. 804-807 (1991).

97. Koul, A. K.; Au, P.; Bellinger, N.; Thamburaj, R.; and Wallace, W., "Development of a Damage Tolerant Microstructure for Inconel 718 Turbine Disc Material," *Sixth International Symposium on Superalloys, Superalloys 1988*, held in Champion, PA, September 18-22, 1988, The Metallurgical Society of AIME, Warrendale, PA, pp. 3-12 (1988).

98. Brooks, J. W., and Bridges, P. J., "Metallurgical Stability of Inconel Alloy 718," Sixth International Symposium on Superalloys, Superalloys 1988, held in Champion, PA, September 18-22, 1988, The Metallurgical Society of AIME, Warrendale, PA, pp 33-42 (1988).

99. Thompson, R. G., "Microfissuring of Alloy 718 in the Weld Heat-Affected Zone," *Journal of Metals*, Vol. 40, No. 7, pp. 44-48 (July 1988).

100. Poole, J. M., "Homogenization of VIM-VAR Inconel Alloy 718," *Special Melting and Processing Technologies*, held in San Diego, CA, April 11-15, 1988, Noyes Publications, Park Ridge, NJ, pp. 508-539 (1989).

101. Ruiz, C.; Obabueki, A.; and Gillespie, K., "Evaluation on the Microstructure and Mechanical Properties of Delta Processed Alloy 718," *Superalloys 1992*, held in Champion, PA, September 20-24, 1992, The Minerals, Metals, and Materials Society, Warrendale, PA, pp. 33-42 (1992).

102. Loria, E. A., "Recent Developments in the Progress of Superalloy 718," *Journal of Metals*, Vol. 44, No. 6, pp. 33-36 (June 1992).

103. Denda, T. H.; Bretz, P. L.; and Tien, J. K., "Inclusion Size Effect on the Fatigue Crack Propagation Mechanism and Fracture Mechanics of a Superalloy," *Metallurgical Transactions A*, Vol. 23A, No. 2, pp. 519-526 (February 1992).

104. Denda, T.; Himeno, S.; Shimizu, F.; Mori, N.; Bretz, P. L.; and Tien, J. K., "Electron Beam Cold Hearth Refining of IN 718 and Resulting Properties," *High Temperature Materials for Power Engineering 1990. II*, held in Liege, Belgium, September 24-27, 1990, Kluwer Academic Publishers, Dordrecht, The Netherlands, pp. 1675-1686 (1990).

105. Tien, J. K.; Denda, T.; and Bretz, P. L., "A Functional Dependence Between Inclusion Size and LCF Life," *Electron Beam Melting and Refining – State of the Art 1991*, held at Reno, NV, October 25-27, 1992, Bakish Materials Corporation, Englewood, NJ, pp. 200-210 (1991).

106. *Metals Handbook*, 10th Edition, Vol. 1, American Society for Metals, pp. 969-983 (1990).

107. Holmes, R. R.; Burns, D. H.; and McKechnie, T. N., "Vacuum Plasma Spray Forming NARloy-Z and Inconel 718 Components for Liquid Rocket Engines," *Thermal Spray Research and Applications*, held in Long Beach, CA, May 20-25, 1990, ASM International, Metals Park, OH, pp 363-368 (1991).

108. Heubner, U.; Kohler, M.; and Prinz, B., "Determination of the Solidification Behavior of Some Selected Superalloys," *Superalloys 1988*, held in Champion, PA, September 18-22, 1988, The Metallurgical Society of AIME, Warrendale, PA, pp. 437-447 (1988).

109. Antolovich, S. D., "The Effect of Metallurgical Instabilities on the Behavior on IN 718," *Superalloy 718 – Metallurgy and Applications*, E. A. Loria, Editor, The Minerals, Metals and Materials Society, pp. 647-653 (1989).

110. Brooks, J. W.; and Bridges, P. J., "Long Term Stability of Inconel Alloy 718 for Turbine Disc Applications," *High Temperature Alloys for Gas Turbines and Other Applications, 1986, II*, held in Liege, Belgium, October 6-9, 1986, D. Reidel Publishing Company, Dordrecht, The Netherlands, pp. 1431-1440 (1986).

111. Fayman, Y. C., "Microstructural Characterization and Elemental Partitioning in a Direct-Aged Superalloy (DA 718)," *Materials Science and Engineering*, Vol. 92, pp. 159-171 (August 1987).

112. Sundararaman, M.; Mukhopadhyay, P.; and Banerjee, S., "Some Aspects of the Precipitation of Metastable Intermetallic Phases in Inconel 718," *Metallurgical Transactions A*, Vol. 23A, No. 7, pp. 2015-2028 (July 1992).

113. Sundararaman, M., and Mukhopadhyay, P., "Carbide Precipitation in Inconel 718," *High Temperature Materials and Processes*, Vol. II, No. 1-4, pp. 351-368 (January 1993).

114. Robertson, W. M., "Hydrogen Permeation and Diffusion in Inconel 718 and Incology 903," *Metallurgical Transactions A*, Vol. 8A, pp. 1709-1712 (November 1977).

115. Goldberg, I. B.; Mitchell, M. R.; Murphy, A. R.; Goldfarb, R. B.; and Loughran, R. J., "Magnetic Susceptibility of Inconel Alloys 718, 825, and 800 at Cryogenic Temperatures," *Advances in Cryogenic Engineering Materials, Vol. 36A*, held in Los Angelos, CA, July 24-28, 1989, Plenum Press, New York, NY, pp. 755-762 (1990).

116. Baker, E. A., "Long-Term Corrosion Behavior of Materials in the Marine Atmosphere," ASTM STP-965, American Society for Testing and Materials, Philadelphia, PA, pp. 125-144 (February 1988).

117. Senor, D. J.; Peddicord, K. L.; and Strizak, J. P., "Effects of Hydrogen on the Fracture Morphology of Inconel 718," *Materials Letters*, Vol. 11, No. 10-13, pp. 373-378 (August 1991).

118. Hicks, P. D., and Altstetter, C. J., "Hydrogen Embrittlement of Superalloys," *Hydrogen Effects on Material Behavior*, held in Moran, WY, September 12-15, 1989, The Minerals, Metals, and Materials Society, Warrendale, PA, pp. 613-623 (1990).

119. Walter, R. J.; Kendig, M. W.; and Meisels, A. P., "Influence of Hydrogen Oxidation Kinetics on Hydrogen Environment Embrittlement," *Scripta Metallurgica et Materialia*, Vol. 27, No. 4, pp. 419-424 (August 1992).

120. Hicks, P. D., and Altstetter, C. J., "Internal Hydrogen Effects on Tensile Properties of Iron- and Nickel-Base Superalloys," *Metallurgical Transactions A*, Vol. 21A, No. 2, pp. 365-372 (February 1990).

121. Hicks, P. D., and Altstetter, C. J., "Hydrogen-Enhanced Cracking of Superalloys," *Metallurgical Transactions A*, Vol. 23A, No. 1, pp. 237-249 (January 1992).

122. Paul, L. D., "Residual Strength Testing of Hydrogen Charged Alloy 718 Sheet Material," Report RDD:92:8606:58-01:02, from Babcock and Wilcox Company, Alliance, OH to Analex Corporation, Brookpark, OH (February 1992).

123. Pound, B. G., "Hydrogen Trapping in Precipitation-Hardened Alloys," *Acta Metallurgica et Materialia*, Vol. 38, No. 12, pp. 2373-2381 (December 1990).

124. Lenglet, M.; Guillamet, R.; Lopitaux, J.; and Hannoyer, B., "Initial Stages of Oxidation of Inconel 718 by FTIR Spectroscopy," *Materials Research Bulletin*, Vol. 25, No. 6, pp. 715-722 (1990).

125. Stoltzfus, J. M.; Benz, F. J.; and Homa, J., "The Pv Product Required for the Frictional Ignition of Alloys," ASTM STP 1040, American Society for Testing and Materials, Philadelphia, PA, pp. 212-223 (1989).

126. Steinberg, T. A.; Rucker, M. A.; and Beeson, H. D., "Promoted Combustion of Nine Structural Metals in High-Pressure Gaseous Oxygen: A Comparison of Ranking Methods," ASTM STP 1040, American Society for Testing and Materials, Philadelphia, PA, pp. 54-75 (1989).

127. Mills, W. J., "Fracture Toughness Variations for Alloy 718 Base Metal and Welds," *Superalloy 718 – Metallurgy and Applications*, A. E. Loria, Editor, The Minerals, Metals, and Materials Society, pp. 517-532 (1989).

128. Han, Y., and Chaturvedi, M. C., "Steady State Creep Deformation of Superalloy Inconel 718," *Materials Science and Engineering*, Vol. 89, No. 1-2, pp. 25-33 (May 1987).

129. Han, Y., and Chaturvedi, M. C., "A Study of Back Stress During Creep Deformation of a Superalloy Inconel 718," *Materials Science and Engineering*, Vol. 85, pp. 59-65 (January 1987).

130. Chaturvedi, M. C., and Han, Y., "Effect of Particle Size on the Creep Rate of Superalloy Inconel 718," *Materials Science and Engineering*, Vol. 89, No. 1-2, pp. L7-L10 (May 1987).

131. James, L. A., "Fatigue Crack Propagation in Alloy 718: A Review," *Superalloy 718 – Metallurgy and Applications*, E. A. Loria, Editor, The Minerals, Metals, and Materials Society, pp. 499-515 (1989).

132. Smith, H. H., and Michel, D. J., "Effect of Environment on Fatigue Crack Propagation Behavior of Alloy 718 at Elevated Temperatures," *Metallurgical Transactions A*, Vol. 17A, No. 2, pp. 370-374 (February 1986).

133. Ghonem, H.; Nicholas, T.; and Pineau, A., "Elevated Temperature Fatigue Crack Growth in Alloy 718. I. Effects of Mechanical Variables," *Fatigue and Fracture of Engineering Materials and Structures*, Vol. 16, No. 5, pp. 565-576 (May 1993).

134. Woollin, P., and Knott, J. F., "Effects of Temperature and Environment on the Long Crack Growth Behavior of Inconel 718," *ICF 7. Advances in Fracture Research, Vol. 2*, held in Houston, TX, March 20-24, 1989, Pergamon Press plc, Oxford UK, pp. 1859-1868 (1989).

135. Weerasooriya, T., "Effect of Frequency on Fatigue Crack Growth Rate of Inconel 718 at High Temperature," ASTM STP 969, American Society for Testing and Materials, pp. 907-923 (1988).

136. Kreuger, D. D.; Antolovich, S. D.; and Van Stone, R. H., "Effects of Grain Size and Precipitate Size on the Fatigue Carck Growth Behavior of Alloy 718 at 427C," *Metallurgical Transactions A*, Vol. 18A, No. 8, pp. 1431-1449 (August 1987).

137. Weerasooriya, T., and Nicholas, T., "Hold-Time Effects in Elevated Temperature Fatigue Crack Propagation,"

AFWAL-TR-84-4184, University of Dayton, Dayton, OH (March 1985).

138. Petrovich, A., and Ziegler, W., "The Influence of Several Combined High/Low Cycle Loading Parameters on the Crack Growth of a Turbine Disc Alloy," *Journal of Vibratory Acoustic Stress Reliability and Design*, Vol. 108, No. 3, pp. 262-267 (July 1986).

139. Nicholas, T.; Heil, M. L.; and Haritos, G. K., "Predicting Crack Growth Under Thermo-Mechanical Cycling," *International Journal of Fracture*, Vol. 41, No. 3, pp. 157-176 (November 1989).

140. Chang, K.-M., "Time-Dependent Fatigue Crack Propagation in Inconel 718 Superalloys," *Mechanical Behavior of Materials. V. Vol. 2*, held in Beijing, China, June 3-6, 1987, Pergamon Press plc, Oxford, UK, pp. 1139-1147 (1988).

141. Chaudhury, P. K., and Zhao, D., "Atlas of Formability: Inconel 718," N00140-88-C-RC21, National Center for Excellence in Metalworking Technology, Johnstown, PA (July 1992).

142. Smith G. D., and Yates, D. H., "Superplastic Forming of Inconel Alloy 718SPF," *Advancements in Synthesis and Processes*, held in Toronto, Canada, October 20-22, 1992, Society for the Advancement of Material and Process Engineering, Covina, CA, pp. M207-M218 (1992).

143. Smith, G. D., and Flower, H. L., "Superplastic Forming of Alloy 718," *Advanced Materials and Processes*, Vol. 145, No. 4, pp. 32-34 (April 1994).

144. Knorovsky, G. A.; Cieslak, M. J.; Headley, T. J.; Romig, A., Jr.; and Hammetter, W. F., "Inconel 718: A Solidification Diagram," *Metallurgical Transactions A*, Vol. 20A, No. 10, pp. 2149-2158 (October 1989).

145. Baeslack W. A., III, and Nelson, D. E., "Morphology of Weld Heat-Affected Zone Liquation in Cast Alloy 718," *Metallography*, Vol. 19, No. 3, pp. 371-379 (August 1986).

146. Thompson, R. G.; Radhakrishnan, B.; and Mayo, D. E., "Intergranular Liquid Formation, Distribution, and Cracking," *Superalloy 718 – Metallurgy and Applications*, E. A. Loria, Editor, The Minerals, Metals, and Materials Society, pp. 437-455 (1989).

147. Radhakrishnan, B., and Thompson, R. G., "The Effect of Weld Heat-Affected Zone (HAZ) Liquation Kinetics on the Hot Cracking Susceptibility of Alloy 718," *Metallurgical Transactions A*, Vol. 24A, pp. 1409-1422 (June 1993).

148. Bradley, E. L., III, and Thompson, R. G., "The Effect of Weld Heat-Affected Zone Hot Cracks on the Fatigue Crack Growth Behavior of As-Cast Alloy 718," *Superalloy 718 – Metallurgy and Applications*, E. A. Loria, Editor, The Minerals, Metals, and Materials Society, pp. 457-466 (1989).

149. Bavarian, B., and Emmons, J. R., "Microfissuring in the Heat-Affected Zone of Inconel 718 Weldments," *ISFTA 90*, held in Los Angeles, CA, October 29-November 2, 1990, ASM International, Metals Park, OH, pp. 363-383 (1990).

150. Thompson, R. G.; Cassimus, J. J.; Mayo, D. E.; and Dobbs, J. R., "The Relationship Between Grain Size and Microfissuring in Alloy 718," *Welding Research Supplement*, pp. 91s-96s (April 1985).

151. Kelly, T. J., "Elemental Effects on Cast 718 Weldability," *Welding Journal*, Vol. 68, No. 2, pp. 44s-51s (February 1989).

152. Mills, W. J., "Fracture Toughness of Thermally Aged Alloy 718 Weld Metal," *Welding Journal*, Vol. 66, No. 4, pp. 113s-119s (April 1987).

153. Dahotre, N. B.; McCay, M. H.; McCay, T. D.; Hubbard, C. R.; Porter, W. D.; and Cavin, O. B., "Effect of Grain Structure on Phase Transformation Events in the Inconel 718," *Scripta Metallurgica et Materialia*, Vol. 28, No. 11, pp. 1359-1364 (June 1, 1993).

154. Murata, Y.; Morinaga, M.; Yukawa, N.; Ogawa, H.; and Kato, M., "Solidification and Precipitation Behavior of Inconel 718 and Waspaloy," *The First Pacific Rim International Conference on Advanced Materials and Processing*, held in Hangzhou, China, June 23-27, 1992, The Minerals, Metals, and Materials Society, Warrendale, PA, pp. 269-274 (1993).

155. Filoni, L., and Rocchini, G., "Thermal Conductivity of Iron, Plain Carbon and Stainless Steels, and Inconel 718 from 380 to 900K," *High Temperature-High Pressure*, Vol. 19, No. 4, pp. 381-387 (1987).

156. Nicholas, T., and Ashbaugh, N. E., "Fatigue Crack Growth at High Load Ratios in the Time-Dependent Regime," ASTM STP 969, American Society for Testing and Materials, Philadelphia, PA, pp. 800-817 (1988).

157. Jewett, R. P.; Walter, R. J.; and Chandler, W. T., "Hydrogen Embrittlement of Metals," NASA CR-2163 (March 1973).

158. Walter, R. J., and Chandler, W. T., "Influence of Gaseous Hydrogen on Metals," NASA CR-124410 (October 1973).

159. *ibid*, p. 100.

160. *ibid*, p. 123.

161. Private Communication, M. Kommann, Battelle-Europe, Geneva, Switzerland, to J. L. Shannon, Jr., NASA-Lewis Reserach Center, Cleveland, OH (December 12, 1993).

162. Chandler, W. T., "Hydrogen Embrittlement and Its Control in Hydrogen Fueled Engine Systems," Mini-Symposium on Recent Advances in Hypersonic Flight, held at NASA-Langley Research Center (September 1978).

163. Whiteley, R. V., "Determination of Oxygen Levels in Ni-H_2 Cells: Hubble Space Telescope Program," Lockheed Report No. EPS-243 (August 23, 1988).

164. Cullen, W. H., "Fracture Mechanics Materials Properties Tests. Final Report. Vol. 1 Technical Information and Conclusions," Materials Engineering Associates Report 2440, prepared for Space Systems/Loral (March 8, 1991).

165. Wilde, B. E., and Shimida, T., "Surface Modification: A Potential New Approach to Combatting Hydrogen Induced Fracture in Steel," *Scripta Metallurgica*, Vol. 22, p. 551 (1988).

166. Private Communication toWilliam D. Klopp, from W. F. Brown, Jr., NASA-Lewis Research Center (October 15, 1994).

167. Reuter, W. G., "Design Data for the 1/4-in. Thick Alloy 718 In-Pile Tube," Idaho National Engineering Laboratory Report TREE-NUREG-1087 (May 1977).

168. "Annual Book of Standards," ASTM (1994).

This page is blank.